COOPERATIVE AGREEMENT
No. OASRTRS-14-H-MICH

FINAL REPORT:
Health Assessment and Risk Mitigation of Railroad Networks Exposed to Natural Hazards using Commercial Remote Sensing and Spatial Information Technologies

Report Authors:
Prof. Jerome Lynch, University of Michigan, Ann Arbor, MI
Dr. Mohammed Ettouney, Thornton Tomsetti, New York, NY
Dr. Sharada Alampalli, Prospect Solutions, Loudonville, NY
Dr. Andrew Zimmerman, Civionics LLC, Ann Arbor, MI
Katherine Flanigan, University of Michigan, Ann Arbor, MI
Rui Hou, University of Michigan, Ann Arbor, MI
Nephi Johnson, University of Michigan, Ann Arbor, MI

Principle Investigator:
Jerome P. Lynch
Professor, Civil and Environmental Engineering
Professor, Electrical Engineering and Computer Science
2380 G. G. Brown Building
University of Michigan
Ann Arbor, MI 48109-2125
jerlynch@umich.edu

Program Manager:
Caesar Singh, P.E.
Director, University Grants Programs
OST - Office of the Assistant Secretary for Research and Technology
U.S. Department of Transportation
1200 New Jersey Avenue, SE, E33-306
Washington, DC 20590

Date of Report:
May 31, 2017

TABLE OF CONTENTS

GLOSSARY OF TERMS

AAR	Association of American Railroads
ASCE	American Society of Civil Engineers
AREMA	American Railway Engineering and Maintenance-of-Way Association
BMP	Bridge Management Program
CLR	Component Load Rating
CRS&SI	Commercial Remote Sensing and Spatial Information
DB	Database
D2D	Data-to-Decision
DHS	Department of Homeland Security
DLF	Dynamic Load Factor
DMT	Decision Making Tool
ELR	Enhanced Load Rating (utilizing pertinent information from RST, SHM, VI, SA)
ESM	Engineering Structures Management (UP inspection and rating database)
FE	Finite Element
FEM	Finite Element Method
FORM	First-Order Reliability Method
FRA	Federal Railroad Administration
GAO	Government Accountability Office
GEV	Generalized Extreme Value
GPS	Global Position System
GUI	Graphical User Interface (also termed dashboard)
HBD	Hot-box Detector
IL	Influence Lines
LSF	Limit State Function
MC	Monte Carlo
PI	Principle Investigator
REL	Reliability
RES	Resilience
RI	Risk
ROI	Return on Investment

RST	Remote Sensing Technologies
RV	Random Variables
SA	Structural Analysis
SHM	Structural Health Monitoring
SORM	Second Order Reliability Method
STB	Surface Transportation Board
TAC	Technical Advisory Committee
TTCI	Transportation Technology Center, Inc.
UAV	Unmanned Aerial Vehicle
UP	Union Pacific
USDOT	United States Department of Transportation
VI	Visual Inspection
WILD	Wheel Impact Load Detection

EXECUTIVE SUMMARY

The overarching goal of this project was to integrate data from commercial remote sensing and spatial information (CRS&SI) technologies to create a novel data-driven decision making framework that empowers the railroad industry to monitor, assess, and manage the risks associated with their aging bridge inventories, especially those exposed to natural hazards. Among the CRS&SI technologies explored, wireless sensing was a primary focus. Wireless monitoring systems were designed and deployed to monitor railroad bridges exposed to train and environmental loads. Coupled with structural inspection data, wheel impact load detection (WILD) data, and train location data, the wireless monitoring data was interrogated to assess train loads on bridges, assess the health and reliability of bridges, and quantify the consequences of exceeding performance limit states. A data-to-decision (D2D) framework was established to automate the processing of the CRS&SI data to convert it into actionable information that empowers risk-based decision-making. The team partnered with Union Pacific (UP) Railroad who provided access to operational railroad bridges, data and expertise. The project instrumented the Harahan Bridge and the Parkin Bridge in the New Madrid fault zone for demonstration of the system.

This project produced a large number of critical findings that advanced the use of CRS&SI technologies for risk management rail bridges:

1. Two permanent wireless monitoring systems were designed and deployed on the Harahan (Memphis, TN) and Parkin (Parkin, AR) Bridges. These bridges are critical elements of the Memphis sub-junction and were selected due to their exposure to natural (*e.g.,* seismic, aging) and man-made (*e.g.,* vehicular collisions) hazards. The Harahan and Parkin Bridges were instrumented with 36 and 30 wireless sensing channels, respectively, ranging from strain to acceleration measurements. As part of these monitoring systems, a real-time alert service was implemented to provide email alerts to UPRR engineers and inspectors regarding structural responses exceeding pre-defined response thresholds.
2. A relational database was developed to provide a comprehensive data repository to store inspection data, CRS&SI sensor data and analytical models of railroad bridges. Unifying these three forms of data/information empowers more extensive data analysis to assess the health of railroad bridges and aid railroads with risk management of their networks.
3. A reliability framework was created to assess the health of bridge components monitored. The reliability index calculated using the first-order reliability method was found to be an ideal scalar metric for assessing component health. Lower limit states were defined to trigger inspection and maintenance of bridge elements using monitoring data. The reliability index, when coupled with the consequences of exceeding defined limit states, allows owners to assess and manage the risks associated with their bridges and rail networks. The reliability framework was successfully validated on the Harahan Bridge.
4. The loads imposed on short-span rail bridges were quantified using long-term monitoring data. Specifically, the maximum static response and dynamic load factor as a function of train velocity were assessed for the Parkin Bridge. A novel approach to bridge load rating was developed using structural monitoring data; results indicated AREMA-specified load rating procedures are likely conservative for well-maintained rail and bridges.
5. An extensive return-on-investment (ROI) analysis was performed to assess the return rate for railroads that elect to invest in structural monitoring systems. Using the data-driven load rating methodology developed, the revelation of greater bridge capacity allows railroads to

carry larger loads at higher train velocities. This ensures the return on investment is positive and reaped rapidly after technology adoption.

6. The research effort also resulted in scholarly publications including four conference proceeding and two journal papers. Members of the research team provided 16 presentations in which aspects of the research effort in advancing CRS&SI technologies were presented to broad set of audiences across the United States.

A key objective of the project was the development of a commercialization plan for the CRS&SI technologies developed. The commercialization plan was produced based: market analysis, interviews with prospective technology adopters, and feedback provided by the project Technology Advisory Committee (TAC). The market analysis indicated a robust market both domestically and internationally for data-driven risk management methods based on CRS&SI data. Specifically, Class I and II railroads were identified as prospective customers domestically. However, interviews with technology adopter revealed a strong preference for short-term monitoring due to the perceived high costs associated with placing permanent monitoring systems in the field. Based on this feedback, the team devised a go-to-market strategy centered on short-term monitoring. A rapid-to-deploy commercial solution based on Civionics' wireless monitoring system and the Prospect Solutions' Decision Making Toolchest was developed. In partnership with the Transportation Technology Center, Inc. (TTCI) in Pueblo, Colorado, the team validated the commercial system using a short-span steel girder bridge loaded under a controlled loading regime. A wireless monitoring system measuring bridge strain and accelerations was deployed in minimal time and at minimal cost. Monitoring data was used to assess the load rating of the bridge using the data-driven load rating method developed by the team.

SECTION 1
PROJECT OVERVIEW

Introduction and Motivation

A critically important segment of the United States' transportation portfolio is its extensive rail network. Rail is the primary mode of transportation for the nation's coal, intermodal containers, chemicals, and agriculture products and is responsible for carrying 39.5% of the total ton-miles of national freight movement; the next largest is trucking carrying 28.6% (FRA 2014). Rail is an economically efficient means of transporting freight resulting in safer and less congested highways and reductions in greenhouse gas emissions. The national freight rail network is extensive with over 140,000 miles of rail managed by national Class I (7), regional (21), and local railroads (510) (Palley 2013). Along the national rail network are over 76,000 bridges with 80% of these bridges owned and maintained by Class I railroads (GAO 2007). It is estimated that more than half of the bridges were designed and constructed before 1920. While an aging fleet of rail bridges is a concern, even more concerning is the increase in freight being moved over the network. From 1990 to 2005, ton-miles per route-mile owned by Class I railroads have almost doubled. Clearly, this increase in load accelerates common load-based deterioration processes (*e.g.,* fatigue).

The 2013 ASCE Report Card for America's Infrastructure graded the state of repair of the nation's rail infrastructure as C+ indicating significant room for improvement in the condition of the railroads' rails, bridges and tunnels (ASCE 2013). Even though the Federal Railroad Administration (FRA) does not mandate (rather offers guidelines) a specific bridge management approach for railroads to follow, the Class I railroads have amassed an impressive safety record due to thorough inspection methods and detailed documentation used to manage their bridges. In contrast, there is greater variation in the inspection and documentation methods used by Class II and III railroads with the FRA voicing safety concerns. Prior to 1998, a number of high-consequence rail accidents occurred due to bridge failures including the 1993 train derailment on the Big Bayou Canot Bridge (Mobile, Alabama). The Big Bayou Canot Bridge incurred structural damage when it was struck by a barge; this failure resulted in 103 injuries, 47 fatalities and $436.2 million of losses (Otter *et al.* 2012). Since 1998, an additional two dozen train accidents have occurred that can be attributed directly to bridge structural failures (GAO 2007). Bridge failures can lead to serious service disruptions within the national rail network resulting in delays in the movement of freight over large regions of the country for prolonged periods of time. In 2006, a study by the U.S. Government Accountability Office (GAO) concluded that the FRA should "develop a systematic, *risk-based methodology*" to ensuring the safety of the nation's rail bridges. In 2010, the FRA established (Title 49 CFR) new requirements within their Bridge Safety Standards that require all national railroads to implement more rigorous bridge management programs that "*reduce the risk* of human casualties, environmental damage, and disruption to the Nation's railroad transportation system that would result from a catastrophic bridge failure."

Current bridge management programs in the railroad industry largely rely on visual inspections with bridges inspected on an annual or multi-annual basis. Post-inspection analyses are then used to assess the load carrying capacity of the inspected bridge using field observations (*e.g.,* section losses) to derive condition ratings for each bridge span. Unfortunately, visual inspection

methods are known to potentially introduce some degree of subjectivity to the evaluation process (Moore 2001). Despite these shortcomings, visual inspections have proven to be an effective bridge management tool. However, the railroad industry simultaneously recognizes the game changing role commercial remote sensing and spatial information (CRS&SI) technologies can play in helping them make more informed and quantitative decisions associated with assessing the condition of their bridges and undertaking more efficient decision making aimed at cost-effectively managing and mitigating risk (Moreu *et al.* 2012). In particular, the adoption of automated, remotely deployed structural health monitoring (SHM) systems has been cited as one CRS&SI technology that could offer the railroad industry a continuous and more quantitative basis for condition-based management of their bridges (Otter et al. 2012).

Commercial remote sensing and spatial information (CRS&SI) technologies are widely used in the railroad industry to plan and manage their infrastructure, maintain system operations, and manage emergency situations. CRS&SI technologies such as satellite imagery, laser scanning and global position system (CPS) tracking are widely used by the industry. At the same time, new CRS&SI technologies are also emerging in the railroad industry including wheel impact load detection (WILD) stations measuring axle loads and hot bearing detectors (also known as hotbox detectors) assessing the condition of the wheels and bearings of the rolling stock. Other CRS&SI technologies may also benefit the railroad industry in the future such as wireless monitoring systems, unmanned aerial vehicles (UAV), and photogrammetry systems.

Project Goals and Objectives

The overarching goal of this project is the integration of CRS&SI technologies with cloud-based analytical systems to create a comprehensive data-to-decision (D2D) framework that empowers railroad bridge owners to more accurately assess the condition of their bridges and to undertake quantitative risk-based asset management methods. The specific objectives of the proposed research program are as follows:

- *Apply and validate wireless sensing technologies as a cost-effective CRS&SI technology well suited to monitor the response of railroad bridges exposed to normal operational loads such as trains and natural hazard events.* Wireless monitoring systems have been previously deployed on highway bridges but not commonly applied to railroad bridges. Wireless monitoring systems remotely operated in the field must be capable of long-term reliable operations. The project will explore deployment of remote wireless monitoring systems on two bridges: Harahan Bridge in Memphis, TN and the Parkin Bridge in Parkin, AR.

- *Integrate WILD data from the rail network to track train loads.* WILD stations are commonly placed in a rail network to track trains including their speeds, axle counts, and axle weights. In this project, tracking train loads provides an important basis for assessing the consequences of bridges not performing as intended. In addition, WILD data can offer a baseline reference when assessing train loads directly from bridge responses.

- *Develop a comprehensive database system for CRS&SI data.* As railroads adopt more CRS&SI technologies, there is a need to integrate these data sets with traditional data and

information that currently serves as the basis for decision making. An objective of the project is the development of a relational database system that integrated three primary data sets: CRS&SI data, structural inspection data, and information on bridges for the development of analytical models.

- *Advance a reliability analytical framework that rationally combines measures of bridge demand and capacity derived from CRS&SI data to calculate reliability indices for critical bridge components and bridge spans.* Reliability frameworks are especially valuable because of their strong probabilistic basis. In this effort, reliability methods are used to assess the probability of exceeding a wide variety of limit states around which railroad decision making can be based.

- *Develop a risk-based decision making process by enumerating the costs and consequences of poor bridge performance at span- and network-levels when rail networks exposed to natural hazard events.* The reliability framework adopted provides the probabilities of exceeding limit states but when combined with the consequences of exceeding these limit states, risk can be assessed, monitored and managed.

- *Provide Railroad Owners with a Decision Making Toolchest (DMT).* Railroad decision makers are seeking tools to aid them to make better decisions using data they collect. The project will develop a platform that visualizes the data collected and stored in the database system while aid railroads in their decision making. Specifically, load rating and risk analyses will be offered using the CRS&SI data collected.

- *Commercialize the final wireless monitoring and DMT solutions.* An important objective is to translate the project outcomes into a commercially viable solution. The team will work collaboratively to develop a go-to-market strategy and initiate commercialization of the technology.

To ensure the project objectives are in alignment with the needs of the industry, the team will partner with UP which is the largest Class I railroad in the United States. UPRR will offer access to the Harahan Bridge in Memphis, TN and the Parkin Bridge in Parkin, AR for instrumentation; they will also provide access to various data sets that pertain to bridge health assessment including inspection data for these bridges.

Technical Approach

The project technical approach (Figure 1) is divided into three major thrust categories interrelated to create a CRS&SI-based D2D framework for risk management of a network of rail bridges exposed to a variety of natural and man-made hazards. In the first thrust (Thrust 1), the team will focus on the aggregation of CRS&SI technologies to collect data pertinent to bridge management. First, wireless monitoring systems for the monitoring of railroad bridges will be designed and deployed as a critical CRS&SI for bridge management. Furthermore, the team will collect data from a network of WILD stations throughout the UPRR network to acquire load information. As part of Thrust 1, the team will work in partnership with UPRR to validate the wireless monitoring system on UPRR bridges in the Memphis sub-junction due to the close proximity of this subjunction to the New Madrid fault zone. The Harahan Bridge, a long-span steel truss bridge over the Mississippi River, is selected for its natural hazard profile including

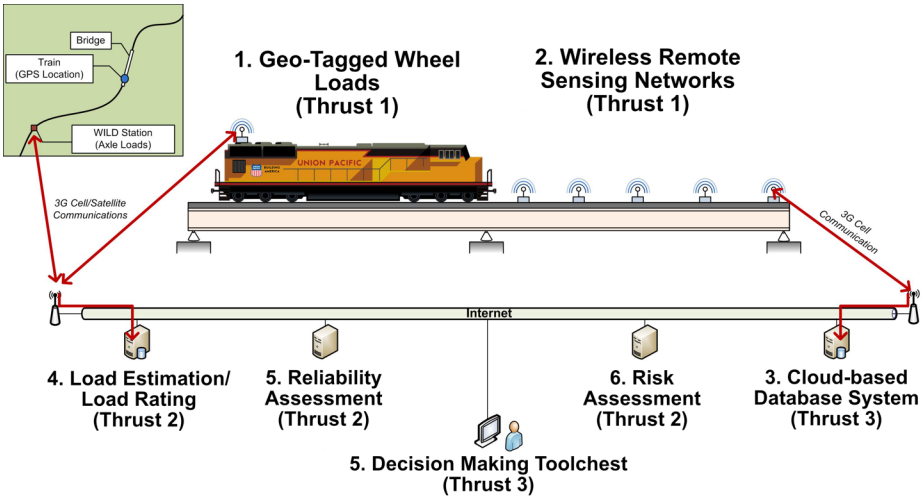

Figure 1. Overview of research effort in advancing wireless monitoring as a CRS&SI technology for the health assessment and risk management of railroad bridges.

seismic and river-based (*e.g.,* barge collisions, scour) natural hazards. Aging is another natural hazard due to the age of Harahan Bridge which is over 100 years. The Parkin Bridge is a short-span steel girder bridge located to the west of Harahan on the same subjunction. This bridge is selected due to its short-space allowing train loads to be estimated. It is also exposed to seismic hazards, aging hazards, and man-made hazards in the form of vehicular collisions from a road beneath the bridge.

The second thrust (Thrust 2) focuses on utilization of CRS&SI data (train loads and bridge responses) to estimate perform a health assessment of the bridges instrumented and a risk analysis of the rail network which the bridges service. The project will undertake three major analytical efforts. First, a reliability approach is taken to process bridge response data to assess the probabilities of bridge components exceeding limit states defined by the bridge owner. To prototype this approach to bridge health assessment, a critical tensile truss element on the Harahan Bridge will be focused on with limit states defined based on fatigue and load distributions. The second analysis is the load rating of bridges using measured bridge responses. The Parkin Bridge is used for this effort with the strain response of the bridge used to assess the static response and dynamic load factor associated with train load events. An empirical assessment of the live load demand is offered to provide a more accurate load rating of the bridge thereby revealing excess capacity not evident when performing traditional AREMA load ratings. The third analytical effort associated with Thrust 2 is the development of a risk assessment framework to evaluate the risk profile of the bridges. Finally, the health assessment and risk analyses performed are utilized to more broadly evaluate the resiliency of the rail network.

The third thrust (Thrust 3) is devoted to providing a user-friendly front-end to the D2D framework. First, the CRS&SI data collected, including the wireless monitoring data, will be stored in a relational database system developed by the team and deployed in the Microsoft Azure cloud. Additional data such as the inspection history of bridges will be stored in the database to provide analytical tools a more complete set of data and information that may be required during data interrogation. The analytical tools of Thrust 2 will be developed to query

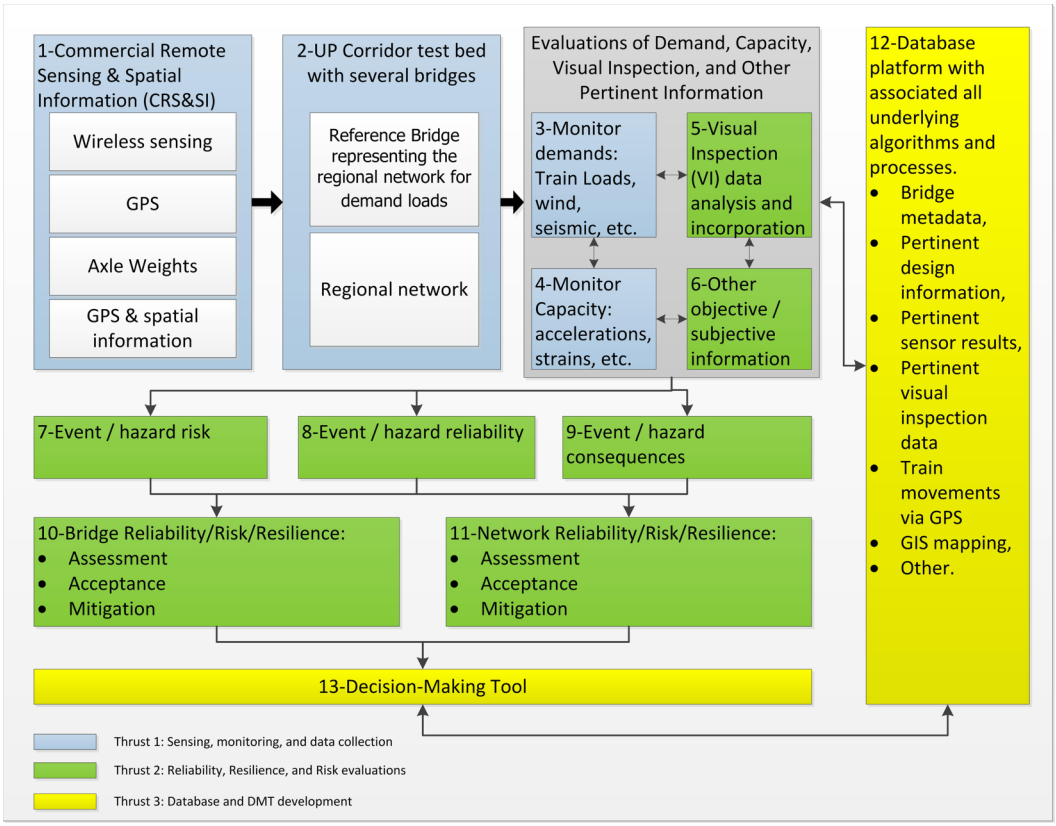

Figure 2. Architectural overview of D2D framework

the data in the database for analysis. The second part of Thrust 3 is devoted to the development of a graphical user interface (GUI), or dashboard, for the visualization of bridge response data and to provide users a convenient means of executing the embedded load rating, reliability, and risk analyses. The final tool is termed the Decision Making Toolchest, or DMT.

The interrelated flow of the three thrusts and their associated tasks are presented in Figure 2. Appendix A provides an overview of the project deliverables established at the outset of the project. The deliverables encompass the technical outcomes associated with the three thrust areas in addition to commercialization and reporting requirements of the project established by the United States Department of Transportation (USDOT).

Report Outline

This final project report is organized as follows. Section 2 presents the CRS&SI data sources considered in this project. Specifically, it focuses on introducing wireless monitoring systems for bridge structural health monitoring and WILD detectors for measurement of train loads. Section 3 introduces the Harahan Bridge which is a steel truss bridge crossing the Mississippi in Memphis. The design of the wireless monitoring is presented in detail. In a similar fashion, Section 4 introduces the short-span steel girder Parkin Bridge. Section 5 introduces the reliability analyses performed on the Harahan Bridge using the data collected from eyebar truss elements. The reliability index, β, is used as a scalar health metric that assesses the probability

of component failure using measurement data collected. The framework is sufficiently general that lower limit states can be used in lieu of the failure limit state. Section 6 is devoted to load rating of the Parkin Bridge using the strain response of the bridge recorded by the wireless monitoring system. Section 7 extends the project analytical framework to consider the resiliency of the sub-network while Section 8 is devoted to the development of the risk monitoring framework along with a detailed return on investment analysis. Section 9 presents the DMT platform as the primary user interface for the technologies developed. Finally, Section 10 details the team effort in developing a commercialization plan for the project technologies. Appendix A provides a detailed review of the achievement of the project deliverables and Appendix B summarizes the invited talks and papers produced under the funded effort.

SECTION 2
CRS&SI DATA SOURCES

A primary objective of the project is the utilization of commercial remote sensing and spatial information (CRS&SI) technologies to improve the asset management of railroad bridges. The primary remote sensing technology used in this study were wireless sensors deployed on railroad bridges. Wireless sensor networks represent a lower cost alternative to traditional wired monitoring systems. In existence since the mid-1990's, wireless monitoring systems are growing in popularity (Kane *et al.* 2014). Already, numerous highway bridge structures now have permanent wireless monitoring systems installed on them (Peckens *et al.* 2014). In this study, wireless sensors were used to monitor bridge environments (*e.g.,* temperature), bridge vibrations (*e.g.,* accelerations) and component strain responses. A second CRS&SI data source utilized were wheel impact load detectors (WILD). Railroads typically employ WILD stations throughout their networks to determine the static weight of a train and to ensure cars do not overload the railroads' infrastructure. WILD stations typically consist of transducers installed on the rail to assess the axle weights of the locomotives and train cars that ride past them. WILD technologies are typically accurate to ± 2% and provide a measure of the axle static weights for the railroad. In this study, WILD were an important tool for measuring the loads imposed on the bridges monitored thereby providing a quantitative measure of bridge demands.

Wireless Sensors

The *Narada* wireless sensing node (Swartz, et. al, 2005) was used as the wireless sensor platform for this project. The *Narada* sensing node has been successfully deployed as part of permanent wireless monitoring systems on other operational bridges including the Telegraph Road Bridge in Monroe, MI (O'Connor *et al.* 2017) and the New Carquinez Bridge in Vallejo, CA (Zhang *et al.* 2017). *Narada* is a wireless sensor that was developed specifically for structural health monitoring applications. *Narada* (Figure 3) has a very high 16-bit ADC resolution which makes

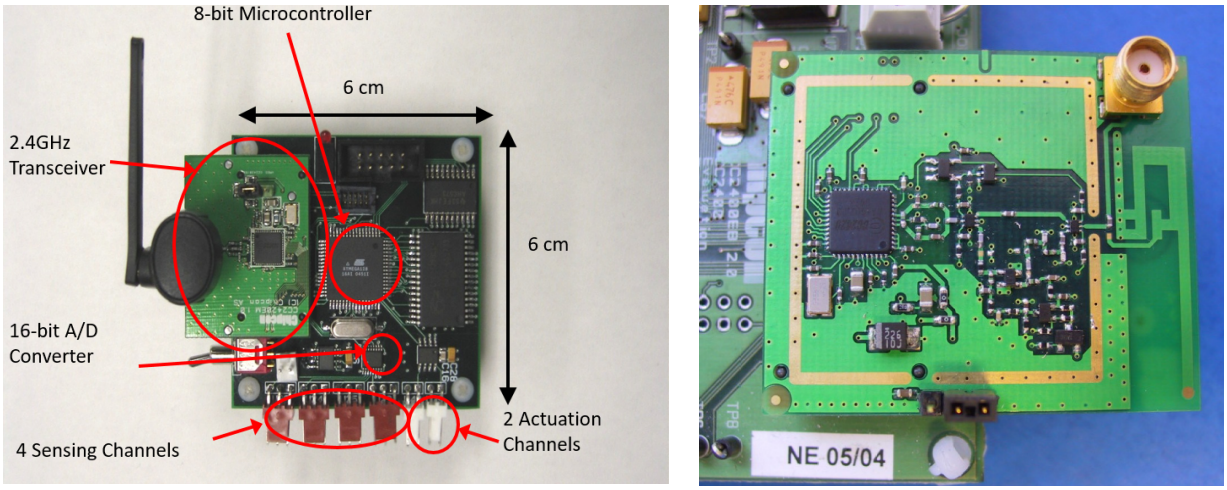

(a) (b)

Figure 3. (a) *Narada* wireless sensor; and (b) power amplified IEEE802.15.14 radio

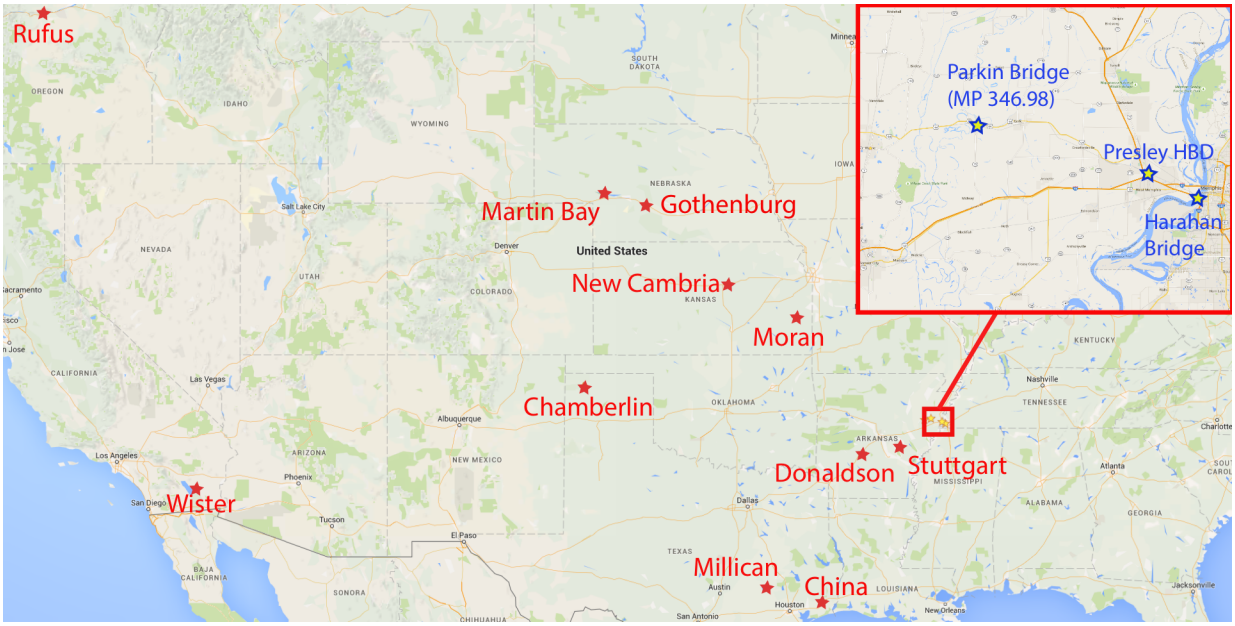

Figure 4. WILD stations in the Union Pacific (UP) network (red stars indicate WILD stations while blue stars indicate bridges and hot-box detectors (HBD))

it an excellent candidate for bridge monitoring and has four sensing channels which can accommodate different combinations of sensors. A wide variety of different sensor transducers have been interfaced including strain gages, accelerometers, thermistors, linear displacement transducers, among many more. *Narada* utilizes an IEEE802.15.4 radio that offers it interoperability with other wireless sensors operating on the same 2.4 GHz IEEE802.15.4 channels. Finally, the device has an 8-bit microcontroller with 128 kB of on-chip Flash memory (for program storage). An additional 258 kB of external static random access memory is included on *Narada* for data storage.

Wheel Impact Load Detectors

WILD stations are installed directly to the track and are designed to measure the vertical axle loads imposed by train cars and locomotives on the track. The station consists of strain gages welded to the track with dummy gages also installed for thermal compensation. A data acquisition is used to collect strain data and to convert the data to a vertical load measurement. The intended use of WILD is to detect excessive vertical loads and wheels with excessive wear in a rail network. UP has a total of 17 WILD stations installed across their network; Figure 4 presents a map of a select set of WILD stations. The WILD stations provide the following information for each train: 1) AAR car type; 2) number of axles per locomotive/car; 3) average and peak axle vertical forces; 4) average and peak axle lateral forces; 5) train speed; 6) train direction; 7) train identifier; 8) axle distances.

In this study, the team acquired complete sets of WILD data from UP. Unfortunately, the Memphis subjunction (along which are the two study bridges) did not have a WILD station but instead had a hot-box detector (HBD) which provides a cruder set of data including: 1) total

number of axles of a train; 2) total number of cars; 3) total number of locomotives; 4) train direction; 5) train speed; 6) day and time of passing; and 7) train identifier. Along the Memphis subjunction is a HBD at Presley (as shown in Figure 4) which is between the Parkin and Harahan Bridges. Hence, the analysis performed consisted of using the HBD to identify the train traffic on the Memphis subjunction and to use train identifiers to find the same train at a WILD station anywhere in the UP network. This approach allowed the train loads to be studied and modeled using the WILD data. Appendix C has a complete review of the analysis performed.

SECTION 3
HARAHAN BRIDGE MONITORING SYSTEM

Introduction

The Harahan Bridge, pictured in Figure 5(a), spans the Mississippi River near Memphis, Tennessee and is part of the Memphis subjunction of the UP network. The Harahan Bridge finished construction in 1916 and is a five-span cantilever truss bridge. The carbon and alloy steel structure supports two rail lines carrying trains 4913 feet (1497.5 m) across the Mississippi River just west of Memphis. The main bridge (five spans) stretches 2550 feet (777.2 m) but to the west of the five main spans is a tower girder and viaduct that continues 2363 feet (720.2 m). The majority of the cross-section (Figure 5(b)) carries railroad traffic but one of the two side roadways (that are not owned by UP) serves as a pedestrian walkway. As seen in Figure 5(b), the cross-section of the bridge consists of four smaller floor stringers supporting the lightly/unused roadways, two truss chords located at the bottom of each truss, and four interior floor stringers. The Harahan bridge stands to benefit greatly from system monitoring because of its exposure to multiple hazards. It is located in the New Madrid fault zone, may experience scour or flooding events from the Mississippi River, and is susceptible to barge collisions. Weathering and loading can also contribute to deterioration of individual structural members including corrosion and fatigue; these effects are deemed to be an aging "hazard". Thus, both global and local sensing approaches are needed.

Finite Element (FE) Modeling

Prior to the design of the wireless monitoring system, an FE model of the Harahan Bridge (Figure 6(a)) was constructed using CSiBridge which is an add-on to the software package SAP2000 (Computers and Structures Inc.). Creating an FE model of the Harahan Bridge played an important role in selecting and validating a sensor instrumentation plan. Once the initial material properties, section properties, boundary conditions, connection properties, and member geometries were specified, the model was carefully calibrated. The original engineering reports that accompany the design drawings of the Harahan Bridge include notes regarding prescribed dead and live loads in addition to the loads that are induced in many of the members due to these prescribed loadings. The accuracy of the FE model was verified by applying the dead loads that are prescribed in the engineering report (including self-weight) and comparing the resultant loads in each member of the FE model to the loads that are recorded in the engineering report for each respective member. The FE model results (which will be more precise than the engineering report) were within 15% of the engineering report values which is reasonable considering there are several potential sources of error including inconsistent descriptions of dead loads in the report and simplifications in the distribution of the bridge self-weight made by the engineer during the original design in 1916. A key benefit of using CSiBridge is that it is capable of capturing structural responses due to simulated dynamic moving loads. Hence, moving unsprung train loads were simulated on the FE model using actual axle loads and axle spacing values that

(a) (b)

Figure 5. (a) View of Harahan Bridge looking south from east bank; and (b) cross-section of Harahan Bridge showing trusses and the floor system (including floor beams and stringers)

are collected in a WILD database maintained by the railroad (see Appendix C for a detailed analysis of the train types and loads extracted from the WILD data).

One of the main benefits of constructing the FE model of the Harahan Bridge using CSiBridge is that the program can simulate dynamic train loads on the bridge. Using this capability of CSiBridge, the team was able to capture more realistic dynamic structural responses of the bridge members by actual axle loads and axle spacing from WILD data. Dynamic moving train load simulations were used to validate a sensor instrumentation plan using modal, strain, and displacement analyses in order to confirm that the members identified by the bridge owner were in fact critical members that should be monitored. Figure 6(b) serves to help explain the moving load case that was used to inform the instrumentation plan and to perform model validation. As seen in Figure 6(b), once the leading train locomotives have exited the bridge, the bridge is fully covered with freight. After 100 seconds, the train is covering the entire length of the bridge, and after just 50 seconds the locomotives are far enough along the bridge that the trends in member strain stabilize. For this reason, the analyses that required the moving train load considered data for the first 55 seconds after the train enters the bridge.

In consultation with the bridge owner (and verified using the FE model), the eyebar elements in the Harahan Bridge truss system are of great interest. The Harahan Bridge has 67 (28 top chord, 4 bottom chord, 31 diagonal truss, and 4 vertical truss) such elements which each consist of six parallel eyebar plates (in most cases) that are generally long chord elements designed to carry high axial loads in tension. Eyebars are prone to fatigue damage over time (as was observed in the recent case of the San Francisco-Oakland Bay Bridge (Gostautas and Tamutus 2015; Reid 2010)). In addition, the load distribution across the parallel eyebars can change due to changes in boundary conditions of the pins, which can lead to greater axial loads and accelerated accumulation of fatigue damage. Due to these concerns, the monitoring system selected eyebar chords at section US0-LS0 (on the north and south truss systems) as the primary components to monitor with the monitoring system. To acquire insight into the train locomotive and car axle loads, the team also elected to monitor the lower LC5-UC5 chord, which is a vertical hanger element adjacent to the eyebar chords in the same truss panel. This element is a built-up box section with a length of 27 feet 4 ¼ inches (8.3 m) and a gross cross-sectional area of 39 in^2 (251.6 cm^2). Since the vertical truss chord only has longitudinal chords framing into the chord

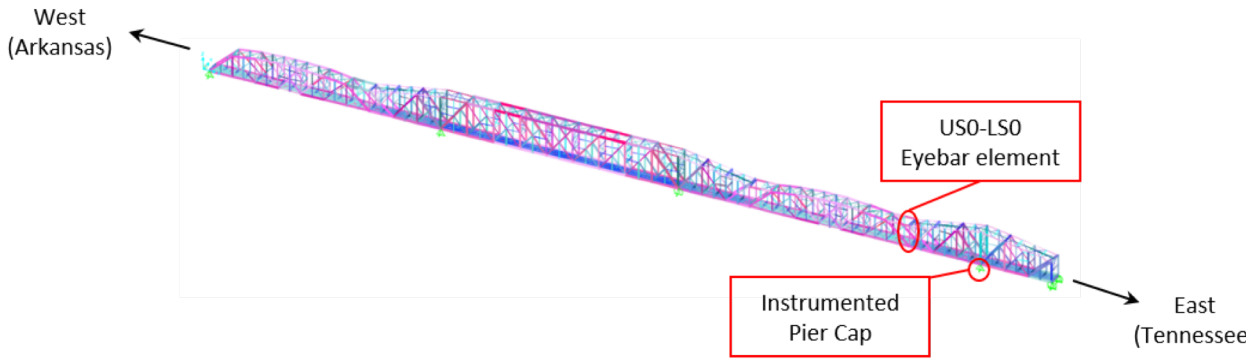

(a)

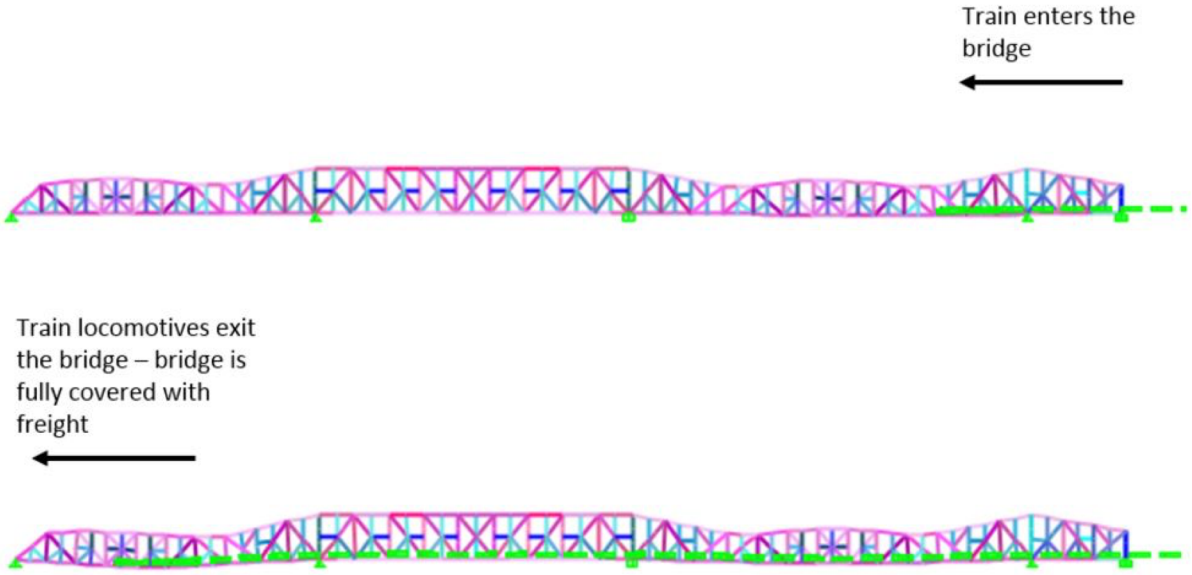

(b)

Figure 6. (a) FE model of Harahan Bridge designed in CSiBridge; (b) displacement response of the bridge to a moving train load (displacement is not to scale)

lower node, in theory it should carry the entirety of the train axle loads. Thus, it was hypothesized that monitoring axial strain in LC5-UC5 would give a crude measure of train axle loads.

Monitoring System Architecture

The wireless monitoring system was designed to be a permanent fixture on the bridge collecting data based on trigger events such as train loads and lateral motions. The monitoring system was interfaced to the Internet where data is pushed to an SQL data server for storage and data processing. When an approaching train triggers the system, the base station sends a command for

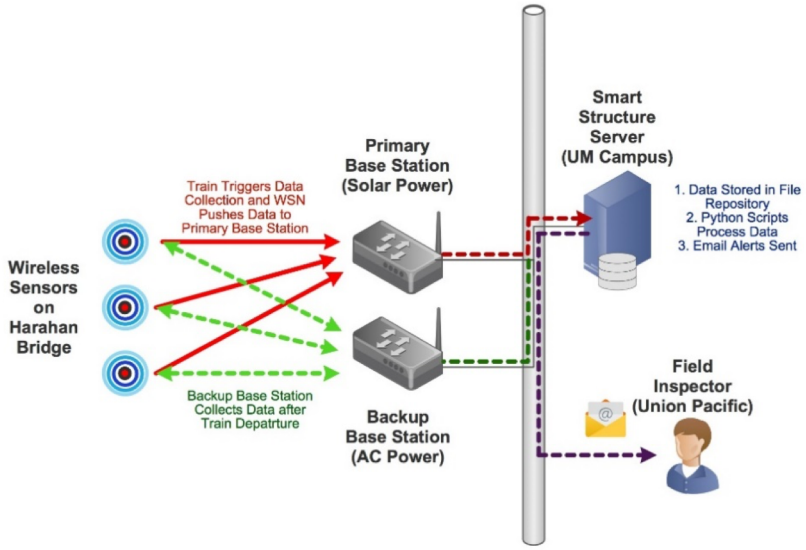

Figure 7. Monitoring framework and alert systems

every *Narada* wireless sensor to wake up from a low-power mode and begin collecting data. After data is collected at each wireless sensor node, the data is transferred wirelessly to the base station (a second base station was installed for redundancy which will be discussed in the instrumentation section). In addition, geophones were installed with the system base stations and continuously collect data (*i.e.,* never enter sleep mode) to capture any unexpected extreme loading events (*i.e*., barge collisions, earthquakes) that occur in real-time. The data stored in the base station is transferred via the Internet to a dedicated data server at the University of Michigan. This server then automatically performs the following tasks: 1) stores the data in an organized SQL database; 2) processes the data (*e.g.,* fatigue analysis, load distribution, reliability analysis); and 3) sends email alerts to interested parties (*i.e.,* UP field inspectors and managers) when there is a collision or unexpected structural response. The functionality of this framework is summarized in Figure 7.

Selection of Sensor Types and Locations

The sensor selections are provided in Table 1 and the final monitoring system layout is shown in Figure 8. Note that a single sensor can serve multiple functionalities. The system contains 36 wireless measurement channels and 14 *Narada* wireless sensing nodes. There are also two wired channels for the geophones located inside the two base stations. Each wireless sensor node (Figure 9(a)) consists of two waterproof plastic boxes that house a rechargeable battery (powered by a 10W solar panel), solar charger controller, *Narada*, and additional conditioning circuits. The monitoring framework focused on the critical elements on the east portion of the bridge. However, this same sensing methodology could be expanded to other critical elements on the remainder of the bridge. The remainder of this section focuses on the specific sensors that are installed and a description of the elements they monitor.

Table 1. Monitoring system equipment summary (Harahan Bridge)

Equipment Type	Model	Type of Measurement	Quantity
Weldable strain gages (1 channel each)	Hitec HBWF-35-125-6-10GP-TR	Local Strain	12
Uniaxial accelerometers (1 channel each)	Silicon Design 2012-002	Local Acceleration	12
Triaxial accelerometers (3 channels each)	Silicon Design 2422-005	Global Acceleration	4
Geophone (wired to base station)	GeoSpace Geo-11D 4.5-380 VT	Global Velocity (trigger)	2
Wireless channels {wired channels}	-	-	36, {2}
Narada wireless sensor nodes	-	-	14

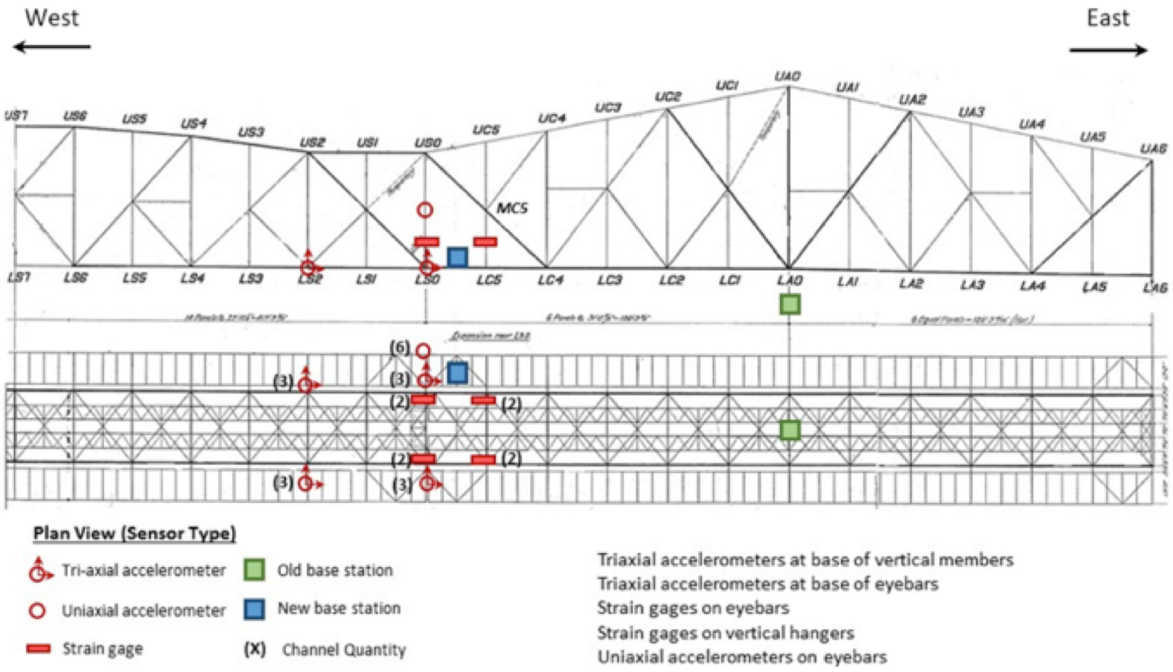

Figure 8. Harahan Bridge instrumentation plan

Global Modal Properties and Lateral Loads: there are four triaxial accelerometers magnetically mounted on the floor beams near the outer truss chords at cross-sections S2 and S0 (Figure 8). These accelerometers were oriented with the x-axis longitudinal to the bridge, y-axis transverse to the bridge, and z-axis vertical. The combination of the four triaxial accelerometers contributes to the understanding of the bridge global modal properties. Modal properties extracted from these sensors provided a robust parameter with which the FE model of the bridge was calibrated. It should be noted that they can also act as indicators of global changes to the bridge structure (*i.e.*, changes induced by major damage such as damage originating from an earthquake). They also contribute to the lateral load monitoring and quantify the effects of wind as well as potential earthquakes or barge collisions acting on the bridge.

(a) (b)

Figure 9. (a) Typical *Narada* wireless sensor node containing battery, solar controller, *Narada,* and conditioning circuits; (b) primary base station on Harahan Bridge including (from left to right) cell antenna, server enclosure, camera, ZigBee antenna, and solar panel

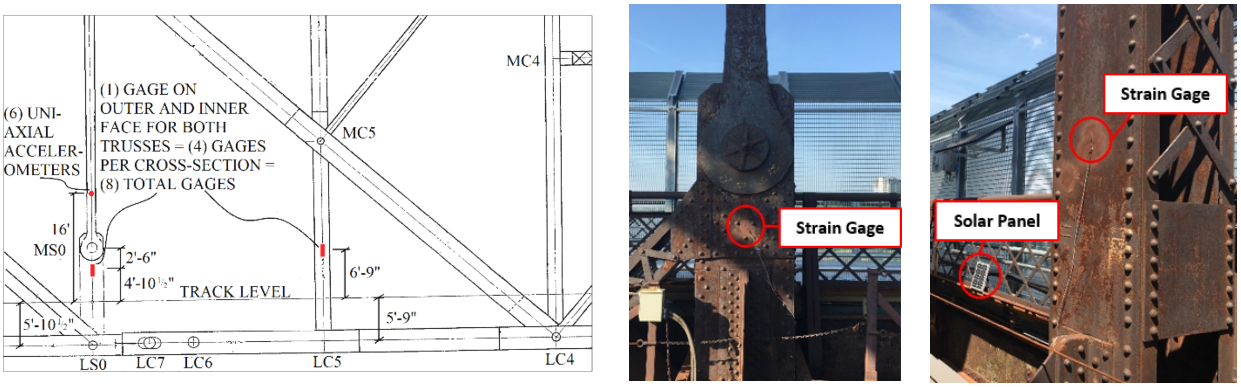

(a) (b) (c)

Figure 10. (a) Schematic of strain gage locations; (b) installed strain gages at US0-LS0 and (c) MC5-LC5

Truss Component Vertical Loads: Strain gages (Figure 10(a)) were instrumented on the bridge to determine the loads imposed on bridge (*e.g.,* train locomotive axle loads and total train global load) and the behavior of key truss elements (*e.g.,* pure axial eyebars). Train information taken from WILD data were correlated to strain readings (matching same train to same data set) at multiple members on the bridge, which provided a rough measure of train axle loads. This set of load data, along with strain data from the Harahan Bridge will serve as the basis for assessing component capacity versus demand, which may change due to component deterioration or changes in component boundary conditions. Weldable strain gages with temperature compensation were installed on the bottom sections of members LS0 and LC5. For each cross-section (US0-LS0 and MC5-LC5) four gages were installed; one on the inner portion (facing the track) and one on the outer portion (facing out from the bridge) of each member on both sides of

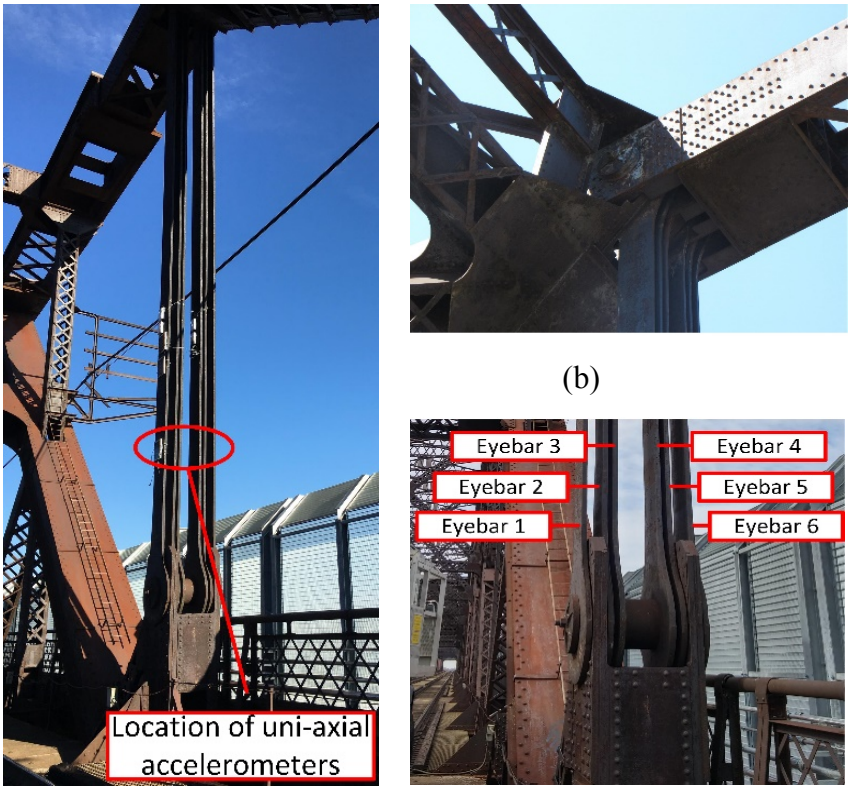

Figure 11. Member north truss LS0-US0: (a) built-up section on bottom portion and 6 eyebars on upper portion; (b) close-up on top and bottom of MS0-US0; and (c) designation of individual eyebars

the bridge (*i.e.,* south and north truss). Both sections were built up sections consisting of steel box tubes. At member US0-LS0 the strain gages were welded on the built-up section below the bottom eyebar pin. Two examples of the installed gages are shown in Figure 10(b) and 10(c). The gages on the built-up section use strain to infer the aggregate effect of the live load on the member. For example, gages are installed on the outer and inner faces of the members in order to detect out-of-plane bending of the members. Having both trusses (north and south side of the bridge) instrumented allows the effects of the bridge torsion and asymmetric loading to be examined. Member US0-LS0 carries only a portion of the individual axle loads locally (due to an angled chord taking load at node LS0); however, it has a large contribution to carrying the entire (global) load of the whole train as it crosses the bridge. As a result, for each train crossing the strain reveals both a large magnitude strain cycle associated with the train weight and much smaller cycles superimposed which correspond to local axle loads carried by the member.

Eyebar Relative Tautness: There are six eyebars on each truss side (12 total) that constitute truss chord US0-LS0. Each of the eyebars on the north truss were instrumented with a uniaxial accelerometer oriented to monitor out-of-plane vibration 16 feet (4.88 m) above the track level (Figure 11). The fundamental frequency corresponding to the axial load being carried by each eyebar relative to the other eyebars can be calculated from these frequencies. Relative tautness is a primary area of maintenance concern noted by the bridge owner and is checked manually by

bridge inspectors regularly. Standard practice for the bridge owner is to inspect these elements by physically shaking each eyebar and counting the number of vibration cycles relative to the other eyebar links to crudely assess relative tautness. The monitoring strategy proposed in this effort can potentially replace this time consuming manual approach

Base Stations

The base station is used to control the wireless sensor network (including data collection triggering), receive sensor measurements, and transmit the data to the University of Michigan server via a cellular link. The base station is powered by a 165W solar panel and consists of one PC-104 single board computer, one solar controller, one 12 V rechargeable battery, one 12V/5V DC converter, one webcam, one geophone, one Sprint LTE USB modem, and one CC2420 RB transceiver (operating on ZigBee 2.4 GHz frequency) that is connected to an external high-gain omni-directional antenna. The metal base station box and external components were mounted to a pedestrian walkway fence located on the north side of the bridge (Figure 9(b)).

The geophone within the base station enclosure was set to measure vertical and horizontal velocity data continuously; this geophone was intended to be a trigger for the system. When a train approaches the bridge it causes the geophone response to exceed a threshold of 1.24 in/s (3.15 cm/s). This triggers the server to send a wake-up command to the wireless *Narada* nodes, giving the nodes sufficient time to power up and begin recording data. This "sleep- mode/wake-up mode" protocol allowed the sensor nodes to be powered by much smaller solar panels (which is vital for deployment on a structure), remain active through the night or overcast weather, and for them to only record data during loading events. The threshold was set after empirically assessing typical velocities for different train events. The final threshold was selected to ensure that as a train approaches the bridge, the threshold is exceeded well before the train reaches the location of the sensors. As a result, the wireless sensors have enough time to wake up and begin taking measurements. Additionally, the threshold was found to be not so low that it limits the number on non-loading vibrations that cause false triggers. Although a trigger is a vital component of the system, the monitoring system can also be triggered manually at any time via an Internet connection to the base station server which has a cellular modem (Sprint LTE USB modem). Unlike the wireless sensing nodes, the two wired geophones continuously collect data and never enter "sleep-mode" so that they can trigger the system to "wake-up" and capture any extreme loading events such as seismic ground motion or lateral vehicle collisions in real-time.

A second base station was installed on the pier cap just to the east of the primary base station where a 110V AC power outlet is available. It was found that this base station did not communicate as efficiently with the sensor nodes due to its distance from the instrumented section of the bridge and the fact that a 9-inch (22.9 cm) thick concrete fire blocking slab (not anticipated during initial instrumentation design) obstructs the line of sight between the sensors and base station. However, because of its reliable power supply it continues to serve as an access point in the event of overcast, low solar power scenarios in which the primary base station may be inaccessible.

SECTION 4
PARKIN BRIDGE MONITORING SYSTEM

Introduction

The Parkin Bridge (MP346.98) is a short-span railroad bridge located in Parkin, Arkansas. The bridge was constructed in 1935 and has undergone several renovations through its history. The bridge carries one railroad track between Bald Knob, Arkansas and Memphis, Tennessee and is owned and operated by UP. The entire bridge spans 56 feet (17m) with 3 spans. The two wing spans are built as thick reinforced concrete slabs while the mid-span consists of four steel girders. The mid-span is 24 ft (7.32 m) supported by reinforced concrete piers with Tyronza Street running underneath (with a clearance of 9.75 ft (2.97 m)). Only the mid-span is of the interest in this project as it experiences the largest structural responses and is more vulnerable to over-height truck collisions that can occur from the road beneath. In the following sections, the Parkin Bridge refers to the mid-span alone for naming simplicity. Overall, this bridge is simple to monitor and model. An image of the bridge is shown in Figure 12. The motivation for monitoring the Parkin Bridge in this study was to provide bridge response data for estimation of train speeds, static axle loads, dynamic load factors, and to count the number of cars. These parameters will serve as inputs for performing a data-driven load rating for the bridge as will be presented in a subsequent section. UP also expressed a strong interest in monitoring the bridge for lateral collisions from large trucks.

The potential hazards that the Parkin Bridge is exposed to include: excessive train loads, aging (*i.e.,* fatigue, corrosion), seismic loads, and vehicular collision (*i.e.,* traffic colliding with the over-pass bridge girders). Among those hazards, excessive train loads and collision were the two primary hazards investigated in this project. As the primary load the bridge carries, train loads are the critical factor related to the structural capacity, serviceability and safety. Meanwhile, with the mid-span being only 9.75 ft (2.97 m) above the surface of Tyronza Road, the bridge could experience a collision from an over-height truck passing underneath the bridge. This type of collision can cause permeant deformation to the bridge which, unreported and unknown, may threatens the safety of train traffic above.

Figure 12. View of the Parkin Bridge (Parkin, AR) with Tyronza Street running beneath

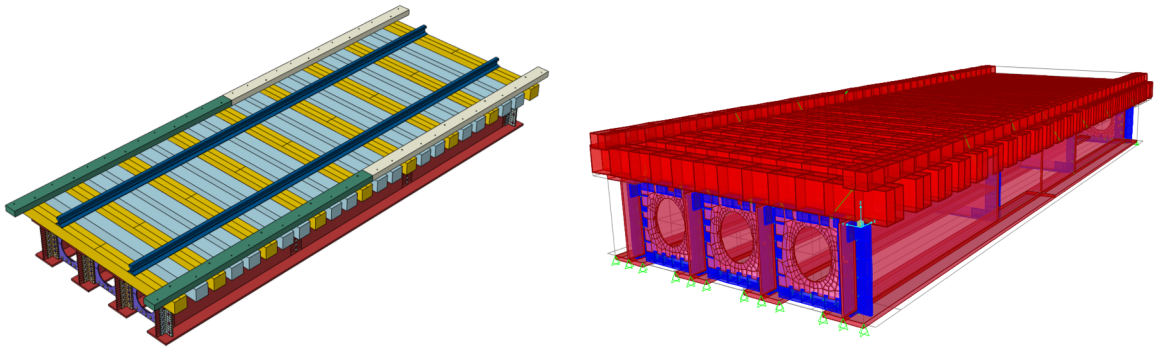

(a) (b)

Figure 13. (a) Abaqus and (b) CSiBridge model of the Parkin Bridge

Finite Element Modeling

The team first conducted a detailed finite element model analysis of the Parkin Bridge. The FE modeling was intended to inform understanding of the bridge behavior under train loads. In addition, FE modeling served as a valuable tool for development of the bridge monitoring system design. Over the course of the project, two finite element models were developed of the Parkin Bridge: an elaborate high-resolution model built in Abaqus Unified Finite Element Analysis (Dassault Systèmes) and a coarser model built in CSiBridge (the same platform used for the Harahan Bridge FE analyses). The high-resolution model was used for structural analysis while the low-resolution model was mainly responsible for the generation of a geometric model that could be used to define the bridge geometries in the project database management systems (see Section 9).

The high-resolution Abaqus model included both the superstructure and the railroad system (*e.g.,* timber ties, track). The physical connection between the different bridge and track components were established in detail which improved the accuracy of the simulation results but at the cost of higher computational costs. Almost all components are built using solid objects while the connection among timber ties are modeled using a tie connection. The Abaqus model is presented in Figure 13a. On the basis of this model, several load and analysis cases were simulated. The low-resolution model, shown in Figure 13b, utilized shell elements for the steel components, solid objects for the timber components, and simplified all connection among components as tie connections. This model has fewer elements compared to the high-resolution Abaqus model which rendered it better suited for defining the bridge geometries in the project database system. In this section, the high-resolution Abaqus model is used to describe bridge behavior.

First, a modal analysis of the bridge was performed in Abaqus using its native Lanczos solver. The intent of performing this analysis was to extract modal parameters including the bridge natural frequencies and mode shapes. Based on that analysis, the natural frequency for the first vertical bending mode was found to be around 50 Hz which is much higher than would be encountered in longer span bridges. The mode shape corresponding to the first mode is shown in Figure 14. Hand calculation of modal frequency based on the mid-span length and cross section flexural rigidities yield similar results. The modal analysis performed was critical for informing

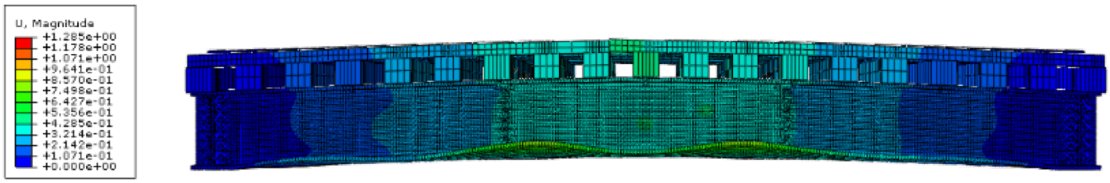

Figure 14. First vertical bending mode shape of the Parkin bridge

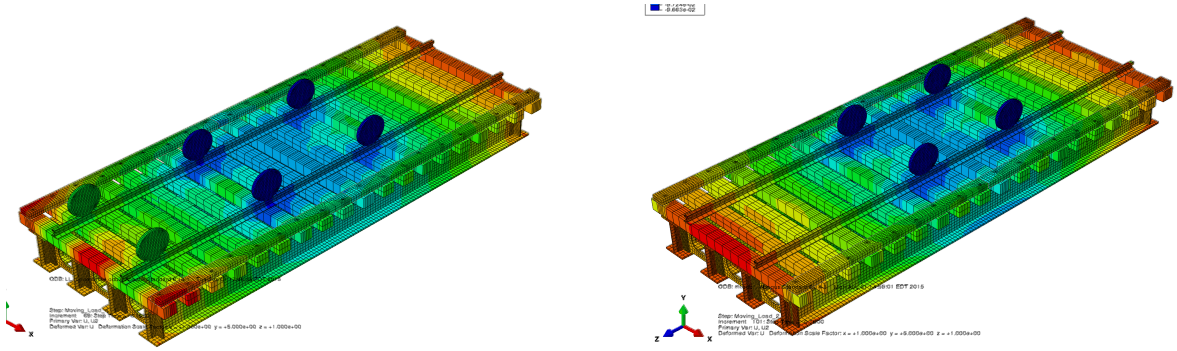

Figure 15. Live load (train wheel loads) simulation: locomotive (left) and freight car (right)

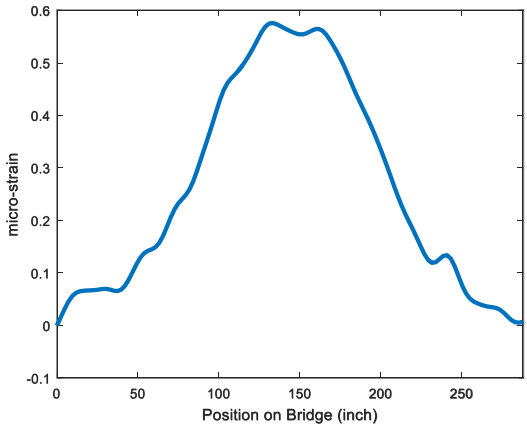

Figure 16. Influence line of mid-span strain on the lower flange of girder 2 as extracted from the Abaqus model for a 1-kip bogie load

the sampling rates of the monitoring system and for identifying locations for accelerometers and strain gages.

To explore the response of the bridge to train loads, a moving load analysis of the Parkin Bridge was performed using representative locomotive and freight car train loads. The simulated response in Abaqus is shown in Figure 15. From the WILD data that UP provided, the vertical wheel loads of a locomotive are much higher than that of a freight car. In view of this fact, the live load to dead load ratio in a locomotive case is around 14, larger than that for the case of a freight car which is around 10. The simulated response of the Parkin Bridge to the modeled train loads was explored for proposed sensor positions. These simulated responses were vital to determining the monitoring system requirements (*e.g.*, measurement range and transducer sensitivity). The responses were also a basis for the updating of the FE model. The influence

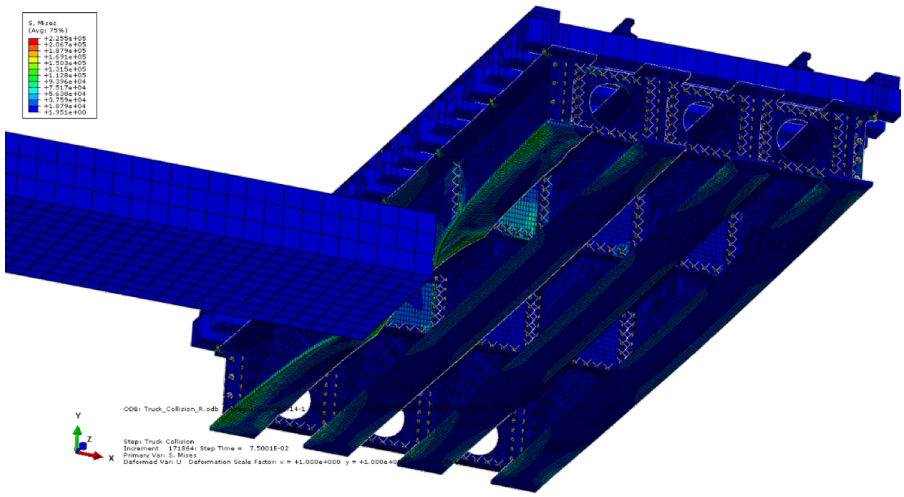

Figure 17. Collision of a 37 kip truck with the Parkin Bridge in the Abaqus model

line from a unit (1 kip) bogie was also extracted from the Abaqus model and will be further used for the estimation of speed and car weights from the measured strain response. The influence line for the bridge strain response at the mid-span lower flange is presented in Figure 16.

The Parkin Bridge is vulnerable to the possibility of a vehicular collision by an over-height truck traveling beneath the mid-span. The scenario of a truck collision was simulated in Abaqus. The truck was simulated as moving at a top speed of 30 mph (48.3 km/hr) with its top roof 10 in (25.4 cm) higher than the bottom flange of the bridge girder. The truck roof was simulated to strike the bridge at the mid-span from one side of the bridge as shown in Figure 17. The truck was modeled as a solid cuboid volume with a weight of 37,000 lb (16,783 kg). The response of the bridge was assessed including maximum deflection, residual deflection, and changes in the modal properties.

Monitoring System Design

Based on the needs of the project and the hazards identified (*e.g.,* aging and vehicular collisions), a permanent monitoring system architecture was designed. The monitoring system aimed to achieve the following functions: 1) extraction of span modal properties; 2) monitoring and identification of train loads; 3) over-height vehicular collision detection; and 4) structural health condition diagnosis. The sensor layout is shown in Figure 18. Table 2 summarizes the number of each sensor type used for the Parkin Bridge instrumentation. The entire sensing system can be divided into two subsystems: 1) train load monitoring subsystem and 2) vehicular collision detection subsystem.

Train Load Monitoring Subsystem

Moving train loads is the principle load type that the Parkin Bridges carries; it is also the load of greatest interest in this project. As will be presented in subsequent sections, a primary objective of the project was to perform a data-driven load rating analysis of the Parkin Bridge using response data collected from the bridge. A train load monitoring system was then designed with the purpose of monitoring the responses of the Parkin Bridge to moving train loads including accelerations and bending strains of the girders. The collected measurements would be used to:

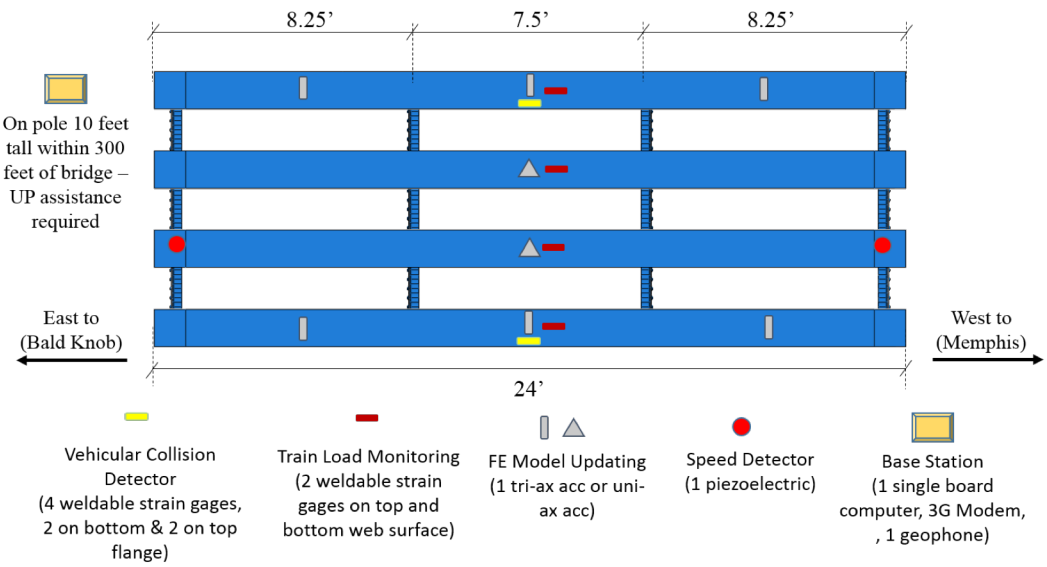

Figure 18. Parkin Bridge instrumentation plan

Table 2. Monitoring system equipment summary (Parkin Bridge)

Equipment Type	Model	Type of Measurement	Quantity
Weldable strain gages (1 channel each)	Hitec HBWF-35-125-6-10GP-TR	Local Strain	18
Uniaxial accelerometers (1 channel each)	Silicon Design 2012-002	Global Vertical Acceleration	6
Triaxial accelerometers (2 channels each)	Silicon Design 2422-005	Global Vert & Trans Accel	2
Piezoelectric Elements (1 channel each)	Piezosystems Piezoelectric Wafers	Vertical Tactile Force	2
Wireless channels {wired channels}	-	-	30, {0}
Narada wireless sensor nodes	-	-	16

1) conduct modal analyses of the bridge for validation of the finite element model of the bridge; 2) identify the speed and magnitude of moving train loads and induced dynamic load factor as inputs to load rating analysis.

First, two piezoelectric pads were installed at the two ends of the mid-span in the gap between the girder and the timber tie, as shown in Figure 19. These piezoelectrics were used to record the instance when the train enters and leaves the bridge so as to estimate the speed and relative position of each car of the train on the bridge. Second, six uniaxial accelerometers were installed to measure the vertical acceleration of the two outer girders. In addition, two triaxial accelerometers were installed at mid-span on the two inner girders to measure vertical and transverse accelerations. All accelerometers were fixed on the bottom flanges of the girders. The data collected by these accelerometers were used for modal analysis including extraction of the natural frequencies and mode shapes of the bridge. Finally, strain gauges were welded to the

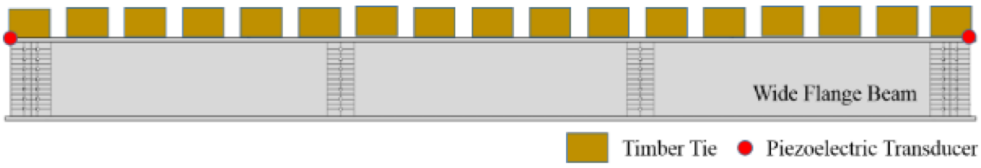

Figure 19. Deployment of piezo-electrics to detect train car entry and exit from the mid-span

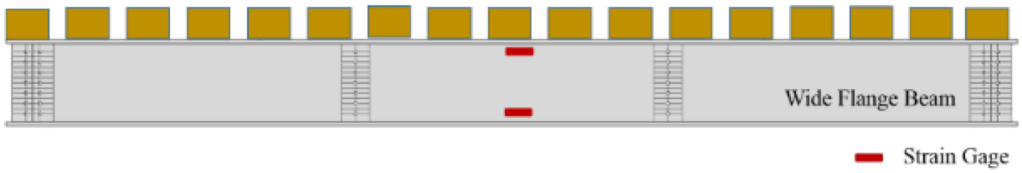

Figure 20. Strain gauge for the train load monitoring subsystem

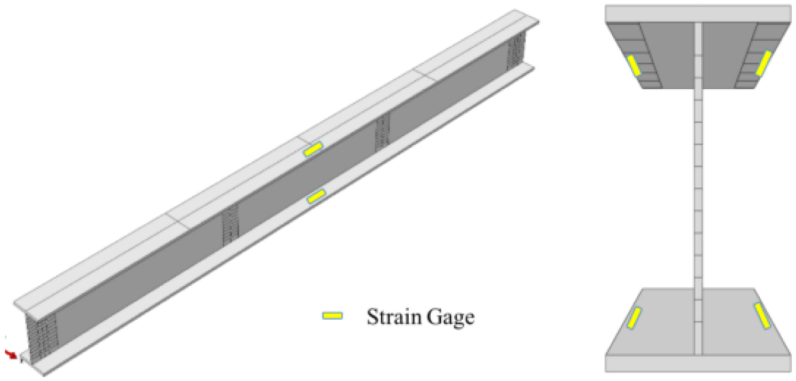

Figure 21. Strain gauge for train load monitoring system

lower and upper web surfaces at the mid-span position of each girder, as shown in Figure 20. The top and the bottom girder strains were used to assess the flexural moment induced at the center of each span; this induced moment was correlated to the weight of the imposed axle load from each train car. The measured strains were also used for the estimation of speed and dynamic load factor.

Vehicular Collision Monitoring Subsystem

In order to detect vehicular collision damage, two weldable strain gauges were installed on the bottom and top flanges of the two outer girders as shown in Figure 21. On each flange, two strain gauges were put in symmetry about the girder web. This subsystem is able to record both the bending and twist behavior caused by lateral vehicular collision should a collision occur. In addition, the two triaxial accelerometers deployed for each intermediate girder can also detect the transversal acceleration caused by lateral collision.

System Installation

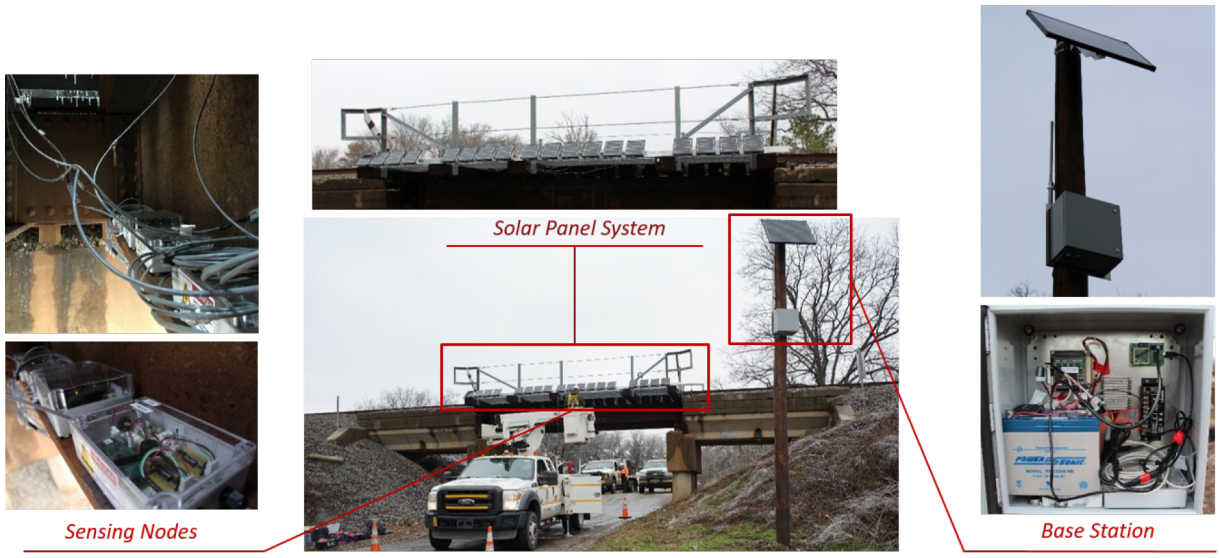

Figure 22. Installation of the Parkin Bridge monitoring system

The instrumented monitoring system was installed at the project outset as presented in Figure 22. Apart from the sensors described above, the sensors were attached to a total of 16 *Narada* nodes for data collection. Each *Narada* node (similar to the Harahan Bridge) was placed in a water tight enclosure with one 12V lead acid battery and charge controller. In addition, one 18V solar panel was connected to each *Narada* node and mounted on the southern girder at an angle to maximize sun exposure. UP installed a wood utility pole in close proximity (about 300 ft (91.4 m) away) to the Parkin Bridge upon which a base station capable of both communication with the Narada nodes (via IEEE802.15.4 telemetry) and with a cellular network (using a cellular modem) was mounted (see Figure 22). The base station contained a single board computer (PC-104) used to: 1) send operational commands to wireless sensing nodes (*e.g.*, start data collection), 2) receive sensor measurements from nodes, and 3) transmit data to an online database. Also included in the base station was a Morningstar 12V solar controller, one Sprint 3G USB modem, one 12V 40 Ah rechargeable sealed lead acid (SLA) battery, one CC2420 RF transceiver (IEEE802.15.4) and one 12V/5V DC converter. The base station was powered by a 100W solar panel also installed to the utility pole.

The monitoring system was designed to trigger based on train or truck collision events. One geophone in a vertical direction was installed in the base station enclosure. This geophone worked as a trigger to wake up the sensing system when there is an incoming train which induced ground vibrations experienced by the pole. When the vibration magnitude measured by the geophone exceeds an established threshold set by the team manually, the geophone sends a message to the PC-104 to start up the sensing system and collect data. An example of the vibration magnitude measured by the geophone is shown in Figure 23. Finally, an inexpensive web camera was installed next to the base station to capture videos of the measured train event. A sample image of a train is shown in Figure 24.

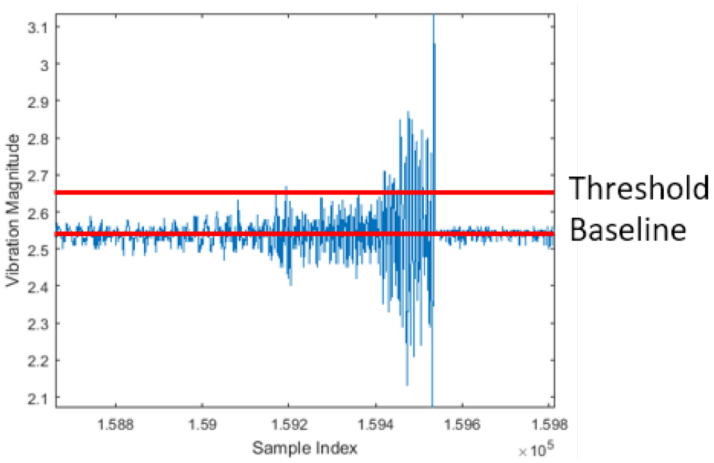

Figure 23. Vibration measured by the geophone with threshold set

Figure 24. Web cam snapshot captured by the installed camera

SECTION 5
RELIABILITY ANALYSIS OF HARAHAN BRIDGE

Introduction

The wireless monitoring system on the Harahan Bridge was designed to primarily monitor the behavior of the long and slender US0-LS0 eyebar elements. Parallel eyebar truss elements such as those on the Harahan Bridge are critical structural element that are designed to undergo high levels of tension. However, they can experience deterioration and damage over their operational lives including section loss due to corrosion, plate-pin locking also due to corrosion, and fatigue. For example, the former eastern span of the San Francisco-Oakland Bay Bridge constructed in 1936 was a double balanced cantilever truss bridge utilizing parallel eyebar elements as tensile elements. In 2009, one of the eyebar elements on the bridge experienced severe fatigue cracking requiring immediate closure of the bridge until an emergency repair could be carried out by the bridge owner (Gostautas and Tamutus 2015; Reid 2010).

In this section, a novel approach to long-term performance assessment of the Harahan Bridge eyebar elements is presented based on a reliability index framework that is driven by monitoring data. Use of a reliability framework is attractive for use in this setting. First, reliability methods are the basis for many of the design codes that govern railroad bridge design (*e.g.,* AREMA). Furthermore, reliability methods can quantify bridge conditions in probabilistic terms. This is very valuable when seeking to perform risk assessments which can be viewed as the combination of probabilities of events (*e.g*., failure) and the consequences of the event. Finally, the reliability framework is flexible and allows for a variety of limit states to be considered. Unlike the use of reliability in design (which largely looks at yield or ultimate limit states), in a structural health monitoring context the reliability framework can be extended to easily consider "lower" limit states that an owner may define such as exceedance of a behavioral threshold for a local component or for the global response of the bridge.

This section is divided into three major parts. First, the performance of the wireless monitoring system on the Harahan Bridge is summarized. The global behavior of the bridge and the local response of the instrumented truss elements are summarized. In particular, axial tensile loads are estimated for the vertical eyebar plates using transverse accelerations analyzed using modal analysis. Second, a fatigue assessment of the vertical eyebar elements is performed using the axial loads in the eyebar elements. This analysis aims to assess the damage accumulate by the elements during a one year period of observation (June 16, 2016 to June 15, 2017). Finally, the remainder of the section focuses on the reliability framework used to track the performance health of the eyebar elements.

Monitoring System Performance and Automated Data Analysis

Communication Reliability

The Harahan Bridge monitoring system has been in full operation and has triggered over 6,000 times since June 16, 2016. In this section, the behavior of the bridge was considered over a one year period of observation (June 16, 2016 to June 15, 2017). The data sets were collected from the strain gages and eyebar acceleration channels at 200 Hz for a period of 30 seconds per trigger

event and from the triaxial accelerometers (for global modal analysis) at 50 Hz for 60 seconds per trigger event. While the trains on the bridge will load the bridge for a much longer time period, the limited amount of memory on the *Narada* wireless sensor nodes limited the amount of data that could be buffered before communication was required. For some train events, the monitoring system might trigger more than once; this can be easily identified based on the time of the triggers.

In general, the wireless monitoring system on the Harahan Bridge performed well over the period of observation. The nodes and second base station were solar powered; as solar powered system elements, access to sun was critical. Unfortunately, the Harahan Bridge is a complex structure that casts many shadows that move with the movement of the sun. As a result, the solar panels installed with the wireless sensor nodes never had extended periods of direct exposure to sun. This resulted in less than ideal conditions for powering the wireless sensor nodes, especially during the winter when the sun is lower on the horizon and up for shorter periods of time. As a result, there were periods of days when the system remained off due to low levels of power. However, during warm weather and sunny days, the system remained on indefinitely and triggered when trains crossed the bridge.

When powered on, the data packet transmission success rate of the wireless monitoring was assessed during the monitoring period. Transmission success rate is defined as the number of data packets received by the base station divided by the number of packets sent by the *Narada* nodes. The transmission success rate ranged between 60 and 70% during the period of observation. The transmission rate was much higher (exceeding 90%) for the *Narada* nodes installed on the north side of the truss and in direct line of sight with the base station. The main challenge encountered during system operation was with the wireless sensor nodes installed on the south side of the bridge. During train events, most of the trains are so long that when the Narada nodes were ready to communicate their data, the train was still crossing the bridge. When tall train cars (e.g., those with double stacked containers) were present, the wireless sensor nodes on the south side essentially had a large metallic obstruction in their way. This condition resulted in many of the wireless sensor nodes on the south side of the bridge not being successful in communicating their data to the base station. The transmission success rate for these nodes were slightly below 50%. Nevertheless, a large number of recorded train events were recorded for most of the wireless sensor nodes installed over the course of one year. In addition, the objective of the monitoring system design was to capture segments of train load events for long-term tracking of structural behavior. Hence, the loss of some portions of the collected data was acceptable and would not affect the integrity of the fatigue and reliability analyses performed.

Global Modal Properties and Lateral Loads

The acceleration data from the four triaxial accelerometers at track level are analyzed in the frequency domain. The objective was to ascertain the modal properties of the bridge based on these acceleration measurements. As seen in Table 3, the fundamental frequencies of the various mode shapes (*e.g.*, transverse, vertical, torsional) are excited below 4 Hz, with component, or local, modes being excited at higher frequencies. Based on the FE analysis, the primary modal frequencies are 0.679 Hz (transverse), 0.878 Hz (transverse), 1.08 Hz (transverse), and 1.39 Hz (vertical), and 1.50 Hz (torsional). The modal frequencies experimentally obtained from long-term modal analysis of the measurement data lined up well with the results of the FE model, however modes 3 and 5 were not clearly evident in the experimental data. Additional calibration

Table 3. Simulated and measured Harahan Bridge modal frequencies

Mode #	Mode Type	Simulated Modal Freq. (Hz)	Measured Modal Freq. (Hz)	Percent Error (%)
1	Transverse	0.679	0.683	0.59
2	Transverse	0.878	0.917	4.3
3	Transverse	1.08	-	-
4	Vertical	1.39	1.23	13
5	Torsional	1.50	-	-

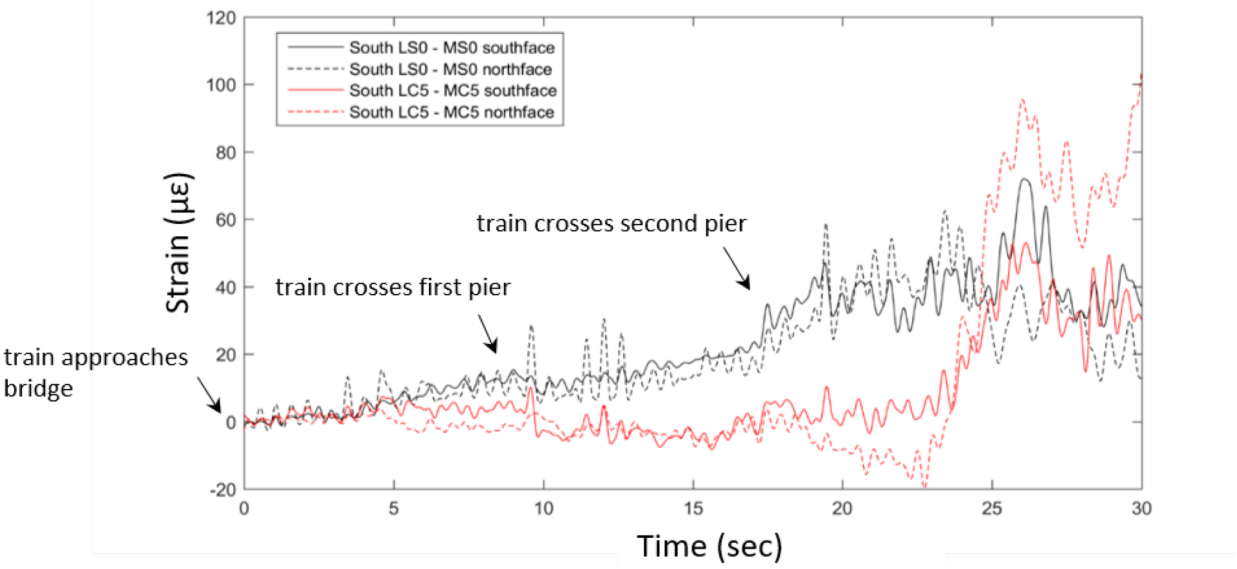

Figure 25. US0-LS0 south truss and MC5-LC5 south truss axial strains (11/14/2016 at 13:56 EST)

of the FE model was performed to align the model better with the experimentally determined modal frequencies.

Truss Component Vertical Loads

Figure 25 shows a sample time history of strain recorded at the south truss at US0-LS0 (*i.e.,* eyebar truss elements) and MC5-LC5 (*i.e.,* vertical truss element) on November 14, 2016 (13:56). It should be noted that the eyebar pin is above the track line and connect to a box section at a node denoted as MS0 (hence, in some instances the eyebar elements will be referred to as MS0-USO). This strain time history captured the train locomotive entering the bridge from its western end and continuing across the bridge affecting the level of strain in the eyebar and vertical truss elements. At around 5 seconds, the train entered the truss structure with the eyebar element beginning to respond with an increasing level of tensile strain. The rising strain, especially after the train crossed the second bridge pier, was due to the global tensile load developing in the eyebar element of the truss. After the train crossed the second pier, it passed the panel that contains element US0-LS0 at which time the strain response consisted of the global response of the truss from the static weight of the train on the bridge and a dynamic component superimposed due to the axle loads that enter the element at the pin at the bottom of the eyebar element. The vertical truss element MC5-LC5 in theory should not experience axial

load under the static weight of the train. However, when train axles crossed the truss panel containing the vertical hanger element MC5-LC5, the element responded by taking the axle load as is seen at 23.5 second and later. The two faces of the vertical truss element MC5-LC5 measured clearly have different levels of strain that were attributed to flexural moments developing at the stringer element that frame into the bottom of element MC5-LC5.

The strain levels in the vertical hangers and eyebars were closely monitored. First, the alert system implemented automated the processing of these strain measurements with alerts sent if the strain response of the elements approached zero (*e.g.,* indicating a disconnected element) or were loaded to a high level of response exceeding 350 με. Second, strain in these elements were also processed to conduct an analysis on the accumulation of fatigue and to conduct structural reliability analyses. The subsequent sections of this chapter use strain and acceleration data to anticipate changes in structural behavior over time so that targeted preventative maintenance decisions can be made.

Eyebar Relative Tautness

Each eyebar plate in the eyebar truss components (US0-LS0) is designed to carry an even portion of the tensile load in the given member. The static tensile axial load (*i.e.,* tautness) in each eyebar can be calculated from the frequency of the member based on out-of-plane uniaxial acceleration measurements. These links are governed by two limit states (*i.e*., yield under tensile axial load and fatigue) that directly correlate to calculated tautness. Similar to the built-up sections (US0-LS0 and MC5-LC5), the eyebars must not exceed a certain stress threshold; additionally, fatigue in the parallel eyebars relative to each other must not be disproportional, otherwise, one or more eyebar links would carry a larger proportion of the load than originally designed for and experience accelerated fatigue accumulation. Standard practice for the bridge owner is to inspect these elements manually with the inspector physically shaking each eyebar and counting the number of vibration cycles relative to the other eyebar links to assess relative tautness in parallel eyebar link members. The wireless sensing strategy allowed for this analysis to be both data-driven and performed continuously rather than manually and periodically.

The axial tensile loads in the eyebar plates were assessed using accelerations of the out-of-plane response of the plates. If accelerations were used when no trains were on the bridge, the axial loads estimated would correspond to the dead load (*i.e.,* self-weight) of the bridge. In contrast, if these axial loads are estimated with the train on the bridge, they correspond to the dead load and live load (*e.g.,* train loads). This strategy was attractive for two reasons. First, if the strain response from these elements were used only the live load could be estimated. Second, measuring out-of-plane acceleration to derive element natural frequencies is nearly identical to the current practice that visual inspectors employ to determine tautness. This section outlines the method adopted that used a continuous dynamical analytical model to extract loads and load proportions from acceleration data. The calculated axial loads were then used for the fatigue and reliability analyses as will be presented in the following sections.

The load in each eyebar plate was calculated using the following equation (Kollar 2003):

$$\frac{\omega_i^2}{\omega_0^2} = 1 + \frac{N_i}{N_E} \tag{1}$$

where, ω_i is the measured first modal (out-of-plane vibration) frequency of the eyebar i, ω_0 is the first modal frequency of the eyebar if it were unloaded, N_i is the total axial load (positive denotes tensile loading) in eyebar i, and N_E is the Euler buckling load for the corresponding eyebar. Rearranging Equation (1) gives:

$$N_i = N_E \left(\frac{\omega_i^2}{\omega_0^2} - 1 \right) \tag{2}$$

with the classical Euler buckling load defined as (Hibbeler 2011):

$$N_E = \frac{\pi^2 EI}{\left(L/n\right)^2}. \tag{3}$$

Here, n is determined based on the boundary conditions of the eyebar (n = 1 for simply supported and n = 2 for fixed-fixed support), and L is the length of the eyebar. The unloaded natural frequency is defined as (Blevins 2016):

$$\omega_0 = k^2 \sqrt{\frac{EI}{A_g \rho L^4}} \tag{4}$$

where, k is determined based on the boundary conditions of the eyebar (k = 3.142 for simply supported and k = 4.730 for fixed-fixed support), EI is the flexural rigidity of the eyebar, A_g is the area of the eyebar, and ρ is the density of the eyebar. The total load for the eyebar truss component is the summation of the load in each link ($N = \sum_{i=1}^{m_{eb}} N_i$) and the ratio of load proportion carried by each eyebar, R_i, is $R_i = N_i/N$. Here, m_{eb} corresponds to the total number of members in the eyebar truss element.

The boundary conditions (which determine n and k) for the eyebar links for out-of-plane bending were determined to be fixed-fixed based on the engineering drawings and from observations of the as-built bridge. This assumption was also validated with dead load-only calculations using measured data and Equation 2 for all six eyebar plates; under fixed-fixed conditions the empirically estimated axial dead load was within 10% of the dead load documented in the engineering drawings. These equations and accompanying properties were combined with the measured fundamental frequency of the eyebar plates to monitor the eyebar loading. Figure 26 plots the load distribution for the eyebar plates on the north MS0-US0 member for 190 events between December 15, 2016 and February 28, 2017.

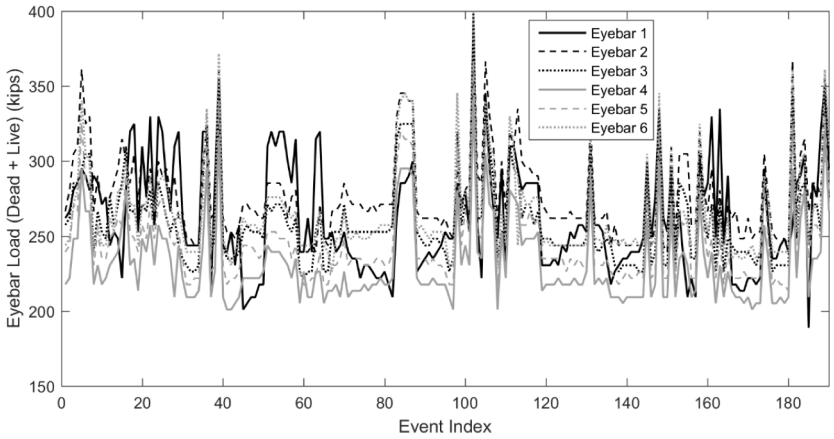

Figure 25. Load distribution for the eyebar elements on the north MS0-US0 member of the Harahan Bridge for 190 train load events between December 15, 2016 and February 28, 2017

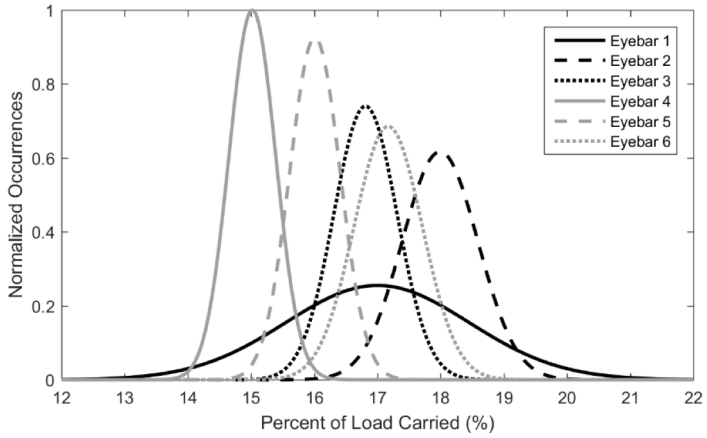

Figure 26. Gaussian distributions that fit the ratio of load carried by each eyebar link on the north MS0-US0 member for 190 train load events between December 15, 2016 and February 28, 2017

A perfect load distribution scenario for six parallel eyebars would result in each eyebar carrying 16.7% of the load. However, the eyebar components exhibited a slightly uneven distribution of loading. The load distribution between eyebars varied between different load events; therefore, the percent of load being carried for each event was accumulated in a separate histogram for each individual eyebar with a normalized Gaussian distribution fit (Figure 26). Nevertheless, the ratio that each eyebar carries remained relatively close to one another for all of the monitored events and there were no eyebars that showed a trend towards carrying an excessive percentage of the load. From Figure 26 it can be seen that the load distributions typically fell between 14% and 19.5% for all eyebars with Eyebar 1 (recall Figure 11(c) for eyebar labeling scheme) varying the most between separate train events.

LONG-TERM FATIGUE ACCUMULATION ASSESSMENT

Fatigue is an important parameter to monitor in railroad bridges because fatigue accumulation is largely controlled by live load, which is high in magnitude as well as in cyclic count for railroad bridges. In this study, it was assumed that the load distribution of dead load was the same as the distribution of live load. Therefore, the dead load in a given eyebar was calculated as the total dead load (1332 kips (5925 kN)) times the load distribution ratio, R_i, and the live load calculated as $L_{Li} = N_i - D_L$. This allowed the fatigue analysis to consider the dead and live loads explicitly.

Miner's Rule (Miner 1945) was followed to calculate consumed fatigue in the eyebars:

$$C_i = \sum_{j=1}^{k} \frac{n_{F_{ij}}}{N_{F_{ij}}} \tag{5}$$

where, i indicates the eyebar, j indicates the stress (load) range, C_i is the fraction of the consumed fatigue, n_{Fij} is the number of cycles accumulated at stress S_{Fij} (where $S_{Fij} = L_{Li}/A_g$), and N_{Fij} is the number of cycles a specimen can withstand at the given stress range (S_{Fij}). AASHTO (AASHTO 2012) provides S-N curves for bridge elements and these same curves have been adopted by AREMA. The S-N curves have an exponential relationship (log-linear slope) between stress range and the number of cycles that follows:

$$N_{F_{ij}} = K S_{F_{ij}}^{-m} \tag{6}$$

where K shifts the curve up or down based on the category of the structural component and m is the log-log slope. Eyebar tensile elements are generally classified as category E, which has a K value of 3×10^{11} and all categories have m equal to 3.

The trigger threshold for the consumed fatigue for each eyebar relative to one another was set to send an alert when the rate of consumed fatigue increases by 50% from that which would be expected if the loading scenario were ideal with 16.7% of the load carried by each eyebar. Relating Equation 5 to 6 (with the help of the AASHTO, category E, S-N curve plotted in Figure 27), this threshold was determined by calculating the stress range that would cause N_{Fij} in Equation 6 to be reduced to 66.7% of its original value. The S-N curve equations show that a 14.5% increase in stress range, S_{Fij} (which directly corresponds to axial load) results in a 33.3% reduction in fatigue life (corresponding to a 50% increase in the rate of fatigue accumulation). That is, for a given train load event, if the load were to change from being distributed evenly to having one or more eyebars carrying 19.08% of the load, the resulting change in stress would cause the member to fatigue at 1.5 times the rate that it normally would for the given load. When this threshold is exceeded consistently, the ratio and overall load should be examined. The fatigue analysis was performed on the eyebar plates; based on the load distributions in the eyebars, the plates are accumulating fatigue relatively evenly. The results of this fatigue analysis also indicated that a reliability-based framework should be put in place to monitor changes in the boundary conditions which can in turn lead to disproportionate loading across the members.

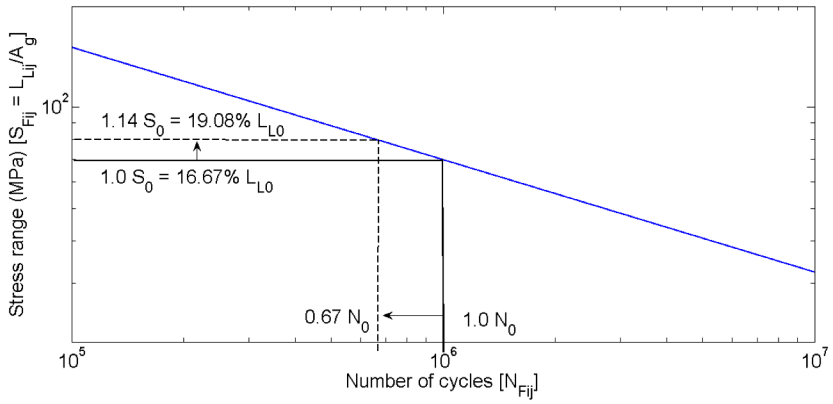

Figure 27. AASHTO/AREMA S-N curve for assessment of eyebar fatigue accumulation

RELIABILITY-BASED CONDITION MONITORING

This study utilized a first-order reliability method (FORM) reliability framework in order to stay consistent with current AASHTO LRFD (Thoft-Christensen and Baker 1982) design procedures. Consider the safety margin, M, defined by structural reliability in terms of capacity, C, and demand, D, as $M = g(X) = C - D$ where the limit state function (LSF), g, is a function of a vector of random variables (RV), X, that characterize the capacity and demand profile of the structural member. Structural design dictates that capacity must be greater than or equal to demand, which leads to the probability of failure defined by $P_f\,(M \leq 0)$. Consequently, reliability is defined as the probability that failure does not occur, or $R = 1 - P_f$.

LSFs governing the axial tensile behavior of the critical Harahan truss elements (*i.e.,* eyebar and vertical hanger members) were analyzed. The most basic case of reliability arises when a LSF's RVs are entirely independent and jointly normal. In this case, $P_f = \Phi(-\beta)$, where the reliability index, β, is given as (Thoft-Christensen and Baker 2016):

$$\beta = \frac{\mu_M}{\sigma_M} = \frac{\mu_C - \mu_D}{\sqrt{\sigma_C{}^2 + \sigma_D{}^2}}\,. \tag{7}$$

However, some of the RVs that are used to characterize the limit states in this analysis were non-normal (as will be discussed), so the RVs had to be transformed into independent standard normal space. Since transformed LSFs are generally non-linear and second-order reliability methods (SORM) can be implemented to improve the accuracy of the calculated reliability index. However, FORM was confirmed to produce sufficient approximations of the reliability indices because they were very similar to the results from Monte Carlo (MC) simulations. Figure 28 outlines the iterative FORM-based framework that was used to analyze the LSF and corresponding reliability indices by finding the minimum distance between the origin (in the standard normal space) and the limit state surface.

Evaluation of Limit States

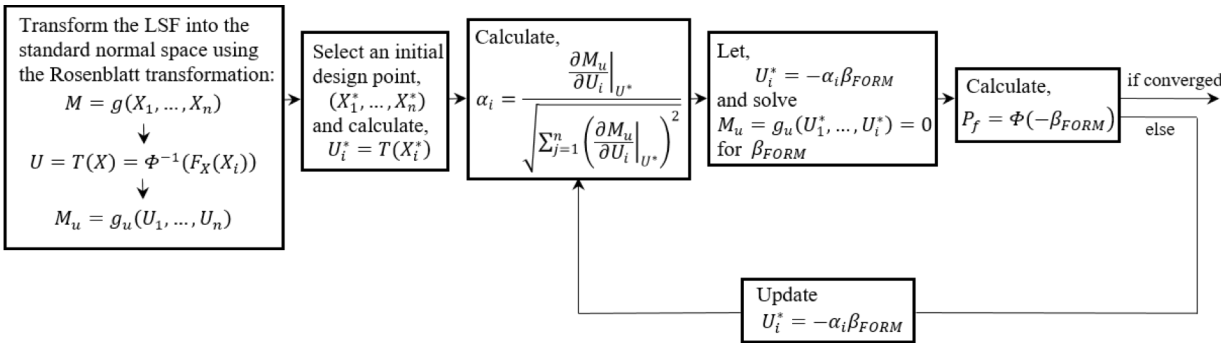

Figure 28. Iterative approach for FORM analysis (Flanigan *et al.*, 2017)

Changes in boundary conditions of the upper and lower pins of the eyebar elements caused by excessive load-induced moments in the box-section or corrosion can cause one or more of the eyebars to carry a disproportionate amount of the load that the members were not designed to carry. In addition, the MC5-UC5 is a vertical hanger that theoretically carries the majority of the load as a train crosses over the C5 section of the bridge. First, the LSFs for the box-section of the US0-LS0 eyebar member and MC5-LC5 vertical hanger were analyzed. This determined the reliability index considering the entire load that each member carries.

The assumed limit state for net-section stress in the US0-LS0 eyebar box section is:

$$M_U = F_{y,U} - \frac{DL_U}{A_{n,U}} - \varepsilon_U \cdot E \tag{8}$$

and the assumed limit state for net-section stress in the MC5-LC5 vertical hanger is:

$$M_M = F_{y,M} - \frac{DL_M}{A_{n,M}} - \varepsilon_M \cdot E \tag{9}$$

Additionally, the assumed limit state for net-section in each eyebar is:

$$M_E = F_{y,U} - \frac{L_{tot}}{A_{n,E}} \tag{10}$$

where the dead loads (DL_U and DL_M) were calculated from design drawings and the FE model, net-section areas ($A_{n,U}$, $A_{n,M}$, and $A_{n,E}$) were taken from design drawings and verified with on-site measurements, peak strains (ε_U and ε_M) were calculated from measurement data, total load (dead load and live load) in each eyebar (L_{tot}) was extracted from the acceleration-based tautness framework outlined in the previous section, and yield stresses ($F_{y,U}$ and $F_{y,M}$) and the elastic modulus (E) were taken from design drawings. The distributions for the dead loads, yield stresses, and the elastic modulus were taken from the literature (Hess *et al.,* 2002) and the statistical parameters for the RVs are presented in Table 4. The distributions extracted from the measured data closely fit generalized extreme value (GEV) distributions, which are described by the probability density function:

Table 4: Random variable parameters for lognormal and constant distributions

Random Variable	Mean	COV	Distribution
US0-LS0 yield stress, $F_{y,U}$ (ksi)	49.6	0.0890	Lognormal
MC5-LC5 yield stress, $F_{y,M}$ (ksi)	37.3	0.0680	Lognormal
Elastic modulus, E (ksi)	29696	0.0179	Lognormal
US0-LS0 dead load, DL_U (kips)	1332	0.0800	Lognormal
MC5-LC5 dead load, DL_M (kips)	115	0.0800	Lognormal
US0-LS0 net-section area, $A_{n,U}$ (in^2)	127.5	-	Constant
MC5-LC5 net-section area, $A_{n,M}$ (in^2)	39	-	Constant
US0-LS0 single eyebar area, $A_{n,E}$ (in^2)	28	-	Constant

Table 5: Random variable parameters used for GEV distributions

Random Variable	Shape Parameter	Location Parameter	Scale Parameter	Distribution
US0-LS0 peak strain, ε_U, (με)	0.0639	114.0	55.4	General Extreme Value
MC5-LC5 peak strain, ε_M, (με)	-0.148	136.5	56.4	General Extreme Value
US0-LS0 eyebar 1 load (kips)	0.202	288.8	14.7	General Extreme Value
US0-LS0 eyebar 2 load (kips)	0.0899	289.4	19.0	General Extreme Value
US0-LS0 eyebar 3 load (kips)	0.148	269.5	17.4	General Extreme Value
US0-LS0 eyebar 4 load (kips)	0.0941	242.1	18.6	General Extreme Value
US0-LS0 eyebar 5 load (kips)	0.210	257.2	17.8	General Extreme Value
US0-LS0 eyebar 6 load (kips)	0.222	273.7	19.5	General Extreme Value

$$f_X = \frac{1}{\xi} exp\left\{-\left[1 + k\left(\frac{x-\eta}{\xi}\right)\right]^{-\frac{1}{k}}\right\}\left[1 + k\left(\frac{x-\eta}{\xi}\right)\right]^{-1-\frac{1}{k}} \quad (10)$$

where k is the shape parameter, ξ is the scale parameter, and η is the location parameter. The parameters that describe the GEV distributions for strain in the US0-LS0 member and MC5-LC5 vertical hanger are provided in Table 5.

For the limit state functions defined by Equations 8 and 9, the results shown in Table 6 indicate that FORM provided an excellent approximation for the probability of failure and was therefore used for the remainder of the analyses (*i.e.,* calculation of reliability indices for individual eyebars) because it has a shorter computational time than the MC simulation. The probability of failure for net-section stress in the US0-LS0 box-section is 2.42×10^{-6} which corresponds to a reliability index of $\beta = 4.57$. The reliability index values of the six individual eyebars in this same member (US0-LS0) are presented in Table 8. The β values for the US0-LS0 eyebars and box section's respective limit states were all well above AASHTO LRFD's reported target value of 3.5 (AASHTO 2012; Nowak 1999). This indicated that the probability of failure calculated from measured data is even lower than would be designed for per AASHTO guidance. For the MC5-LC5 net-section stress limit state, the probability of failure was essentially zero. This vertical hanger is located at the cross-section of the bridge where the cantilever section at the pier meets the span section. As a result, while this vertical hanger experiences slightly higher live loads because there are no other truss elements connected with it, the engineering reports and FE

Table 6: Reliability analysis results for strain-based analysis

Limit State Function	P_f (Monte Carlo)	P_f (FORM)	β_{FORM}
US0-LS0 net-section stress	2.34×10^{-6}	2.42×10^{-6}	4.57
MC5-LC5 net-section stress	~0	~0	-

Table 7: Reliability analysis results for load-based analysis

Limit State Function	P_f (FORM)	β_{FORM}
US0-LS0 eyebar 1 net-section stress	1.22×10^{-6}	4.71
US0-LS0 eyebar 2 net-section stress	2.80×10^{-9}	5.83
US0-LS0 eyebar 3 net-section stress	1.53×10^{-7}	5.12
US0-LS0 eyebar 4 net-section stress	2.35×10^{-9}	5.86
US0-LS0 eyebar 5 net-section stress	3.44×10^{-6}	4.50
US0-LS0 eyebar 6 net-section stress	8.28×10^{-6}	4.31

model confirmed that it carries a very small dead load as compared to the US0-LS0 member which is located in the main span. Due to this discrepancy in the dead loads, the reliability analysis confirms that the probability of failure of this element is zero.

SECTION 6
LOAD ASSESSMENT AND RATING ANALYSIS OF PARKIN BRIDGE

Introduction

Assessment of railroad bridge load capacity is a major component of bridge asset management and is required by the FRA. Bridge load rating is a standard practice railroads use to assess bridge capacities under anticipated load conditions, especially those originating from rail equipment running on track. In the United States, bridge load rating methods are based on the AREMA Manual for Railway Engineering (Chapter 8). They largely are based on estimating the safety margin of structural components based on analysis of bridge responses to standard train load models (so called Cooper E loads) using empirically observed impact factors that account for dynamic responses associated with bridge, track and train parameters. Such methods are relatively conservative approaches which ensure safety of railroad bridges.

A key component of the load rating analysis is the dynamic load factor (or impact factor) which accounts for the dynamic components of train loads as they naturally interact with the track and bridge. The dynamic load factor (DLF) is influenced by a number of factors including the bridge properties (*e.g.,* span length, flexural rigidity, intrinsic damping), train properties (*e.g.,* train speed, train static weight, train suspension system, wheel conditions), and track properties (*e.g*., track condition). Structural monitoring provides an opportunity to observe the DLFs of a bridge being monitoring allowing monitoring to inform the load rating process. This can reduce conservativeness in load ratings which in turn may allow heavier train loads and/or higher train speeds. This can increase the overall freight capacity of a rail network without jeopardizing the safety of the network.

This section presents a load rating analysis that is informed by bridge monitoring data. Specifically, the approach takes direct observation of the live load response of a monitored bridge to determine an appropriate impact factor for use in load rating analyses. The method was implemented using strain response data of the Parkin Bridge. In subsequent sections, the method serves as a basis for risk and resilience assessment of the Parkin Bridge.

Conventional Load Rating Estimations

Load rating, LR_x, for a structural component in a railroad bridge is expressed by the following equation (AREMA 2006):

$$LR_x = \left(\frac{Cap-DL}{LL_x(I+1)}\right) \tag{11}$$

where,

$$E_x = x(E_{10}) \tag{12}$$

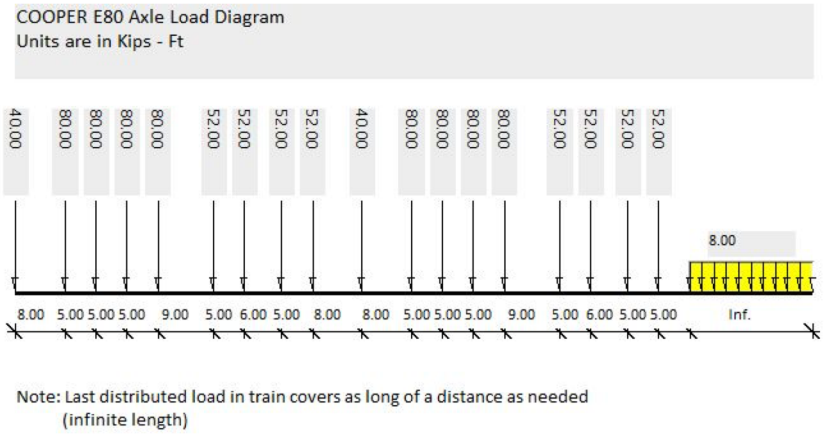

Figure 29. Cooper E80 Train Load

with *Cap*, *DL*, LL_x, and *I* representing the capacity of the component, dead load response of the component, live load response due to the desired standard Cooper train load, E_x, of the component, and impact factor at the component level, respectively. The factor x represents a multiplier which identifies the required ratio of the level of required design train load, E_x, to the standard Cooper train load, E_{10}. As the train load demands have increased gradually since the original definition of E_{10} as a standard, the value of x increased. Recently, it is customary to use x = 8 which illustrates the standard distribution of E_{80} (*e.g.,* see AREMA (2006)). A figure representing the load distribution of E_{80} is shown in Figure 29.

Clearly the load rating of Equation 1 is an expression of safety margin for train load demands. It is conventionally computed using structural analysis process. Where the values of *DL* and LL_x are obtained by applying the own weight (dead load) and the desired E_x (train load) to an appropriate structural analysis model and performing two separate computations for the dead load and the train load, respectively. The impact factor, which accounts for the dynamic effects of the train passage is conventionally prescribed by AREMA (2006).

SHM Estimation of Load Rating

Close examination of Equation 11 reveals that it is a fairly conservative equation. The main reasons for the conservatism are the train load response value, LL_x and the impact factor value, *I*. The LL_x term is often estimated based on analysis with the impact factor, *I*, informed by past empirical observation of railroad bridges under varying structural (bridge and track) and operational conditions (train speeds and weights). However, structural monitoring provides an exciting opportunity to estimate more realistic, yet still safe, values for LL_x and *I* that can save costs while maintaining the desired level of safety. Thus, Equation 1 can be modified for a data-driven load rating process using structural health monitoring (SHM) data for a component to be

$$LR_x|_{SHM} = \left(\frac{Cap-DL}{LL_x|_{SHM}(I_{SHM}+1)}\right) \tag{13}$$

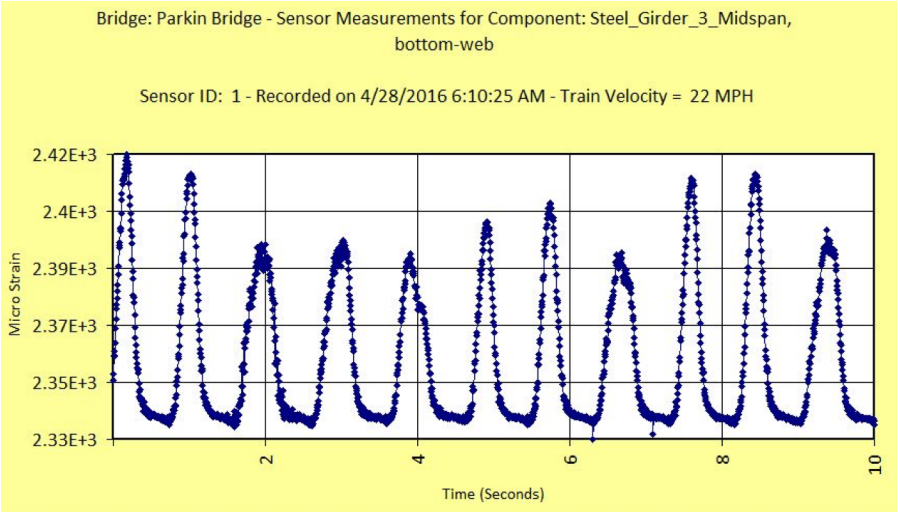

Figure 30. Parkin Bridge strain response at mid-span of girder line 3 on the bottom web surface (note that the strain measurement has a zero-strain bias)

Conventional evaluation of the component static response due to an E_x train load involves applying the loading E_x to an appropriate structural analysis model and performing the needed calculations. Since E_x is a standard loading, it was not feasible to perform an SHM experiment which will result in an actual measurement of $LL_x|_{SHM}$ during this project. So, for this project, the SHM-based rating was:

$$LR_x|_{SHM} = \left(\frac{Cap-DL}{LL_x(I_{SHM}+1)}\right) \tag{14}$$

The only SHM-based improvement for this project is thus the improvement of the impact factor. The team used two methods to obtain the improved impact factor in this project as detailed next.

Signal Processing Technique

The SHM-based impact factor I_{SHM} can be evaluated from the measured time histories of train passage using signal processing techniques. The strain measured at mid-span from the girders can be used to assess the speed of the train and the static weight based on filter processing methods. This is feasible due to the short-span nature of the Parkin Bridge which ensures the bridge strain response under flexural bending is highly correlated to the static weight and speed. Specifically, low-pass filtering is adopted to extract from each passage of a train car and locomotive a rough estimate of the train static response that has the dynamic component removed; in doing so, the impact factor can be estimated. As an example, a typical raw strain measurement (with bias) at one of the girders of Parkin Bridge (Figure 30) was analyzed and produced an estimated an impact factor of I_{SHM} = 6.01% (a DLF of 1.0601). The train speed for that particular event was estimated by the bridge response to be 22 miles per hour (MPH). The process was repeated for numerous train events with the speed, static weight and impact factor estimated for each train car and locomotive. The resulting train speed versus DLF estimates are shown in Figure 31. Studying the figure closely reveals that: 1) there is a modest spread of the measured DLF for a given train speed and 2) there is a fairly small trending upward of DLF as the train speed increase. The second observation is of interest, since the empirical AREAM estimates show a trend which increases rapidly as the train speed increase as shown in Figure 32.

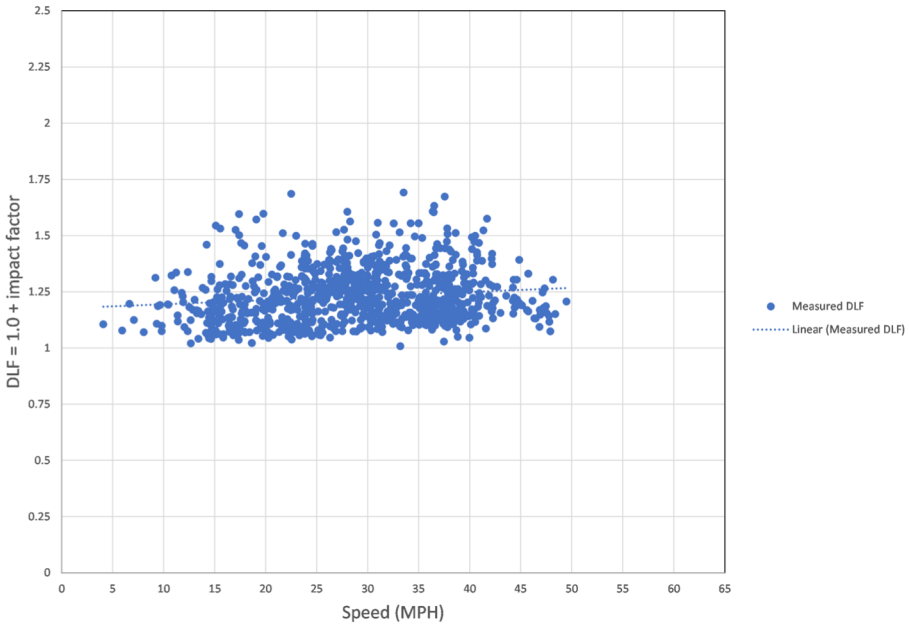

Figure 31. Estimated DLF of Parkin Bridge using measured strain responses at mid-span as a function of train speed.

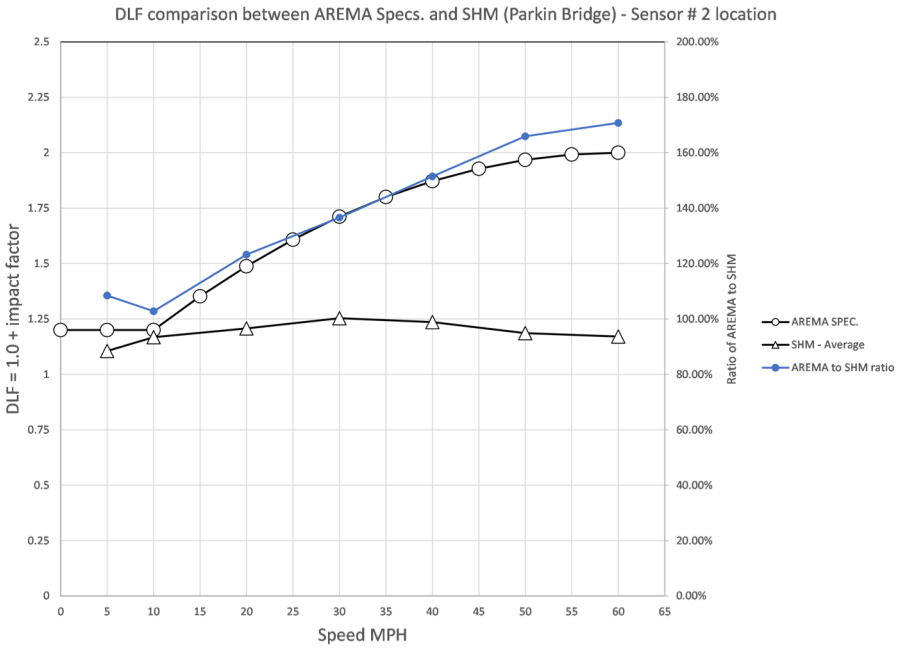

Figure 32. DLF versus train speed for one of Parkin Bridge girders: a comparison between AREMA specified and SHM-based methods

The figure also shows that the ratio of empirical DLF versus SHM-measured DLFs increases as the train speed increase. This is a further indication of the high degree of conservatism in the conventional load rating methods under current use by the railroad industry. Continuing further to estimate the actual load ratings obtained, Table 8 shows a comparison between $LR_x|_{SHM}$ and LR_x for one of the girders of Parkin Bridges at different train speeds where we took advantage of

Table 8: Conventional Load Rating vs. SHM-based Load Rating of Parkin Bridge

Speed (MPH)	E_{10} Rating Conventional	E_{10} Rating SHM
10	70	80.5
25	45	51.8
40	30	34.5
60	20	23

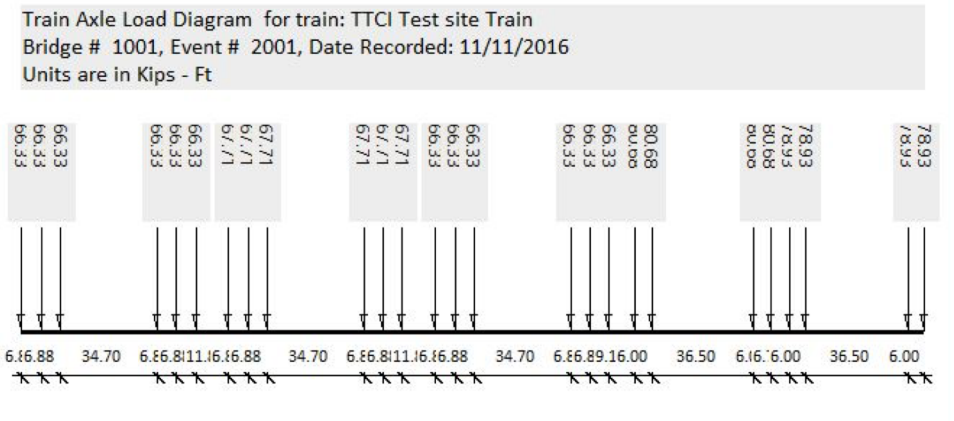

Figure 33. Train load diagram for the TTCI Girder bridge

the SHM-based impact factor measurements. Clearly, SHM-based impact factor estimations produce much smaller values at all train speeds than those offered by AREMA.

SHM-based Load Rating with Train Weights

The signal processing technique described earlier is useful when the train weight information is not available as was the case of the Parkin Bridge. When the train weight information is available, we can use a different technique to evaluate the train impact factor (or DLF) more accurately. To illustrate, the team utilized a short-span (24 feet) steel girder rail bridge at the Transportation Technology Center (TTCI) in Pueblo, CO for experimentation (as will be described in Section 10). Termed the West Steel Bridge, the bridge is similar to the Parkin Bridge but the train loads used to excite the bridge are controlled by TTCI. The flexural response of the bridge is monitored with strain gages on the top and bottom web sections of the girders at mid-span as well as a linear displacement transducer also at mid-span. During experimentation, the train weight was available as shown in Figure 33. Furthermore, the cross-section properties of the steel girders were also known.

A simple strain influence line which was generated at the location of the strain sensors that were placed on the bridge girder (Figure 34) while a static strain diagram representing a moving train was also generated (Figure 35). During the train passage on the TTCI Bridge, the resulting dynamic strains were measured. Figure 36 shows a sample time history of a single train passage

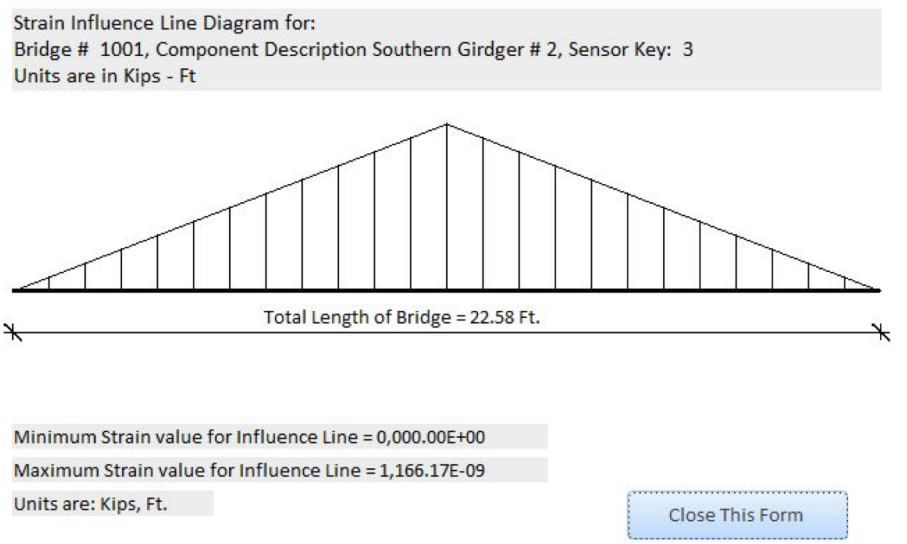

Figure 34. Strain influence line for the TTCI girder

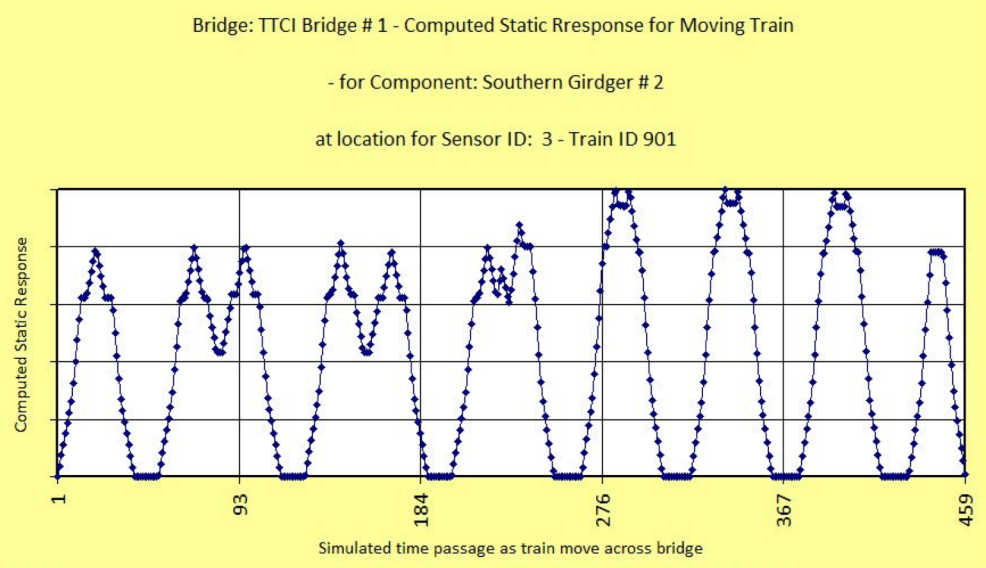

Figure 35. Static Strains that Result from a Moving Train Load (TTCI Train)

on the bridge. By computing the ratio of the dynamics strain[1] to the static strain we computed the impact factor and the DLF for each train event. Table 9 shows the ratio of load rating of the girder of the TTCI Bridge using empirical/conventional AREMA approach and the SHM approach for different train passage event. The conservatism of using AREMA empirical approach as well as the advantages of using SHM in evaluating load rating are obvious.

[1] We used the maximum dynamic strain resulting from each train passage event.

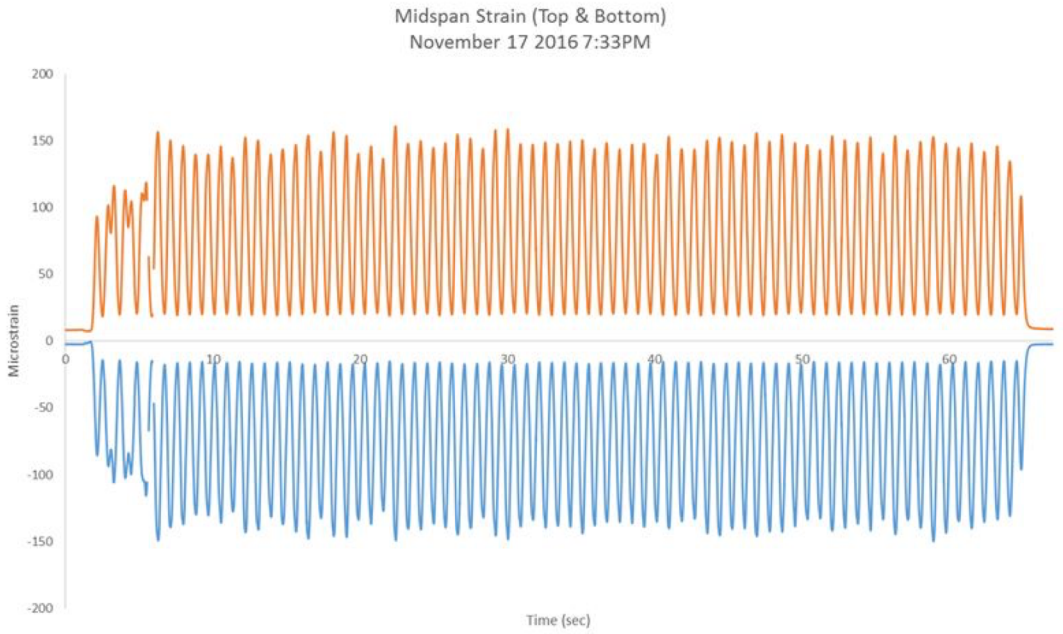

Figure 36. Measured Strains during a single TTCI Train Event

Table 9: TTCI Impact Factor, DLF, and Load Rating Comparisons (AREMA vs. SHM-based measurements)

Lap #	SHM Results		Max Static Strains (micro strain, computed from I. L.)	Train Speed (MPH)	SHM DLF = (max dynamic strains / max static strain)	AREMA Impact Factor	AREMA DLF = 1+Impact Factor	Ratio of Increased Rating Due to SHM
	Max Measured Dynamic Strain (micro strain)	Max Disp (in)						
14	215.114	0.014	172.500	42	1.25	0.90	1.90	152%
26	215.659	0.008	172.500	42	1.25	0.90	1.90	152%
31	211.301	0.008	172.500	43	1.22	0.91	1.91	156%
40	214.387	0.121	172.500	42	1.24	0.90	1.90	153%
52	213.934	0.008	172.500	42	1.24	0.90	1.90	153%
65	215.749	0.009	172.500	42	1.25	0.90	1.90	152%
76	215.568	0.008	172.500	42	1.25	0.90	1.90	152%
82	222.377	0.006	172.500	40	1.29	0.87	1.87	145%

Conclusion

We presented two distinct methods for computing SHM-load rating of components. Either of these methods can be used separately or they can be combined for verification and increasing confidence of accuracy. In both situations, we observed that the use of SHM-based load rating estimations can result in higher ratings, especially for higher train speeds. We will present a risk-based methodology showing how to translate these higher ratings into an objective

(monetary) estimated benefits for bridge owners / operators so as to justify using SHM as a basis for load rating with objective and measured return on investment (ROI).

SECTION 7
RESILIENCE MONITORING

Introduction

Natural and manmade hazardous events can impose a devastating cost to society. As EM-DAT (2017) and Munich RE (2014 and 2014) show, the costs of some of these disasters in the US alone can be staggering. Stakeholders of civil infrastructure have a vested interest in reducing these costs by improving and maintaining operational and physical performance. Throughout history, infrastructure resilience has been defined in numerous ways, the most widely used and most objective by the National Infrastructure Advisory Council (NIAC) (2009), which states:

> "Infrastructure resilience is the ability to reduce the magnitude and/or duration of disruptive events. The effectiveness of a resilient infrastructure or enterprise depends upon its ability to anticipate, absorb, adapt to, and/or rapidly recover from a potentially disruptive event." (NIAC 2009)

The NIAC (2009) also determined that resilience can be characterized by three key features:

- "*Robustness:* the ability to maintain critical operations and functions in the face of crisis. This includes the building itself, the design of the infrastructure (office buildings, power generation, distribution structures, bridges, dams, levees), or in system redundancy and substitution (transportation, power grid, communications networks).
- *Resourcefulness:* the ability to skillfully prepare for, respond to and manage a crisis or disruption as it unfolds. This includes identifying courses of action and business continuity planning; training; supply chain management; prioritizing actions to control and mitigate damage; and effectively communicating decisions.
- *Rapid recovery:* the ability to return to and/or reconstitute normal operations as quickly and efficiently as possible after a disruption. Components [of rapid recovery] include carefully drafted contingency plans, competent emergency operations, and the means to get the right people and resources to the right places."

We propose that resilience has another key feature: redundancy. Sometimes, these four resilience features are simply called the "4Rs". Resilience is multidisciplinary and needs the cooperation of different disciplines for successful outcomes. Without multidisciplinary cooperation and contributions, there cannot be successful or efficient resilient infrastructure.

A beneficial illustration of resilience was introduced by Bruneau *et. al* (2003). We recast the concept in terms of operational quality in Figure 37 and Figure 38. Figure 37 shows graphically how we can objectively estimate resilience of a bridge (or bridge network) by utilizing resilience charts which plot the operational level/quality of an asset or system versus recovery time. The area above the curve is classically defined as the metric assessing resilience with smaller areas suggesting greater resilience. We then use Figure 38 to show a comparison of resilience of two bridges (or bridge networks). The illustration shows how an undesirable event might affect two bridges (or bridge networks). The operations of a bridge (or bridge network) "A" will immediately lose some operational quality, then start recovering until returning back to full operational quality. As for bridge (or bridge network) "B," it will lose much of its operational

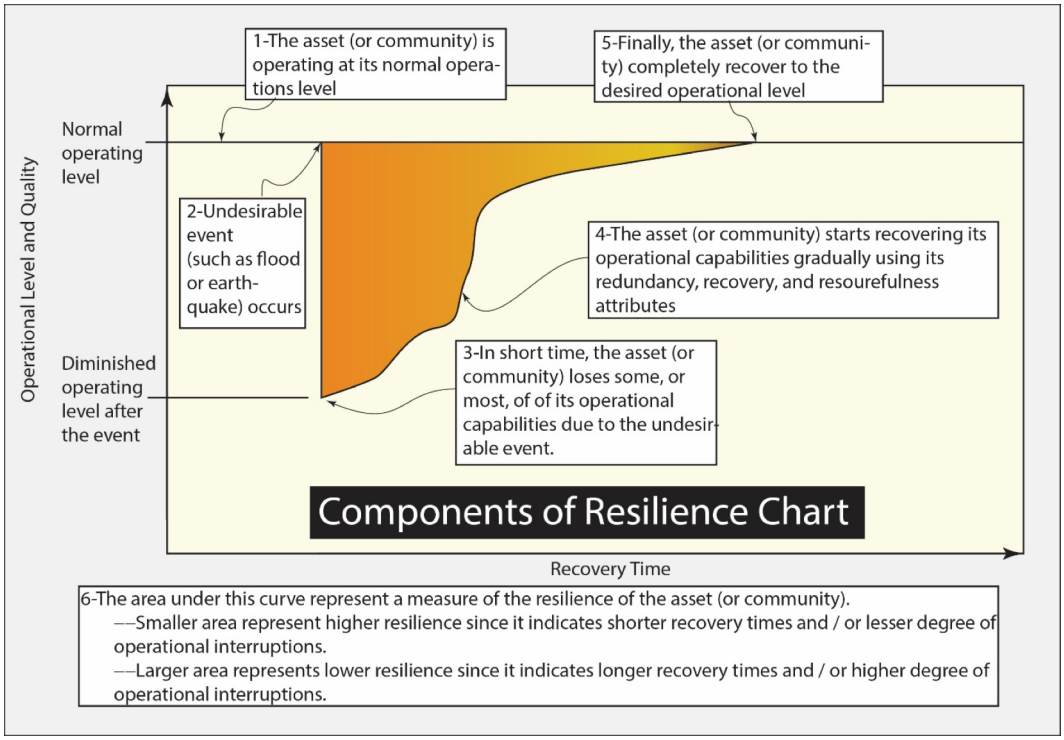

Figure 37. Resilience definition in the time-operational quality space (Ettouney 2014)

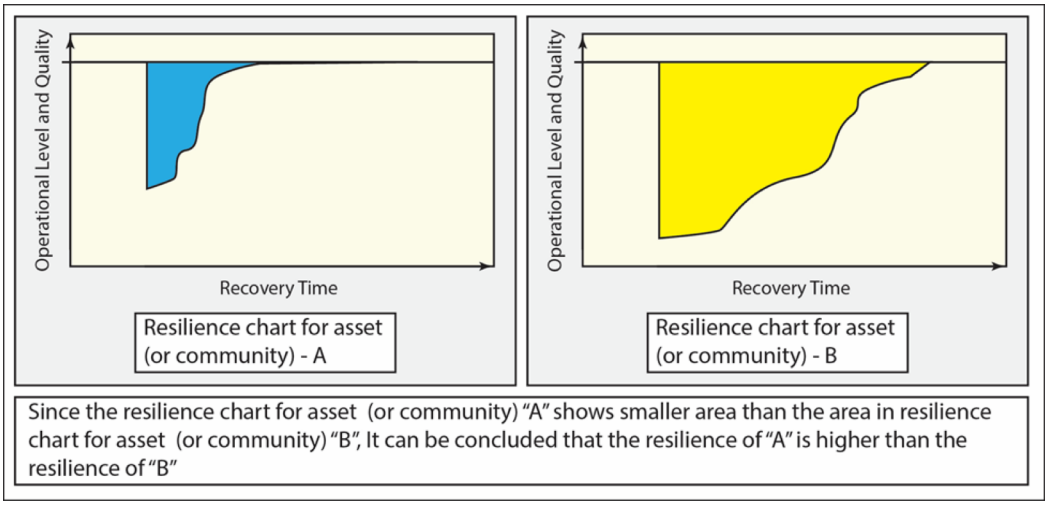

Figure 38. Comparison between the resiliencies of two assets (*e.g.*, bridges) using resilience charts (Ettouney 2014)

quality when subjected to the same undesirable event. It will recover but on a much slower pace than bridge "A." Thus, we can conclude that "A" is more resilient than "B." We can use the area under the curve describing the time-operational quality behavior of the bridges (or bridge networks) to objectively assess the resilience of those bridges (or bridge networks).

The purpose of this section is to show how we incorporated resilience assessment / monitoring processes within the overall project efforts. See Equation 8 and Table 11, below for differences between resilience assessment and resilience monitoring. The main goals of the efforts are: 1) use simple analytical tools, which utilize infield monitoring results as a subset of other information sources to assess resilience in an objective manner; 2) apply those analytical tools for bridge and bridge network resilience estimations; 3) develop different issues parameters, which are needed to evaluate #1, and #2 above; 4) provide reasonable assumptions for parameters needed to complete the applications of bridge and bridge network assessments of #1 and #2 above[2]. We end this section with a brief discussion of return on investment (*ROI*) of resilience management projects.

Theoretical Background: the 4Rs Approach

There are several models for evaluation of infrastructure resilience in an objective manner, see for example, DHS (2011a, 2011b, and 2011c), Hughes and Healy (2014), and Ettouney and Alampalli (2017a and 2017b). Our theoretical model for assessing resilience in this project follows the simpler model of DHS method, see DHS (2011a, 2011b, and 2011c). The method is based on defining resilience of a system as:

$$Res = f\left(R_1, R_2, R_3, R_4\right) \tag{15}$$

The variables R_1, R_2, R_3, and R_4 represents objective expressions for robustness, resourcefulness, recovery, and redundancy of the system under considerations. Following DHS (2011a, 2011b, and 2011c) we use a simple weighted averages approach to compute R_i such that:

$$R_i = \sum_{j=1}^{j=N_i} W_{ij} A_{ij} \tag{16}$$

where W_{ij}, A_{ij}, and N_j are the weighting factor, assessment factor, and number of variables, respectively. These variables will be defined in the next section for bridges and bridge networks.

We note that there are several methods that describe the function $f(\ldots)$ of Equation 15; see a summary of some of those models in Ettouney and Alampalli (2017a and 2017b). These methods vary from a simple power summation of R_1, R_2, R_3, and R_4 (Vose 2009; DHS 2011a, 2011b, and 2011c) to a fairly complex graph network (Ettouney and Alampalli 2017a and 2017b). For simplicity, we choose the model of DHS (2011a, 2011b, and 2011c):

$$Res = \sqrt[n]{\sum_{j=1}^{j=4} \frac{R_j^n}{4.0}} \tag{17}$$

A reasonable value of n in Equation 17 is 10 following DHS (2011a, 2011b, and 2011c).

[2] Given the enormous number of issues, which contribute to bridge and bridge network resilience, obtaining many in-field estimates of the values of those issues were beyond the scope of this work. Hence, we resorted to using a reasonable estimate of those values to help in illustrating the processes of the methodology.

Table 10. Subjective examples of resilience monitoring efforts

Component	Monitoring Techniques
Robustness	Structural health monitoring methods (see Ettouney and Alampalli 2012a and 2012b)
Resourcefulness	Training, courses, management and operational auditing for compliance.
Recovery	Auditing, table top and other types of exercises and drills. Pertinent inspection and maintenance processes.
Redundancy	For physical redundancy, use structural health monitoring methods. See Ettouney and Alampalli (2012a and 2012b). For operational redundancies, use techniques of monitoring resourcefulness and recovery.

We note that Equations 15 through 17 describe resilience assessment at a given instance of time. Since resilience, *Res*, changes as time passes, we can describe as a time-based function:

$$Res = Res(t) \tag{18}$$

We define the effort of assessing *Res*(*t*) as resilience monitoring. Table 10 shows a subjective description of some of the efforts concerning each of the 4Rs. We show later an example of objective monitoring of resilience that resulted from this project.

Bridge Resilience

We use Equation 16 to define each of the 4Rs for bridge resilience and use Equation 17 to define the total resilience of a given bridge. Note that for each of the 4Rs, we define N_j variables, which controls the particular resilience component R_i. Thus there are N_{BR} variables which will control the bridge resilience such that:

$$N_{BR} \le \sum_{j=1}^{j=4} N_j \tag{19}$$

The reason for the inequality sign in Equation 19 is that there might be several variables which may commonly control R_1, R_2, R_3, and/or R_4. Each of the j^{th} variables in Equation 16 is assigned a weighting factor, W_{ij}, which implies the importance of that variable such that

$$0.0 < W_{ij} \le 1.0 \tag{20}$$

The assessment factor $0 \le A_{ij} \le 100$ in Equation 16 indicates the condition of the j^{th} variable at time *t*. It is evaluated using one of four methods:

1. Using an appropriate in field visual observation process by a qualified observer. In this project, we used inspector findings for the evaluation of some of the A_{ij} factors, as pertinent. DHS (2011a, 2011b, and 2011c) recommended the extensive utilization of this

method for finding as many as possible of the A_{ij} factors due to its timeliness and potential accuracy.

2. Using suitable structural analysis results, as pertinent.
3. Using SHM results as pertinent.
4. Using subjective estimates by bridge managers for the remainders of the A_{ij} factors. Due to time and budget constraints, we used our own judgment in estimating these remaining variables as pertinent.

Note that we did not utilize methods #2 or #3 in this project due to time and budget constraints. The resulting bridge resilience as well as each of its 4Rs components will be in the range of 0 to100. The higher the number, the higher the resilience of the bridge under considerations.

Network Resilience

There are some differences between our modeling of bridge resilience and bridge network resilience. The first most important difference is the variables in the bridge resilience model can be either physical or operational, while the variables in the network resilience model are all physical. Second, the physical variable in the bridge network resilience model are only two types: they are either the bridge itself or the linkages between the different bridges in the network. Of course, we can use a higher resolution bridge network model to include all the variables in each of the component bridges, however, such a model can be resource demanding and as such it is beyond the scope of this project.

Based on the above, we rewrite Equations 16 and 17 for components and total bridge network resilience as:

$$R_i\big|_{NETWORK} = \sum_{j=1}^{j=NB} \left(WB_j\right)\left(R_i\big|_j\right) + \sum_{j=1}^{j=NL} \left(WL_j\right)\left(RL_i\big|_j\right) \tag{21}$$

and

$$Res\big|_{NETWORK} = \sqrt[n]{\sum_{j=1}^{j=4} \frac{\left(R_j\big|_{NETWORK}\right)^n}{4.0}} \tag{22}$$

where $R_i|_{NETWORK}$ represents the total network robustness, resourcefulness, recovery, and redundancy for i = 1, 2, 3, and 4, respectively. Individual bridge resilience components are $R_i|_j$ while individual links resilience components are $RL_i|_j$. *NB* refers to the number of bridges in the network while *NL* is the number of links in the network. The importance of the j^{th} bridge or link within the network is WB_j or WL_j, respectively. Note that $Res|_{NETWORK}$ is the total bridge network resilience. Imposing the conditions $0.0 < WB_j \leq 1.0$ and $0.0 < WL_j \leq 1.0$ will result, as before, in a network bridge resilience as well as each of its 4Rs components to be in the range of 0-100. Again, the higher the number, the higher the resilience of the bridge network under considerations.

Applications

The resilience processes just described were encoded in a database as a part of this project. Figure 39 show an output form from the system created which includes the different variables (issues) that control each of the 4 Rs (R_i with i=1,2,3,4). The top list in the figure shows a partial list of issues controlling R_1. The figure indicates that N_1 = 167. Each of these issues has either physical or operational links with other issues (Ettouney and Alampalli 2017a and 2017b). The bottom list in the figure illustrates this linkage for issue #42. It indicates that other non-structural issues are linked (either operationally or physically) with three other issues as shown in the list. Figure 39 also indicate that total resilience-related variables, N_{BR}, for this bridge is 265 issues.

After assessing the resilience of the bridge and applying Equation 16 for each R_i, the resilience components can be estimated. Also, applying Equation 17 will result in the total bridge resilience. Figure 40 shows the form for those results for different bridges in the database. The figure shows a snapshot for Parkin Bridge and its resilience results at different assessment times (resilience monitoring). Note also that the bottom list in the figure indicates the total number of resilience issues, N_i with i=1,2,3,4. The lists in Figure 40 can be of great help to bridge managers in tracking the performance of resilience and its different components as time passes. It shows trends and can be used for forecasting and optimal budget allocations.

Since bridges are part of a larger network of other bridges and links[3] between those bridges, it was of interest, as part of this project, to explore briefly resilience of bridge networks as per Equations 21 and 22. The first step of course is to establish a bridge network. Three sample networks were created for the purpose of the project. Figure 41 shows a form that illustrates topology of the sample network using the latitude and longitude coordinates of bridges in the network. Employing Equation 21 for a given network requires the knowledge of resilience each of its member bridges as well as the resilience of each of the links of the network. Those resiliencies are shown in Figure 42 for convenience. After applying Equations 21 and 22, the final network resilience and it components are shown in Figure 43. The figure shows the history of bridge network resilience. Such information can be of help to bridge managers, on the network level, in understanding network strengths and weaknesses if/when disaster strikes, and forecasting and allocating budgets on network levels.

[3] Note that links can be physical (such as railroad tracks) and operational (such as total budget allocation, manpower, or other resources)

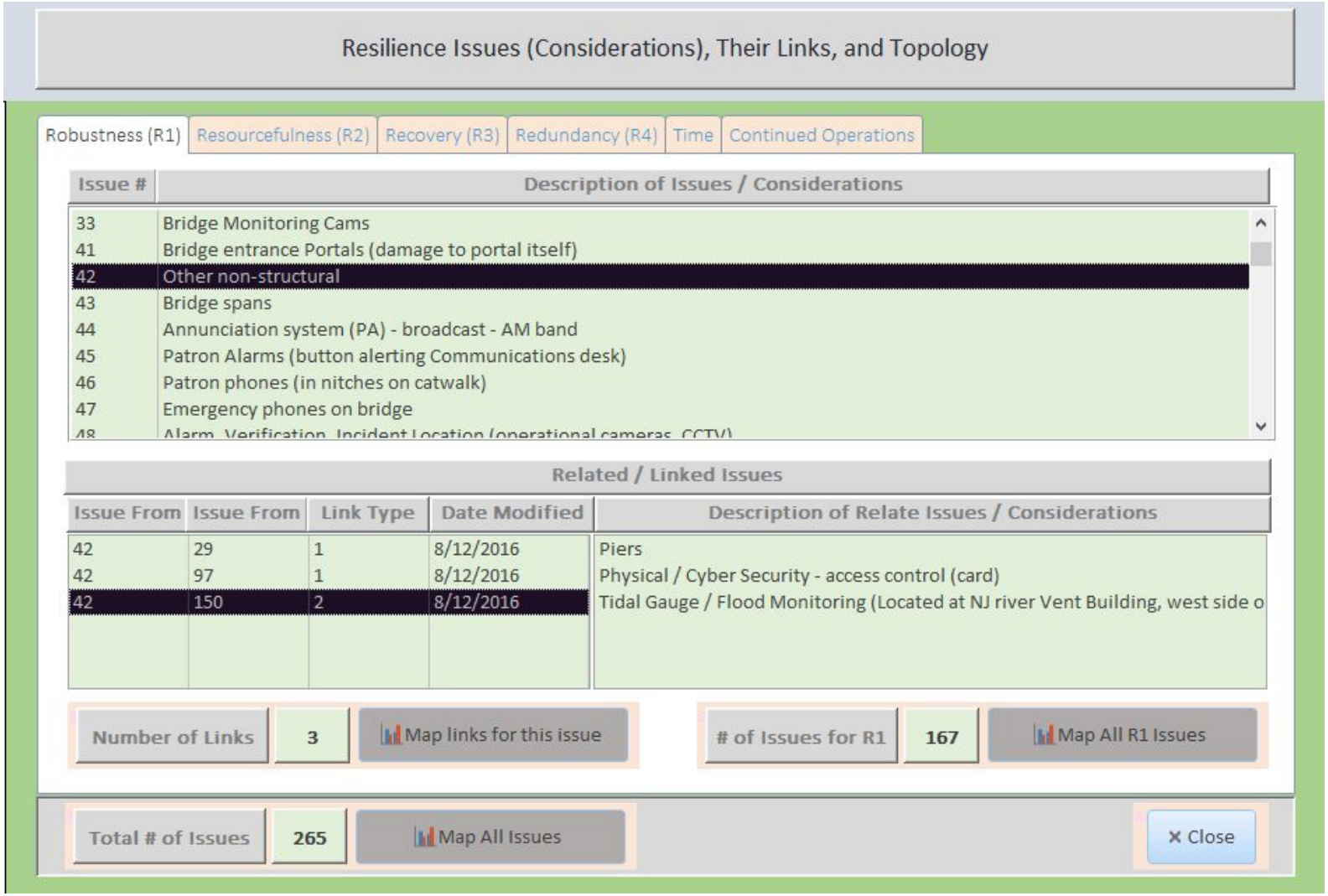

Figure 39. Resilience issues form for single bridge

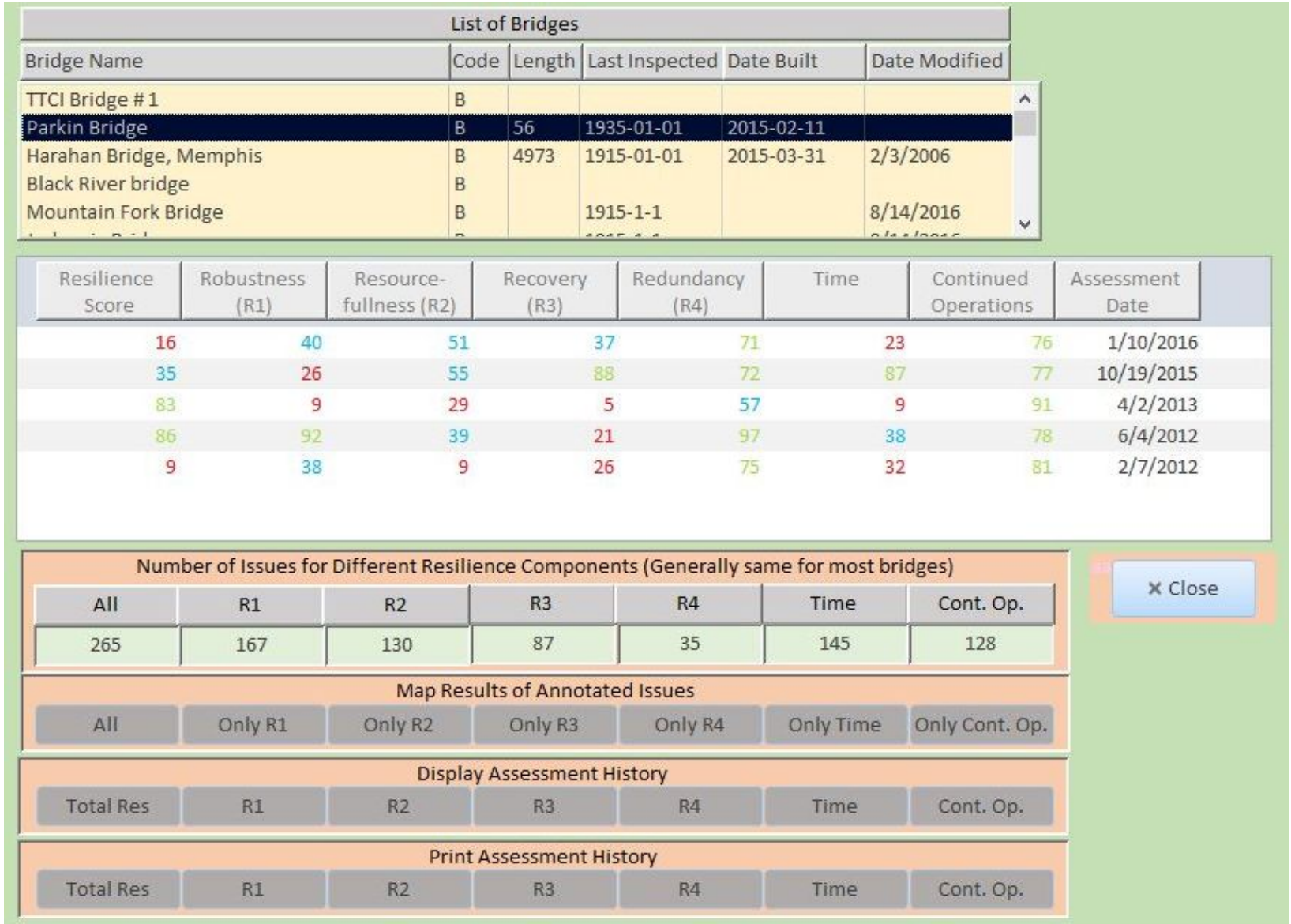

Figure 40. Resilience assessment - monitoring for a single bridge

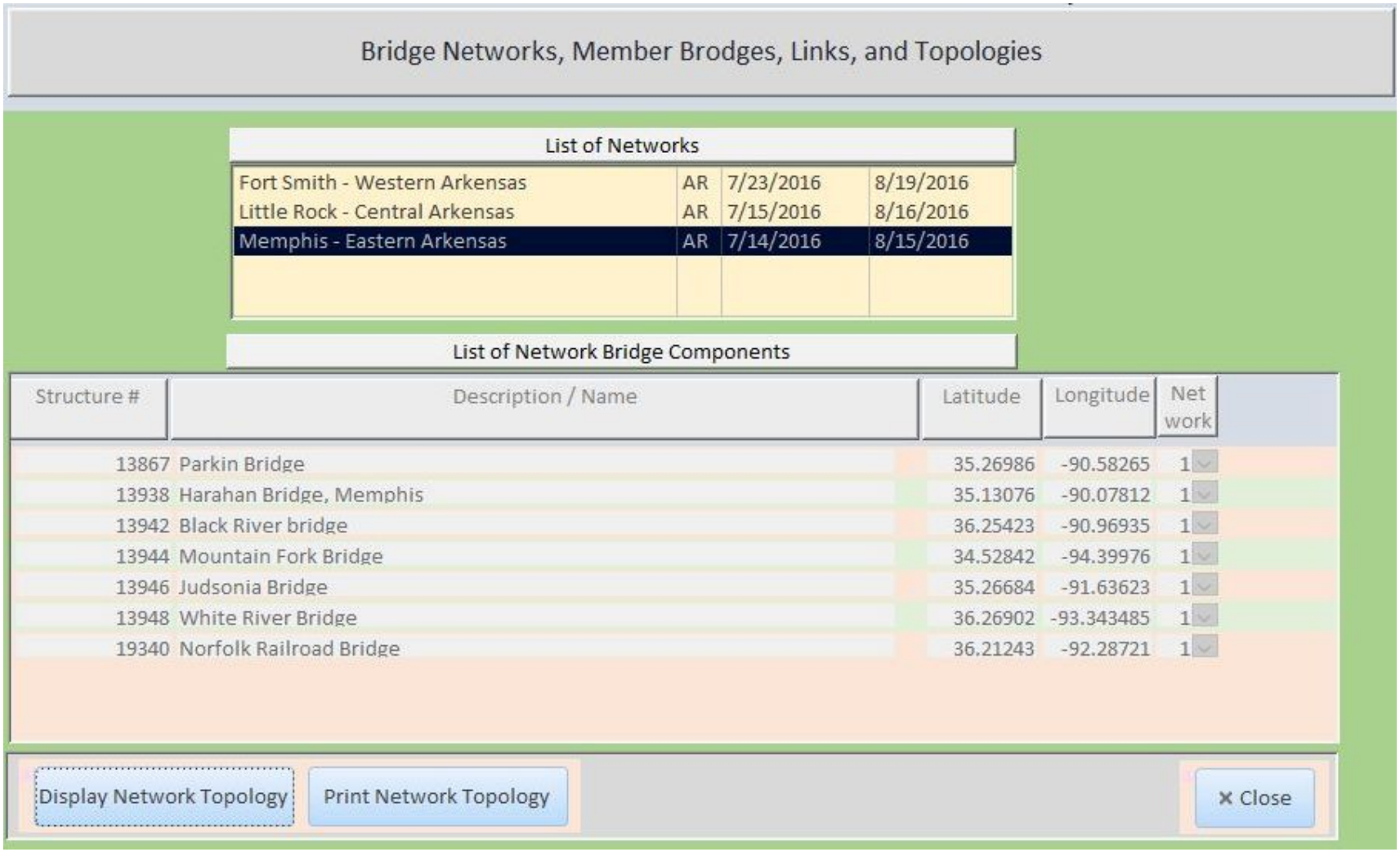

Figure 41. Bridge network topology form

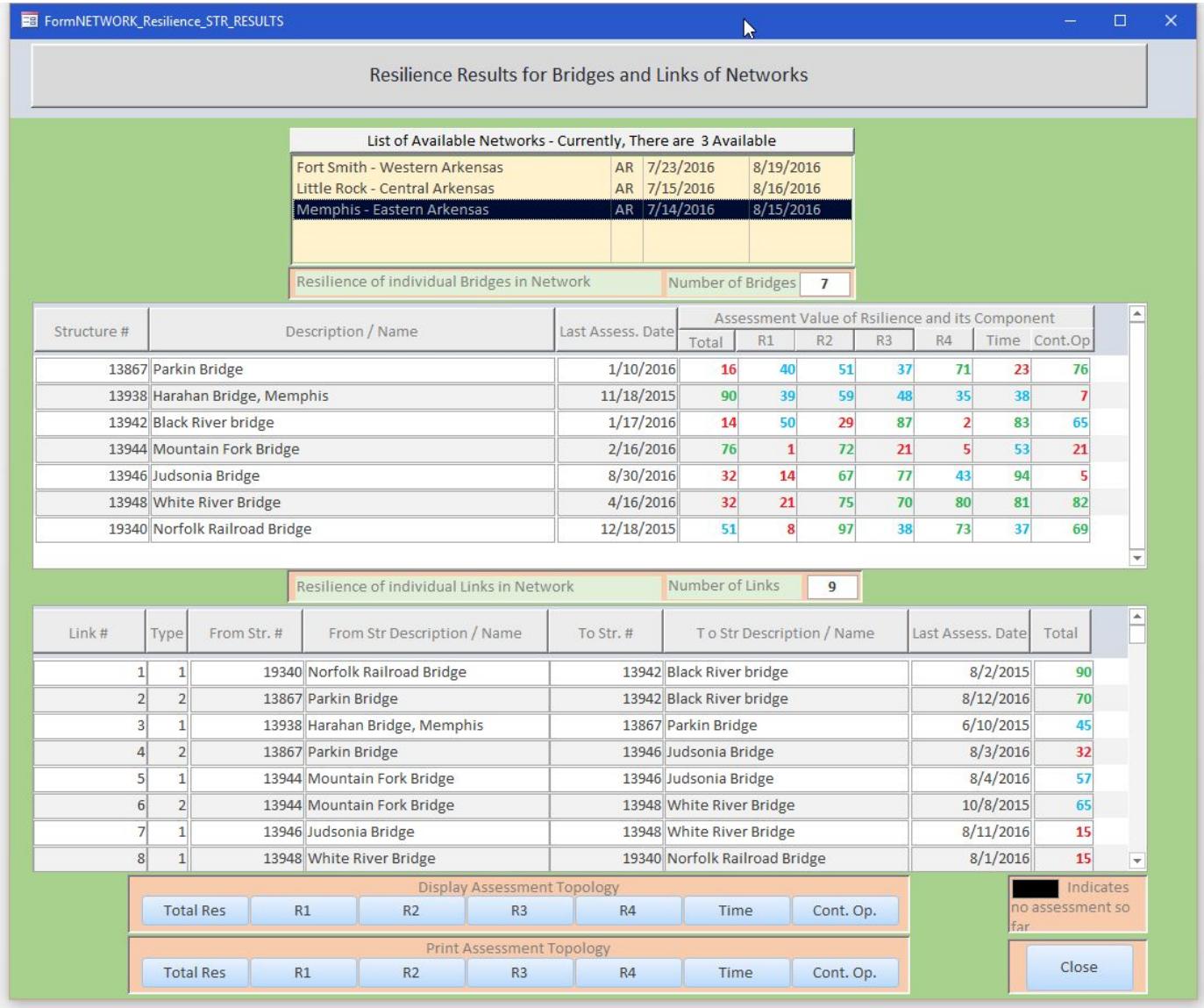

Figure 42. Bridge network resilience form

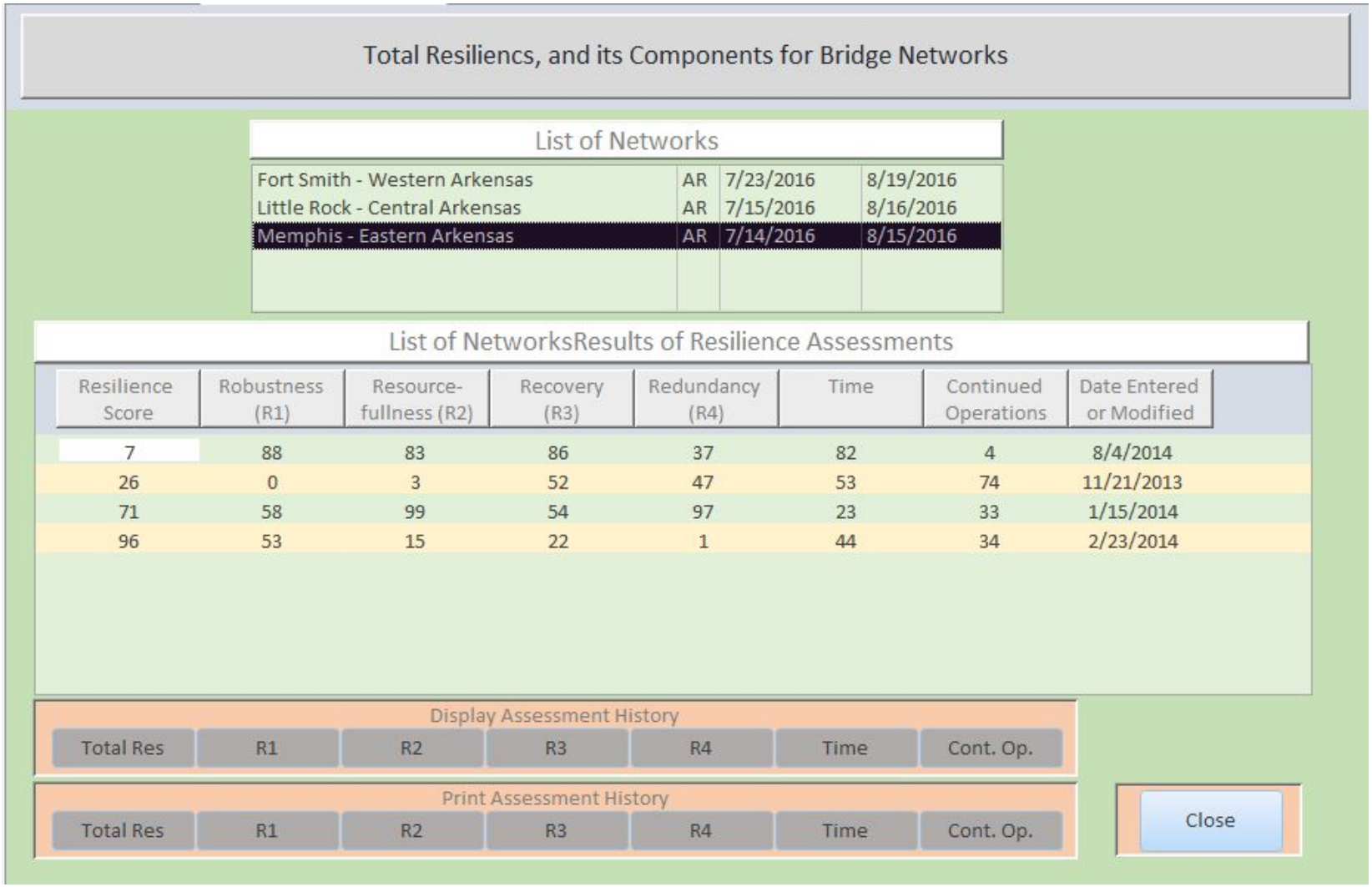

Figure 43. Resilience of bridge network

Return on Investment (ROI) for Resilience Management

Efficient resilience management can bring a great return on investment (*ROI*) for many stakeholders: public organizations (*e.g.,* federal, state, local), civil infrastructure owners, as well as the private industry (*e.g.,* consulting engineers, vendors, constructors). It is a "win-win" proposition for all sides and there are a lot of business applications/opportunities in pursuing different components of resilience management. So, while society benefits from more resilient infrastructure, businesses will also have an opportunity to increase revenue and profits. With that said, finding the *ROI* or cost/benefit ratios of a particular project is not an easy task. Federal Emergency Management Administration (FEMA 1996) and Multihazards Mitigation Council (MMC 2005) have both studied this subject in-depth. MMC concluded that, on average, the benefit from natural hazard mitigation projects is about $4.00 for every $1.00 of cost. We followed their procedures and present a simple case study for resilience enhancement projects *ROI* next. In later sections of this report we introduce a more objective *ROI* method for SHM projects using risk-based analysis.

Let us assume that an organization might be interested in investing funds to improve its financial outlook. We assume that a proposed resilience-related project needs $0.5M in funding. The project has two goals: provide accurate resilience assessment and provide accurate evaluation of a resilience improvement project. The project is in a region often affected by hurricanes, and there are 20 facilities in the region that are susceptible to the destructive force of hurricanes. The hurricane strength of interest is a 50-year hurricane. Such a hurricane is expected, on average, to cause losses per facility per event estimated at $M 2.0. These losses include disruptions in operations, physical damage and other indirect losses. Such losses might be reduced by about 5% if appropriate resilience enhancement measures (learned from an accurate resilience assessment projects similar to those in Figure 39 through Figure 43. Those improvements include enhancing resource management, more efficient disaster planning, increasing network redundancy, improving training, or increasing bridge robustness as a last resort) are enacted. Such savings can be based only on slight modifications in operating practices with limited capital expenditures. Based on this simple example, we can compute an expected cumulative rate of return on investment (ROI) as shown in Figure 44. The ROI after five years from the organization's viewpoint can be considerable.

This example is intentionally conservative in our assumptions on: assumed savings from identifying weak points in the facilities; exposure to a single natural hazard; and assumed savings from optimal project evaluations. Perhaps the most conservative assumption is the expected loss per event. Experience, see for example EM-DAT (2017), and Munich RE (2014 and 2014) show that losses from major disasters can be much higher than those in our simple example. The computed ROI can be several times higher than the ones computed in either of the two cases of the example. Nevertheless, the example shows that even with extremely conservative assumptions, the ROI that organizations can realize from funding resilience-related projects is immense.

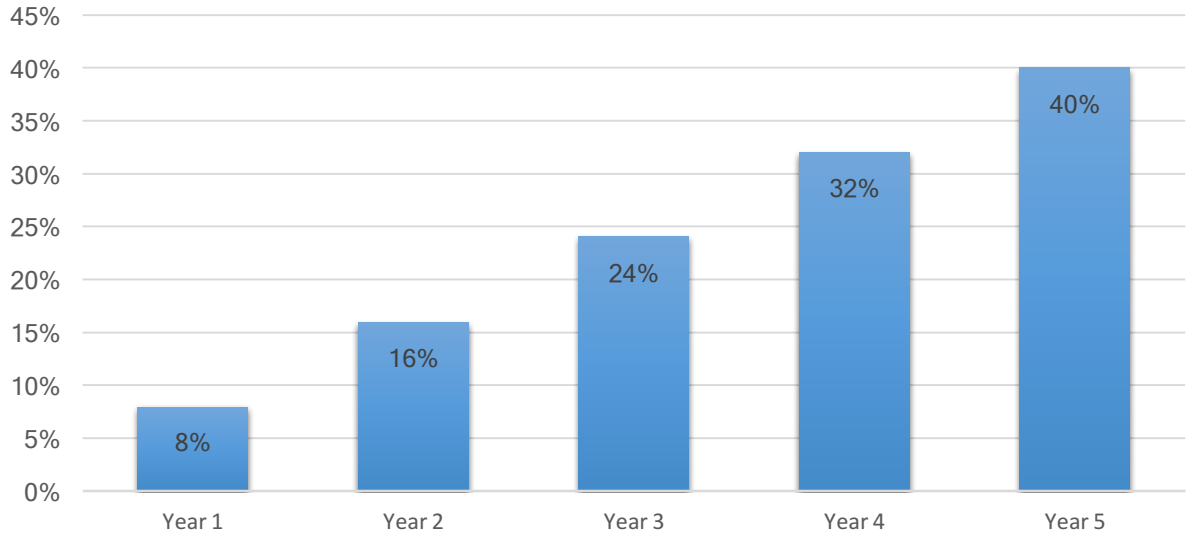

Figure 44. Example of cumulative ROI on a publicly Funded Resilience Project

SECTION 8
RISK MONITORING AND RETURN ON INVESTMENT

Overview

We start this section by using a convenient definition of risk (Ettouney and Alampalli 2017a): *risk is a description of an uncertain objective or subjective alphanumeric expression, which describes an outcome of an unfavorable, uncertain event, which might degrade performance of a single (or community of) civil infrastructure (asset or assets)*. Herein we use the above definition to derive useful objective formulations of risk which we can then use to obtain the rate of return on investments for management operations. We then apply those formulations to perhaps the most important hazards that face railroad bridges by far (live loads and long-term structural deterioration) to quantify risks for these hazards. We then explore the ROI of using SHM (as a management operation) for reducing the risks of these two all-important railroad bridge hazards.

Theoretical Background

Risk and Return on Investments (ROI)

We can now express risk, *Ri*, formally as a function of its three basic components:

$$Ri = f\left(C,T,V\right) \tag{23}$$

This risk expression has been used by many authors including DHS (2011a, 2011b, and 2011c) which applied the above equation to multitudes of hazards, both natural and manmade. The three basic risk components, C, T and V, are consequences, threats (hazards), and vulnerability, respectively. In general, a *hazard* is defined as any process of event which can degrade the performance of civil infrastructure (including rail road bridges). Given these definitions, we can easily recognize that the most potentially damaging hazards to railroad bridges are train loads (live load) and deterioration (which includes many sub-classes of important hazards such as corrosion and fatigue). Closer inspection of Equation 23 as related to the two hazards of interest reveals that the threat, T and vulnerability, V, of the two hazards of interest are intertwined in a complex manner such that identifying each separately cannot be easy. Because of this, we can use a simpler and more suited form of Equation 23 as:

$$Ri = f_1\left(C,E\right) \tag{24}$$

Where E is defined be Ettouney and Alampalli (2017a) as the system exposure. Here, the exposure E is an expression (which can either be objective or subjective) which includes the combined effects of the system vulnerability to (or capacity to resist) the hazard of interest. As such

$$E = f_2\left(T,V\right) \tag{25}$$

We end this brief discussion of risk by noting that risk value as obtained from Equation 23 or Equation 24 can be either subjective or objective. We will use monetary values as a subjective risk description for this project.

Return on Investment:

A suitable definition of return on investment, *ROI*, is:

$$ROI = \frac{Reward}{Investment} \tag{26}$$

We can define $Reward$ as the reduction in risk as a result of $Investment$ such that

$$ROI = \frac{Ri\big|_{Before} - Ri\big|_{After}}{Investment} \tag{27}$$

With $Ri|_{Before}$ and $Ri|_{After}$ representing the estimated risks before and after the investment. Obviously, $Ri|_{Before}$, $Ri|_{After}$ and *Investment* need to be expressed in monetary values.

Live Load (Train) Risk

Recalling that E is an expression that relate vulnerability (or capacity) and hazard level, we can use load rating, *LR*, of the bridge (or a bridge component) to define the exposure of that bridge (or component) to train passage such that:

$$E \approx LR_x \tag{28}$$

With *x* denoting the desired Cooper-E design level of that bridge.

Now, if we compute the consequences, $C=C_x$ (in monetary form) which will be incurred due to LR_x we can estimate the live load risk as:

$$Ri_x = f_1\left(LR_x, C_x\right) \tag{29}$$

We have shown in the load rating section that utilizing SHM can produce a lower load rating, $LR_x|_{SHM}$. As such, the resulting consequences for this lower rating can be computed as $C_x|_{SHM}$. The resulting live load risk due to utilizing SHM can similarly defined as:

$$Ri_x\big|_{SHM} = f_1\left(LR_x\big|_{SHM}, C_x\big|_{SHM}\right) \tag{30}$$

Note that the live load risks of Equation 29 and Equation 30 are both expressed in monetary values. The realization of the individual values of *Ri* and/or $Ri_x|_{SHM}$ can be of use to bridge managers. They can be computed using any of the risk assessment methods proposed previously in the literature (*e.g.,* see Ettouney and Alampalli 2017a). However, for the purposes of this project, we are interested in enumerating the ROI of SHM utilization in load rating evaluations. We will detail the process next.

Return on Investment from SHM Investment for Load Rating

In this section, we will delineate a process by which the ROI of SHM can be analyzed. First, we note that

$$Ri_x\big|_{SHM} < Ri_x \tag{31}$$

Using Equation 27, it can be shown that there will be a positive ROI for using SHM in estimating load rating. Defining the $Reward$ as:

$$Reward = Ri_x - Ri_x\big|_{SHM} \tag{32}$$

We can compute ROI as

$$ROI = \frac{Ri_x - Ri_x\big|_{SHM}}{Investment} \tag{33}$$

A much simpler way to look at Equation 32 and Equation 33 is to reconsider $Reward$ as the increases of load ratings to a bridge. There can be one, or both, of two consequences: 1) reduction of train delay costs as a direct result of increasing permissible train speeds on a bridge while keeping a constant freight weight, and/or, 2) increase of transportable freight weight permissible on a bridge, while keeping train speed constant. In what follows, we give an example of computing the ROI of SHM as a result of reduction of train speeds while keeping train freight load constant.

Reduction of Train Speed on Parkin Bridge:

Figure 45 shows the input dashboard for the analysis developed for the team for the SHM monitoring system installed on the Parkin Bridge. This dashboard includes needed information for computing the *ROI* of SHM (namely, Equation 33) when used to estimate railroad bridge load rating. There are several types of information that are needed for the analysis:

- Train configuration including the number of crew, number of locomotives, and number of different types of train cars;
- Details of cars and their commodity and weights;
- Estimated values of different freight per unit weight;
- Kinematics of train accelerations and decelerations
- Number of trains per day and/or per year (on average)
- Geometry of railroad bridge;
- Results of load rating analysis using both conventional and SHM load ratings at different train speeds.

Needed input for simple model to compute cost of train reduced speeds					
Train		Speed (MPH)	E10 Ratings		
# of crew	3		Conventional	SHM	
# of locomotives	3	10	70	80.5	
# of bulk cars (Total)	50	25	45	51.75	
# of manifest cars (Total)	20	40	30	34.5	
# of intermodal cars (Total)	10	60	20	23	
	Cars per Commodity				
	Perishable	Bulk	Other		
# of bulk cars per type of freight	10	40	0		
# of manifest cars per type of freight	5	5	10		
# of intermodal cars per type of freight	3	3	4		
Car content weight (tons)	80	80	80		
Mohammed Ettouney: Meat / sea food	**Mohammed Ettouney:** Coal	**Mohammed Ettouney:** Machinery			
Value per ton	$ 2,662.00	$ 26.00	$ 6,956.00		
Total value	$ 212,960.00	$ 2,080.00	$ 556,480.00		
	Ft				
Car Length (ft)	53.08				
Locomotive length (ft)	71.39			Meter / sec2	
Bridge Length	24.00		Ave. Acc.	0.3	
Approaches Length	24.00		Ave. Decc.	0.5	
Number of trains per day	40.00				
Number of trains per year	14600.00				

Figure 45. Input dashboard for SHM load rating ROI analysis

Armed with the information in the dashboard the desired *ROI* of SHM can be computed in the output dashboard, which is shown in Figure 46. In the output dashboard, we still need to input the costs (investment) of SHM as shown in the top of the table. Next, a table shows the relationship between the desired bridge ratings and the corresponding speeds resulting from both conventional and SHM-based processes and the difference in speeds. This difference in speeds will cost delays in case of using conventional rating methods. The cost of these delays are then computed per train, per day, and per year. Finally, the *ROI* of SHM can be computed by dividing costs of delays (see Equations 32 and 33) by the cost of SHM investment. Clearly, *ROI* of SHM can be considerable.

Deterioration Risk

We follow the methodology proposed by Ettouney and Alampalli (2017a) for the assessment of deterioration risk. They observed that the subjective bridge inspector findings could be utilized as a subjective measure for deterioration of bridge components. This can be justified by the fact that inspector findings combine the outcome of different hazards that cause deterioration (such as corrosion, fatigue, freeze/thaw, and general wear-and-tear) and the system's response to those hazards (*i.e.,* the capacity of the component under consideration). Thus, it is reasonable to use inspector's finding as a measure for exposure such that:

SHM rating costs			
initial Cost of SHM deployment	$ 100,000.00		
Cost of SHM deployement after one year	$ 200,000.00		
	Speed (S), MPH		Delta_S (MPH)
Desired Rating	Conv.	SHM	
70.00	10.00	15.48	5.48
51.75	20.95	25.00	4.05
45.00	25.00	30.87	5.87
34.50	35.50	40.00	4.50
30.00	40.00	47.83	7.83
23.00	54.00	60.00	6.00
Slowing delays - Desired rating of	70		
From speed (MPH)	15.48		
To Speed (MPH)	10.00		
Delay costs			
Total delay cost per train	**$ 4,809.38**		
Total delay cost per day	**$ 192,375.22**		
Total delay cost per year	**$ 70,216,954.07**		
ROI of SHM system			
ROI after 1st day	92%		
ROI after first year	70117%		

Figure 46: Output dashboard for SHM load rating ROI analysis

$$E \approx V.I. \tag{34}$$

where *V.I.* represents the subjective visual inspection results (inspectors' findings). Substituting Equation 34 in Equation 24 we can express deterioration risk as:

$$Ri_{DET} = f_1\left(C_{DET}, V.I.\right) \tag{35}$$

Here, the consequences of *V.I.* is C_{DET}. For our current purposes, we will use monetary values to express C_{DET}. This will result in a convenient monetary description of deterioration risk, Ri_{DET} (which can be used later to evaluate the desired *ROI*).

Deterioration Risk Example for Three Bridges

We use Equation 35 to quantify deterioration risk on the component level for several components on three bridges. The results are shown in Figure 47. The columns of this table contain the following:

- *Bridge*: bridge number/identifier (three bridges were used in this case study);
- *Component*: component description;
- *Importance of component*: subjective description of the importance of the component for bridge wellbeing (subjective scale used where H is "High", M is "Medium", and L is "Low");

Bridge and Component Properties			Deterioration Risk based on Inspector Findings			
Bridge	Component	Importance of components	Inspector findings (0-pristine to 5-failed/ verge of failure)	Inspectors Notes on observed damage	Supplimental notes from inspector's finding, justifying level of effort	Risk = Cost of not fixing (until next inspection) = f(B,D ,J)
#1	Girder	H	3	Loss of section	Limited loss of section, minimal action	$ 2,217,440.00
#1	Girder	H	2	Bridge vibrations	Some vibrations, nothing to be concerned about	$ 2,137,440.00
#1	Global	H	3	Remaining life	Some alarm	$ 4,314,880.00
#2	Girder	H	3	Loss of section	Loss of section is extensive, a lot more action	$ 4,314,880.00
#2	Global	H	4	Bridge vibrations	Vibartion needs more remedies	$ 4,994,880.00
#3	Eye bar	L	2	Load distribution	Load distribution is ok, subjectively	$ 1,048,920.00
#3	Eye bar	L	3	Remaining life	Some attention is needed	$ 1,054,720.00
#3	Eye bar	L	2	Loss of section	some paint	$ 2,000.00
#3	Global	H	0	Bridge vibrations	None	$ -

Figure 47: Dashboard for deterioration risk based on inspector findings

- *Inspector finding*: subjective condition rating on an integer scale of 0 to 5;
- *Inspectors notes*: descriptive notes of the finding/observations;
- *Supplemental notes*: additional descriptive notes for the component condition;
- *Risk* (Ri_{DET}): monetary description of risk where the computations account for the importance of the bridge, importance of the component, the severity of finding, and the forecasted costs of waiting.

The risk results of Figure 47 can be used by bridge managers to make optimal management decisions as pertinent. As such, the table can be of immense value to bridge managers. However, given the thrust of this project, we are interested in the effects and lessons learned from utilizing SHM as a supplemental tool to help bridge managers in such decisions for improving safety and reducing costs.

SHM Return on Investment (ROI)

Let us now consider Figure 48; it is similar to Figure 47 with the added effects of utilizing SHM. The columns of the table be described as:

- *Bridge:* bridge number/identifier (three bridges were used in this case study);
- *Component:* component description;

Bridge and Component Properties			Deterioration Risk based on SHM and inspector findings are known				SHM-based ROI
Bridge	Component	Importance of components	SHM Finding (0-pristine to 5-failed/ verge of failure)	SHM Cost	Recommended action, based on SHM	Risk = f(B,D,(J+N))	Risk reduction ROI
#1	Girder	H	4	$ 1,200.00	Loss of section is more extensive, a lot more action	$ 801,200.00	**833.33%**
#1	Girder	H	3	$ 1,000.00	Vibartion is a lot more damaging, some action is needed	$ 121,000.00	**500.00%**
#1	Global	H	0	$ 5,000.00	Adequate remaining life	$ 5,000.00	**21174.40%**
#2	Girder	H	2	$15,000.00	Loss of section is not as extensive, only paint is needed	$ 1,103,720.00	**7058.13%**
#2	Global	H	4	$10,000.00	Need some action to fix vibration sources	$ 810,000.00	**10787.20%**
#3	Eye bar	L	4	$ 1,000.00	Needs fixing	$ 3,000.00	**100.00%**
#3	Eye bar	L	3	$ 1,000.00	Some attention is needed	$ 7,000.00	**1000.00%**
#3	Eye bar	L	0	$ 1,000.00	None	$ 1,000.00	**500.00%**
#3	Global	H	0	$ 1,000.00	None	$ 1,000.00	**0.00%**

Figure 48: Dashboard for computing deterioration risk ROI of SHM

- *Importance of component*: subjective description of the importance of the component for bridge well-being;
- *SHM finding*: subjective condition rating on a scale of 0 to 5. This finding is based on SHM results, in addition to the inspectors finding. Note that this value can be 1) greater than, 2) smaller than, or3) equal to the corresponding inspectors finding in Figure 47;
- *SHM costs*: estimation of SHM costs which is the value of *Investment* in Equation 36;
- *Recommended action* (*based on SHM finding*): descriptive notes of the recommended action based on SHM findings. Note that this can be: 1) more repair efforts, 2) less repair efforts, or 3) no action, as compared to Figure 47 actions;
- *Risk* ($Ri_{DET|SHM}$): monetary description of risk. The computations account for importance of the bridge, the importance of the component, the severity of the SHM finding, and the forecasted costs of waiting;
- *SHM* (*ROI*): computed from corresponding risk values in both Figure 47 and Figure 48 as:

$$ROI = \frac{Ri_{DET} - Ri_{DET}\big|_{SHM}}{Investment} \tag{36}$$

Again, the SHM *ROI* is fairly considerable as can be observed in this analysis reported in the last column of dashboard in Figure 48. This holds for every case documented in the analysis for the three bridges and for the variety of damage conditions modeled.

SECTION 9
DECISION MAKING TOOLCHEST

Introduction

A key objective of the project was the creation of a data-to-decision support system for railroads seeking to utilize SHM data to make better decisions around the management of the risk and resiliency of their rail networks. Towards that end, the team designed a scalable database system within a public cloud environment that was designed to archive railroad inspection and structural management data, sensor data emanating from CRS&SI data sources, and structural configuration data pertinent to a variety of analyses owners may seek to perform on their bridges. In this section, the data-to-decision architecture is briefly summarized ranging from data capture to the presentation of data and risk/resiliency analyses in the Decision Making Toolchest (DMT) as shown in Figure 49. The DMT was designed to be an end-user's primary portal to the data and analytical frameworks presented in the previous report sections.

Architecture Overview

The first component of the data-to-decision framework is data capture. This stage primarily consists of gathering information on the bridges being monitored and the networks they are functionally part of. Included in the data capture stage was the acquisition of wireless monitoring, WILD and other CRS&SI data. The data capture stage has already been presented in previous sections of this report (*e.g.,* wireless SHM systems installed on the project bridges, for example). The second stage of the framework is the automated analytics that were used to process the monitoring data as it is gathered – this stage is termed the data extraction stage. For

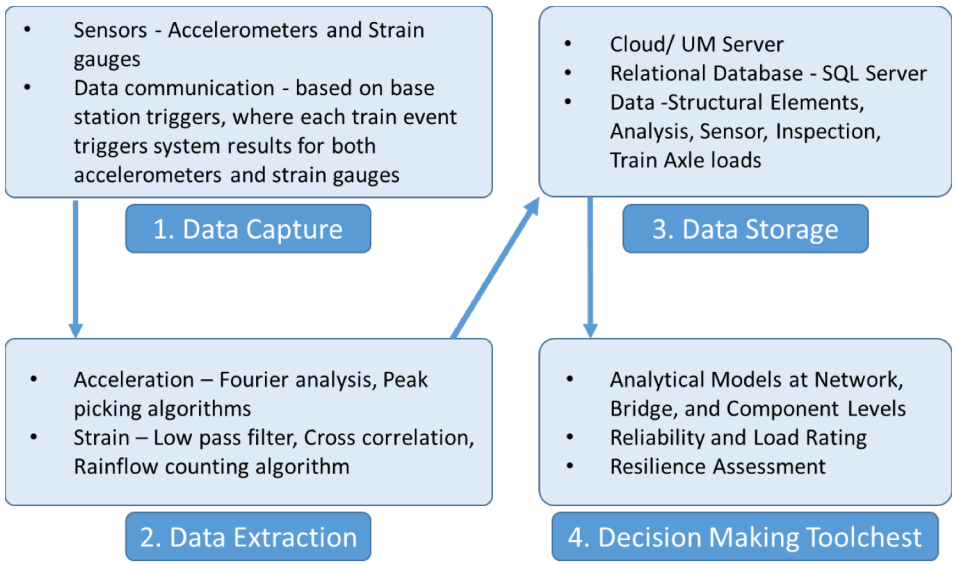

Figure 49. Data-to-Decision Architecture

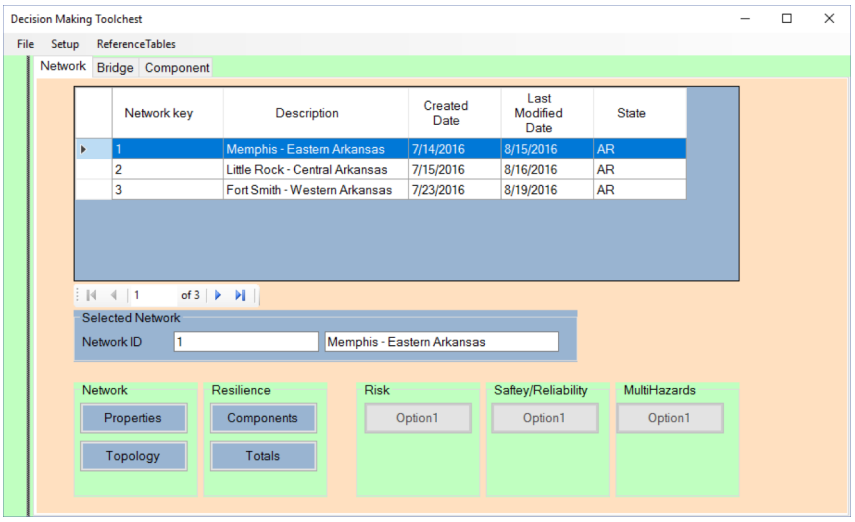

Figure 50. Main screen of the DMT platform

example, a wide variety of analyses presented in the previous sections were implemented such as modal analysis in the frequency domain, peak picking in the time domain, and fatigue assessment (*e.g.*, rainflow counting and Miner's rule). The third stage of the data-to-decision framework is the data storage stage. This stage primarily consisted of the development of a relational database system (Microsoft SQL Server) for the secure storage of information and data. The data held in the database includes structural properties, historical visual inspection data (including the condition of different components and bridges), sensor data, WILD data, structural analysis models such as finite element models of bridges, and bridge management metrics. The database schema was structured and normalized to ensure that data sets are stored efficiently and optimized for the highest level of query performance.

One of the most important aspects of using rich and extensive sets of data (such as those collected in this project) is how data is used to make decisions. To facilitate decision making, data is only effective if it is communicated to end users in a clear and concise manner. Hence, the fourth stage of the data-to-decision framework is the creation of a Decision Making Toolchest (DMT). DMT integrates the aforementioned analytical models (Sections 5 through 8) to evaluate data from different perspectives. Raw data is turned into usable and timely information to understand the actual condition of components and to predict future component behavior. Results are provided to decision-makers through a rich palette of visual dashboards as will be shown in this section. The DMT is a Windows-based application developed in the Microsoft .NET environment using C#. It runs on Windows 10 and requires an SQL database. Analysis in the DMT can be done at three different levels: network-, bridge- and component-levels (Figure 50). The DMT framework allows for scalability as new analytical models can be added at different levels.

Network Level

Each network is stored in the database with a unique key (number). For the selected network, its properties and topology are displayed (Figured 51). DMT incorporates a resilience model at the

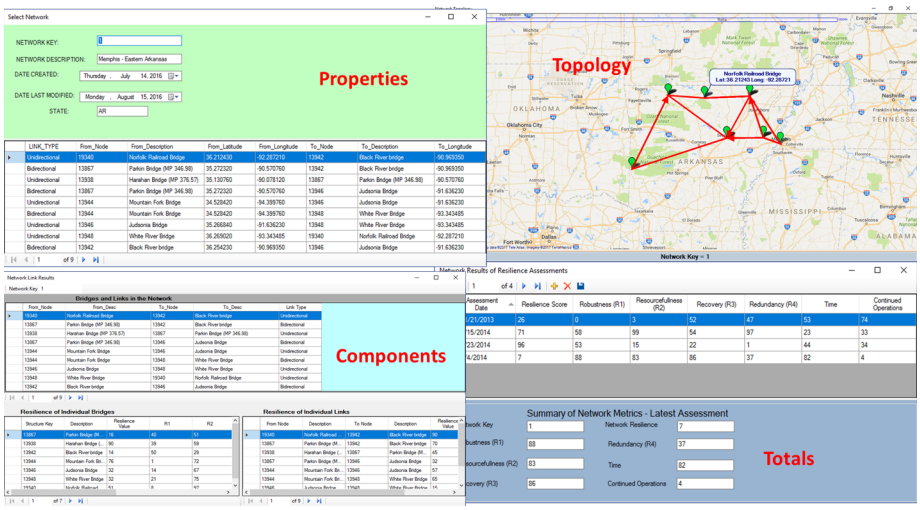

Figure 51. Network Related Screens

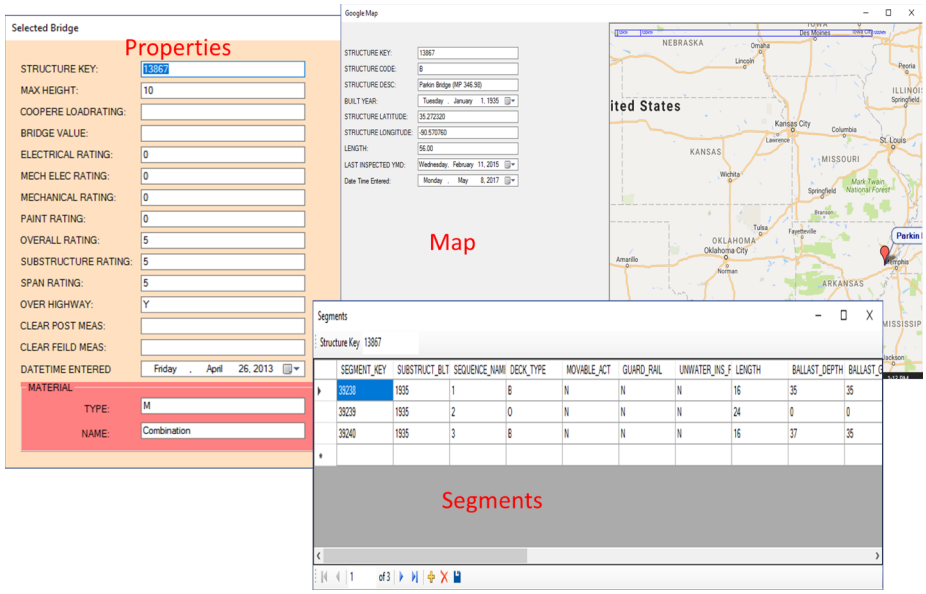

Figure 52. Bridge properties, map and segments screens

network level. The DMT resilience model depends on quantifying the robustness, resourcefulness, recovery, and redundancy (*i.e.*, 4Rs) of a network. Resilience assessment of network components are presented for better visualization. Resilience values along with the 4Rs are presented for an assessed bridge. Similarly, the resilience values of links between bridges are also displayed under components. A section of the dashboard is reserved to displays all the assessments done for the network along with the latest assessment. Assessments provide infrastructure owners the ability to reduce the magnitude and/or duration of disruptive events.

Bridge Level

Each bridge is stored in the relational database with a unique structure key. The bridge-level dashboard screen (Figure 52) lists all bridges stored in the database. A user can select a bridge to

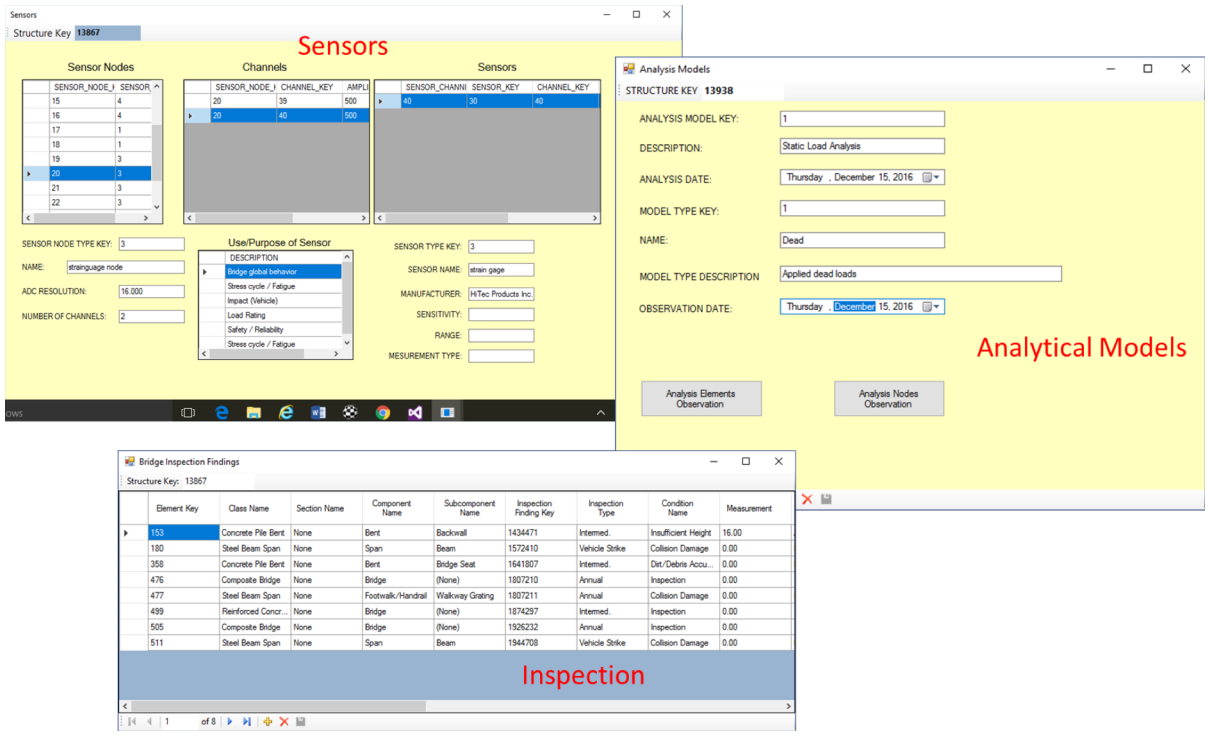

Figure 53. Sensors, inspection, and analytical model screens

display its related information. For a selected bridge, its properties, location, inspection history, sensors, and analysis models can be displayed by clicking on buttons on the bridge-level dashboard screen. Some key features of the bridge-level dashboard:

- Clicking on the structural properties opens a new window displaying properties such as height, ratings, and material;
- a map displays the bridge location on Google Map based on its latitude and longitude coordinates (many of the features in the Google map are integrated in the DMT software);
- a segments screen lists all the segments associated with the bridge;
- the historical inspection data is also presented to the user through the inspection screen (Figure 53);
- the sensor screen displays all sensors installed on the bridge including their node number, number of channels for each node, purpose of each sensor, and sensors attached to each channel (Figure 53).

Analytical models such as the FEM models developed for the bridge can be stored in the SQL database and displayed in the DMT. The software has the capability to store and display any number of analytical models for a selected bridge. The analytical model screen further displays the results from analyses performed including component strains, stresses, and forces, as well as the acceleration, displacement, and velocity response at model nodes. A resilience analysis can also be performed at the bridge-level; the results from such analyses show issues and assessment results (Figure 54).

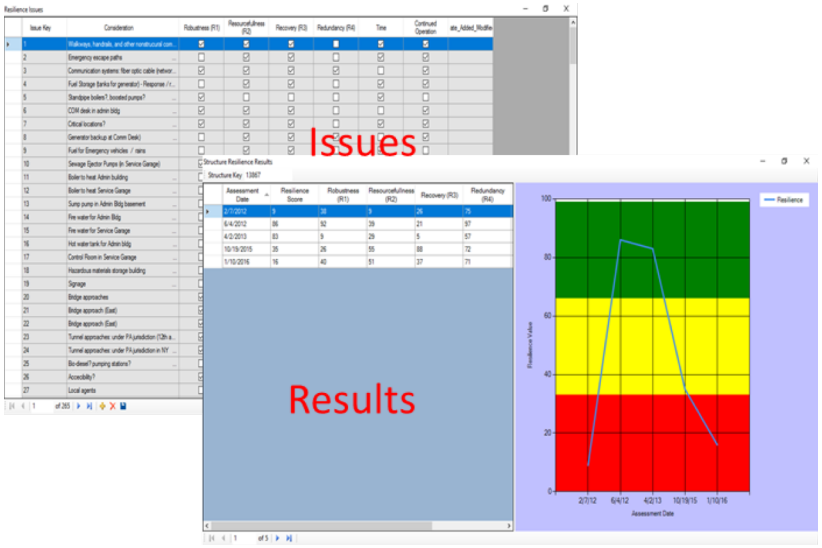

Figure 54. Resilience issues and assessment results screens

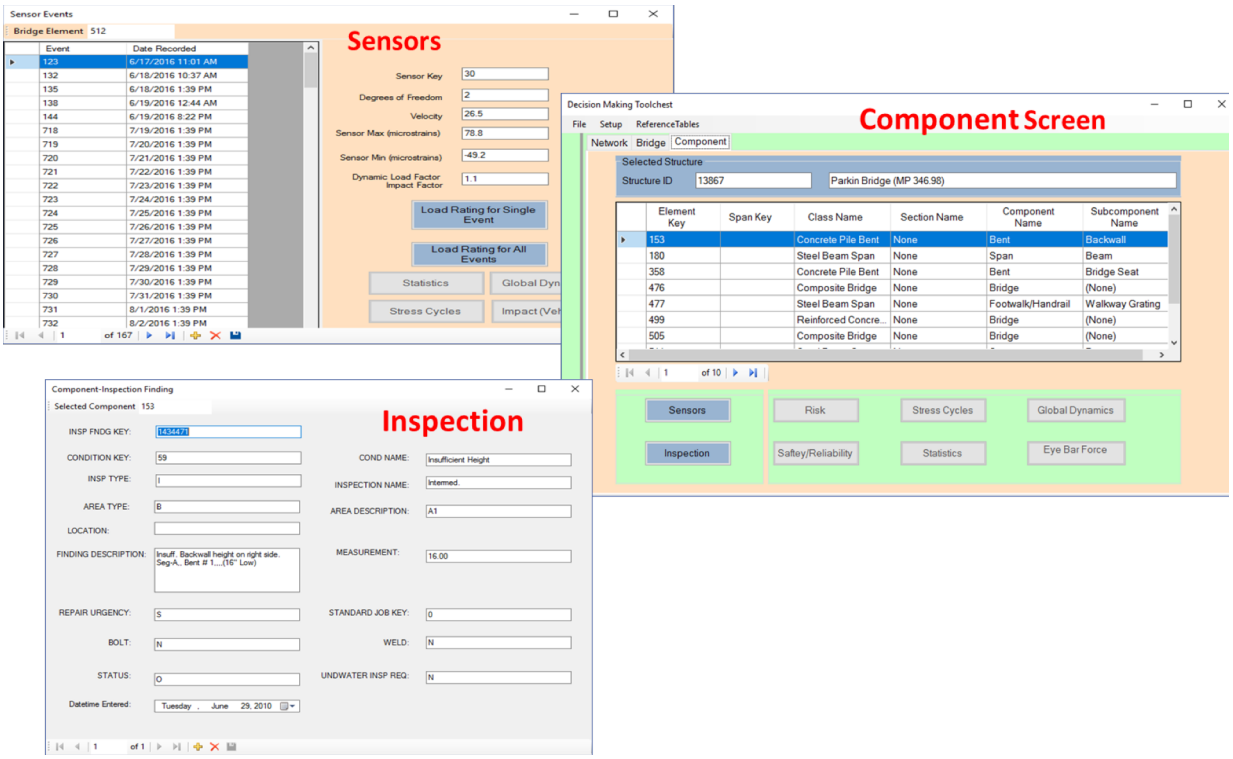

Figure 55. Component, sensors and inspection screens for a selected component

Component Level

The third level of analysis is done at the component level. All components for a selected bridge are displayed on the component screen (Figure 55), where each component is assigned with a unique number. For example, component ID 105 represents a stringer/floor beam connection in the floor system of the lower section of the Harahan Bridge. Inspection findings and sensor

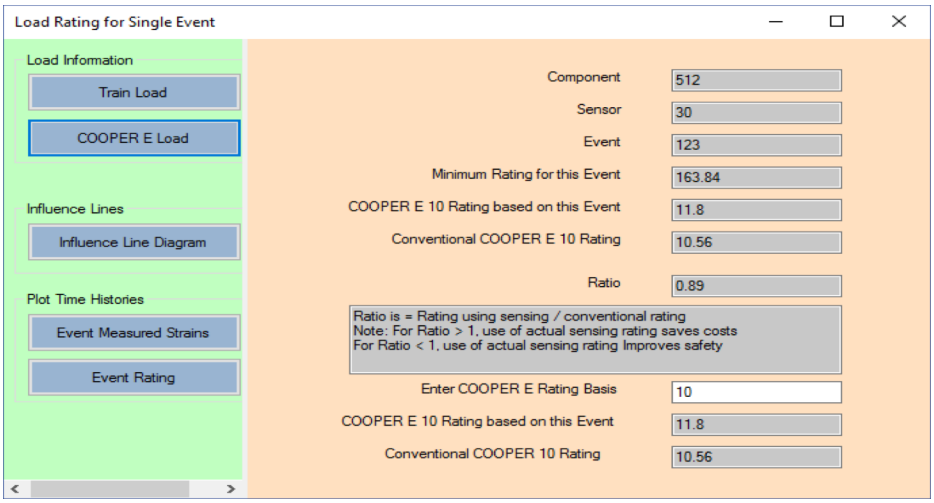

Figure 56. Load rating of a bridge component for a single train event

events related to sensor installed on the component can be accessed for the selected component (Figure 55).

Load rating is one of the analytical models implemented at the component level that has been integrated into the DMT software. Load rating is based on metrics of capacity and demand. Load rating for a single event or based on all train events is computed and presented to bridge owners. Figure 56 provides load rating results for a single event, which shows:

- Minimum rating - calculated using live load (LL) demand and dead load (DL) based on event axle data;
- Cooper E80 rating - calculated by extrapolating event based data to COOPER E80 loading;
- Conventional Cooper E10 rating - based on train LL demand and DL for COOPER E10 loading, and;
- Ratio - computed using sensing and conventional rating to show savings derived from performing a data-driven load rating analysis.

The estimation of dynamic load on the bridge from a train is based on measures of its static axle weights using calibrated monitored bridges. The analysis utilizes CRS&SI data (axle weights, locomotive locations, and bridge responses) to make estimates of the imposed dynamic load for rail bridges in a bridge network and to estimate the residual capacity of the monitored bridge systems in order to develop a reliability analysis (*i.e.*, calculation of reliability indices) of bridge components and spans (Figure 57).

Configuration

Through the DMT setup menu item, structure, bridge, segment, component, and sensors can be added easily to the database. The database has many reference tables, which stores an enumerated set of possible values of a certain field data type that can be accessed through

various screens (Figure 58). This allows users to easily modify their bridge and network information with ease.

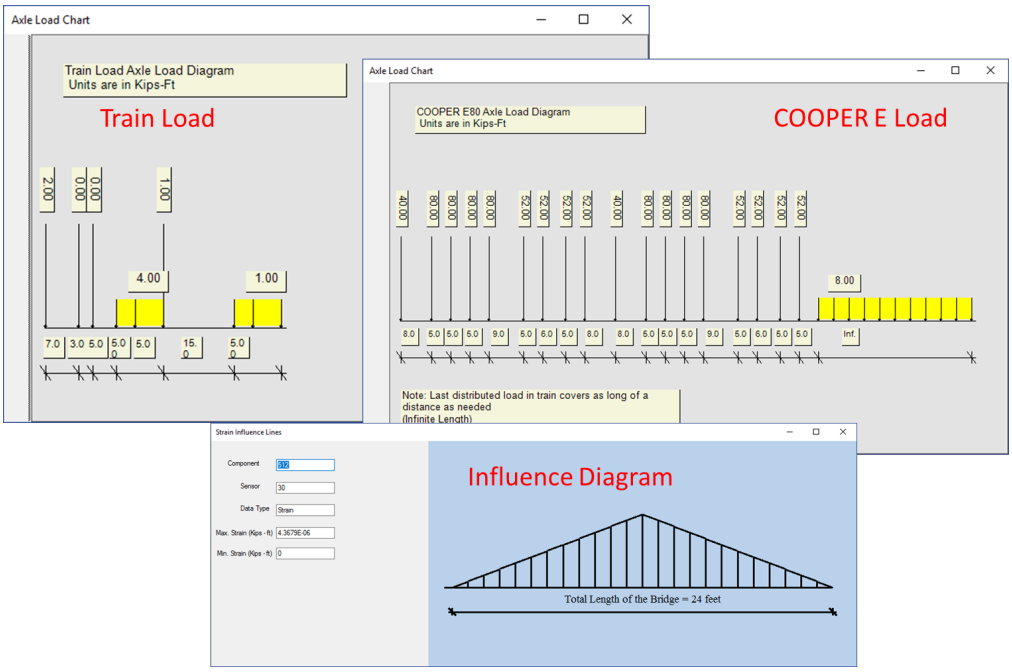

Figure 57. Train Load, COOPER E Load, and Influence Diagram

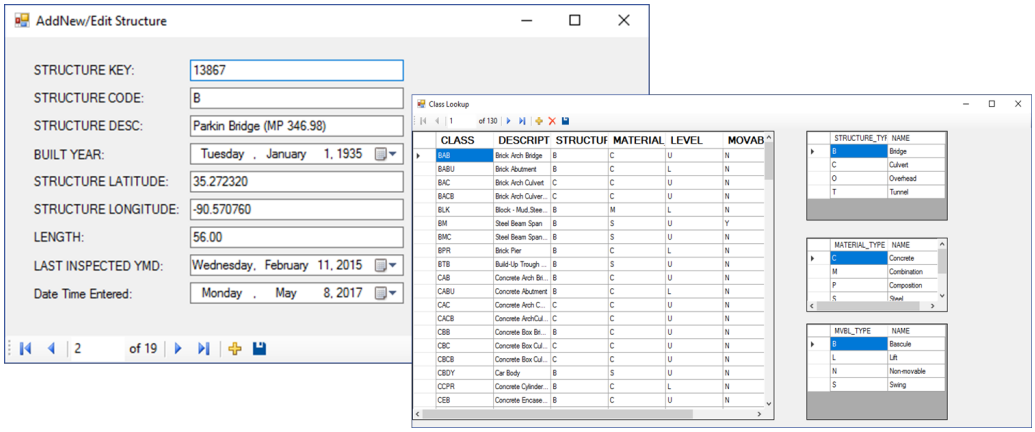

Figure 58. Add/Edit Database Tables

SECTION 10
COMMERCIALIZATION

One of the main goals of this USDOT project was to investigate the market potential of the technologies being developed by the project team, and to leverage this investigation to begin laying the groundwork for true commercialization of this funded research. In accordance with this objective, the commercialization team analyzed several markets that were deemed addressable by the project's technologies, developed an initial strategy to bring these technologies to market, and validated these technologies in a unique testbed aligned with our commercialization objectives.

This commercialization section must be read with the context that the main target user for the technologies developed in this project is UP. UP provided a large contribution to the cost sharing aspect of this project, and as such has shown great interest in the technologies proposed and developed by the project team. Clearly, the adoption and/or purchase of project technology by UP, which is the largest Class I railroad in the United States, could be used as the basis to attract many other potential users and customers. That said, it was important to identify and target a broader set of early stage customers to help accelerate early adoption and create a fertile playing field for commercial growth, and so early on the project team began to identify other stakeholders in related markets who might join UP as early adopters of the project's developed technologies. It is also important to note that because of the agreements signed with UP as part of their cost-sharing arrangement, the project team was not allowed, at least initially, to market the funded research to other US-based Class I railroads.

As with most technologies that are developed in the University environment, the technology advanced in this project has the potential to impact a number of different market verticals. While the obvious focus of the team's effort has been to create a system that addresses the needs of the UP, the commercial opportunities for the resulting technology are wide-reaching. However, in order to prevent our early analysis from becoming too broad and our marketing efforts from being spread too thin, the commercialization team focused their early efforts on analyzing the U.S. domestic railroad market.

U.S. Domestic Railroad Market Analysis

In the United States, the railroad industry is segmented into three "Classes" by the Association of American Railroads (AAR) and the Federal Railroad Administration (FRA). While these class definitions vary depending on the source, most commonly Class I railroads are those that have revenues greater than $467M, Class II railroads are those with revenues greater than $37.4M, and all other railroads are classified as Class III. Table 10 compares and contrasts this U.S. Railroad class system. Note that Class II and Class III data in Table 10 may not be completely accurate, as Class II and Class III Railroads are not required to submit annual data to the Surface Transportation Board (STB).

In order to assess the commercialization potential that exists in this market, it was first necessary to make several assumptions. First, we assumed that a Class II or Class III railroad would have

Table 10: United States Railroad Class System Overview

Class	Number	Miles Operated	Employees	Revenue
Class I	7	95,264	163,464	$67,600M
Class II	21	10,355	5,507	$1,400M
Class III	546	32,858	12,293	$2,600M

Table 11: Assumed financial capacity for a given railroad

Class	Revenue	Infrastructure Spending	Bridges	Available Per Bridge
Class I	$9,657.14 M	$941.57 M	7469	$252,125
Class II	$66.67 M	$6.50 M	271	$48,037
Class III	$4.76 M	$0.46 M	33	$28,115

the same expense structure as a Class I railroad. To this end, we assumed that all railroads spend 15% of their annual revenue on capital expenses (which is true of Class I). We also assumed that 65% of all railroad capital expenses are related to infrastructure (Class I railroads report that between 50% and 80% of their capital expenses are infrastructure related). More practically, we assumed that the number of bridges owned by a railroad scaled linearly with the miles of track owned by that railroad (so if a given railroad owned 10% of the nation's rail, they would also own 10% of the nation's 77,000 rail bridges). Lastly, we made some assumptions as to the financial ability and desire of a given railroad to procure the technology that we are developing in this project. Specifically, we assumed that a given railroad would be capable of siphoning 10% of their yearly infrastructural spending to procure new technology, and we assumed that in order to make this technology valuable, a given railroad would need to be able to outfit 5% of their existing bridges with this technology in a given year (so that a 20-year plan would result in the outfitting of almost all of their bridges with the proposed system). The resulting assumed financial situation (for a given railroad) is presented in Table 11.

From Table 10 and Table 11, it can be deduced that the U.S. railroad market size for our technology is roughly $698.2M ($659.1M Class I, $13.7M Class II, and $25.4M Class III). At a high level, it is clear that the best pathway to commercialization here is through the Class I railroads, and our intent is that UP will be the first adopter of this technology in the marketplace. That said, the purpose of this analysis is to view the commercial potential of the technology outside of this immediate beachhead. To that end, several conclusions can be drawn:

- Class I railroads (outside of UP) represent a huge market opportunity. However, our ability to penetrate that market is hindered by the research contract and NDA that was signed with UP. That said, if this market potential is truly there, it is our belief that there is a business arrangement available between Civionics/Prospect Solutions and UP that would allow us to expand our technology to the rest of the Class I railroads.
- Class II railroads have the potential to be an ideal domestic target for secondary sales outside of UP. The $48K per bridge that we assume will be available for this sort of technology creates enough cash availability to make sales possible, and there are a limited number of customers in the Class II market, making high market penetration a very real possibility. However, as discussed below, individual

- Class III railroads are likely not going to be a viable target market. At a high level, a given Class III railroad would have to spend roughly 1% of their annual revenue on each bridge they outfit with our technology, which is likely not going to fall within their budget range. In speaking with several Class III railroads, we discerned that while they see great value in the product that we are developing (bridge health is an on-going concern for them – with damage mostly being caused by adjoining property owners), they already spend roughly $1K per year per bridge on inspections, and they are unlikely to be willing to expand this budget unless the added technology would also reduce their regulated requirement to visually inspect their infrastructure on a yearly basis.

Go-To-Market Strategy

In order to begin refining our assumptions and go-to-market strategy, the project team spent considerable effort reaching out to stakeholders in the US domestic rail industry. In addition to calls with individual stakeholders, members of the project team also obtained valuable feedback from both a trip to the Q4 2015 USDOT CRS&SI Technologies Program Workshop, and from a Q1 2016 conference call that convened the members of our project's Technical Advisory Council (TAC). After taking into consideration feedback from all of these groups and individuals, it was determined that while a market interest certainly exists in the technologies that are being developed in this project, the product offering that was initially outlined in the project proposal may garner very little commercial traction in the domestic rail market.

Fundamentally, the Class II and Class III railroads (and to a lesser extent the Class I railroads), are hesitant to devote a considerable amount of resources to installing a long-term monitoring solution on the vast majority of their existing infrastructure. In the Class II and Class III case, this hesitancy is driven mostly by the overall hardware/software costs of such an installation (which we have deemed would have to be at least $50,000 per bridge). However, in the Class I case, the bigger issue that arose was the number of labor hours required to perform an intensive installation on a piece of critical infrastructure. While these installation costs could certainly be brought down by having an experienced team perform the installation, all parties (regardless of railroad Class) argued that the more valuable system would be one that could be rapidly deployed on a single bridge, left to sit for a day or two to allow enough data to be collected to perform an informed load rating or fatigue analysis, and then quickly brought down and moved to another location.

To this end, the project team began to discuss the feasibility of using Civionics' existing commercial wireless sensing technologies to create a rapid-to-deploy system for the short-term monitoring and load rating analyses of railroad bridges. A Q2 2016 trip to the Transportation Technology Center (TTCI) in Pueblo, CO provided initial confirmation of the demand for this type of technology, and also presented an extremely accessible testbed for evaluating and demonstrating the capabilities of this rapid-to-deploy system.

After establishing the validity of a market for a rapid-to-deploy technology that can provide quantitative data related to load rating and fatigue analyses, the project team began to outline a short list of stakeholders that would (a) most benefit from this type of product or service, and that

Table 12: Initial Stakeholder List

Entity	Railroads	Miles	Headquarters	Revenue
Union Pacific Railroad	1	32,100	Omaha, NE	$21.9 Billion
Genesee & Wyoming Inc.	120	15,500	Darien, CT	$1.6 Billion
Watco Companies LLC	35	4,500	Pittsburg, KS	$464 Million (est.)
Patriot Rail Company LLC	17	510	Jacksonville, FL	$53 Million (est.)
Pioneer Railcorp	23	600	Peoria, IL	$62 Million (est.)

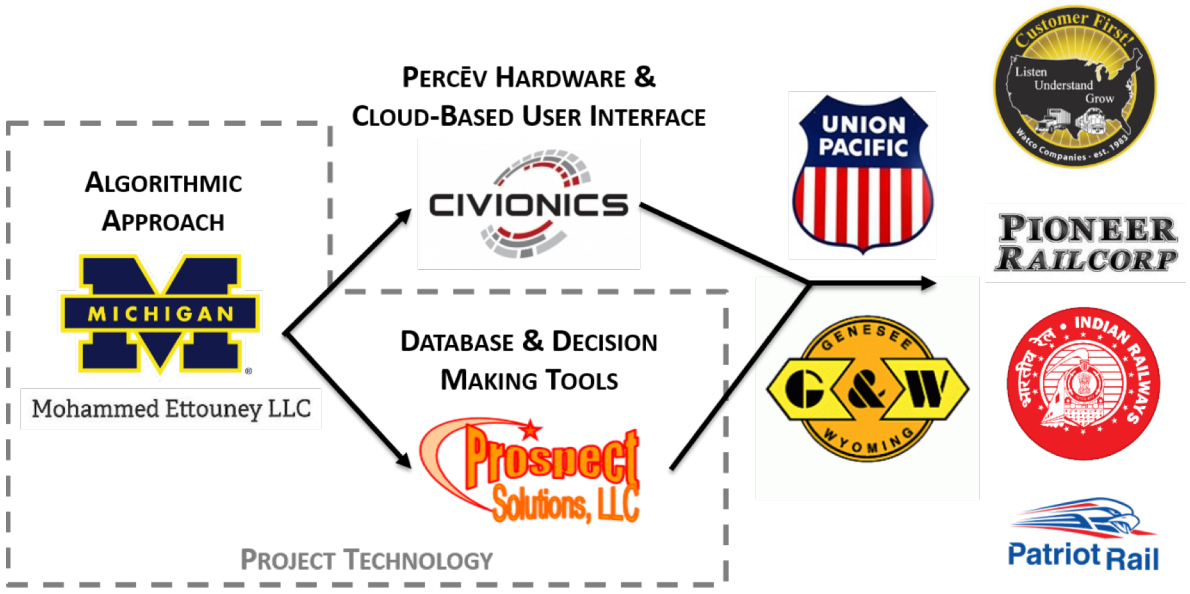

Figure 59. Commercialization flowchart

(b) have the financial wherewithal to serve as initial adopters of this technology. While ultimately all Class I railroads in the United States fit the mold of a potential Stakeholder, the project team's agreements with UP restrict Class I commercial expansion, at least initially, to UP itself. Additionally, when looking outside of the obvious Class I market, it was determined that no one Class II or Class III railroad owns enough infrastructure or has enough available capital to serve as a viable long-term buyer of our proposed product / service. However, many Class II and Class III railroads are owned by holding companies who have large infrastructure-related budgets to cover maintenance and repairs of a considerable amount of track. Table 12 was created to outline the five entities, which the project team intends to target as initial customers of our proposed product/service. In addition to the entities documented in Table 12, the project team has also begun to communicate with the U.S. Department of Commerce, Caton Infra Tech (Bangalore, India), Indian Railways, the Southwest Jiaotong University Railway Development Company (Chengdu, China), and Zhejiang University (Hangzhou, China) about our technology's potential in the international railroad market.

Through the course of the project timeline, the commercialization team worked with the University of Michigan to begin to position ourselves in such a way that project technology could flow to this initial target market with minimal obstruction. Figure 59 demonstrates this

Figure 60. TTCI West Steel Bridge

proposed approach, where technology developed within the confines of the funded research could be licensed by Civionics and incorporated with Civionics' pre-existing Percēv Hardware and Cloud-Based set of data services. Then, a joint partnership between Civionics and Prospect Solutions could provide comprehensive, value-adding solutions to the initial adopters of this technology. In order to protect the project team from potential competition, the project team also negotiated with the University of Michigan to secure the rights to lead the development of a patent application that would comprehensively cover the proposed railroad monitoring solution. As the project is nearing its completion, the patent application text is complete and we are working with our patent attorney to finalize the patent application itself.

Commercialization Testbed

In order to validate the short-term deployment strategy that the commercialization team proposed for attacking our initial beachhead market, the project team was fortunate to leverage the infrastructure owned by the Transportation Technology Center (TTCI) in Pueblo, CO. These commercialization tests took place during two distinct weeks, one in late 2016 and one in early 2017.

In late 2016, two of Civionics' wireless sensing and data processing nodes were deployed to monitor strain, displacement, temperature, and acceleration on the 24' span of TTCI's West Steel Bridge (Figure 60). This span is very similar to the project's Parkin Bridge, allowing for an one-to-one comparison with data being collected and processed by the University of Michigan system. The first objective of this deployment was to show how rapidly the project's technology could be deployed on a typical rail bridge. To this end, a single untrained engineer was able to deploy four strain gauges, one displacement transducer, and two Civionics' wireless nodes in under two hours. This process involved: 1) grinding the steel at each of the four strain gauge installation locations, 2) welding each of the four gauges to the structure, 3) deploying a string potentiometer at the midspan location, 4) running all cables through glands into Civionics' watertight enclosures, 5) connecting those cables to Civionics' data acquisition hardware, 6) installing batteries in each wireless node, and 7) magnetically attaching each wireless node to the bridge. Figure 61 shows the supplies used and one of the wireless nodes post-installation.

Figure 61. TTCI West Steel Bridge

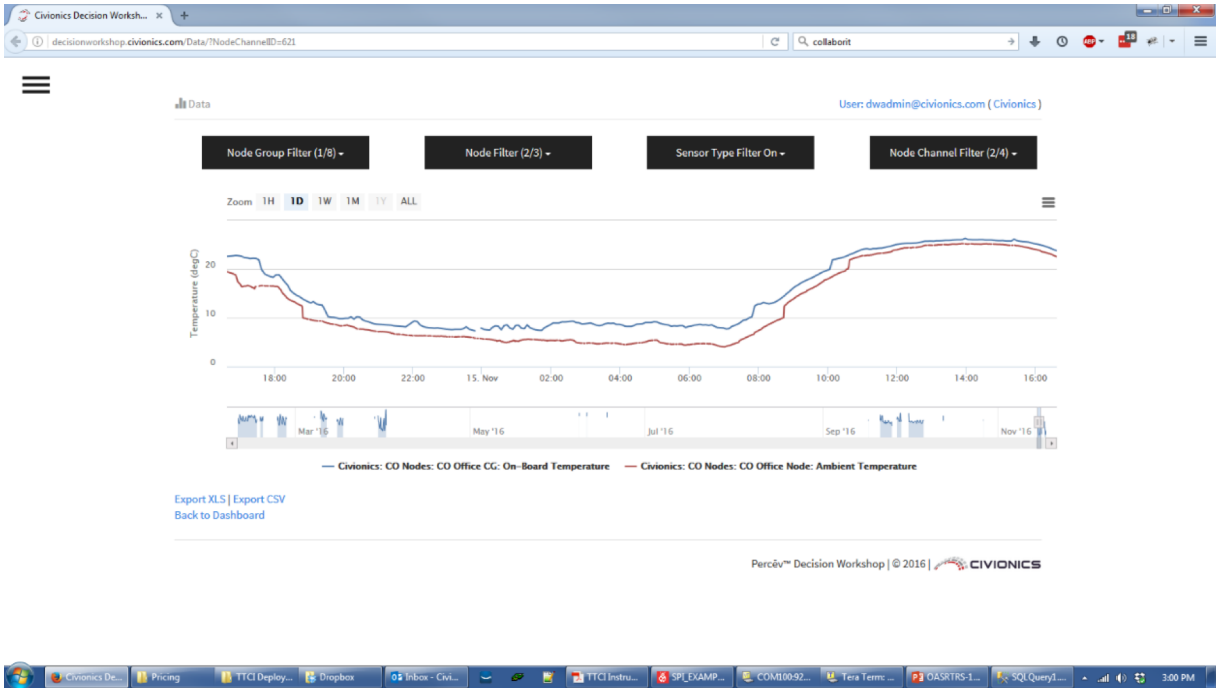

Figure 62. Day 1 temperature data as seen using Civionics' web-based UI

While this bridge is unusually accessible from below, this exercise confirmed that each weldable strain gauge can be installed in under twenty minutes, and each wireless node can be deployed in roughly fifteen minutes. In the future, epoxy-based strain gauges might be used in place of the weldable gauges because 1) epoxy would be easier to work with in less accessible locations, and 2) an epoxied system might allow mounting blocks to be put into place such that the gauges themselves, along with the wireless hardware, could be reused from bridge to bridge.

Once deployed, the technology was used to remotely monitor bridge functionality for a four-night period. Each of these four nights, the TTCI train (three engines, 70 cars) ran the loop of the test track roughly 120 times at a speed of roughly 40 miles per hour. This meant that the monitored bridge was crossed once every four minutes. The Civionics' system performed several different operations during the monitoring campaign. First, it monitored ambient temperature at one minute intervals and reported this data to the cloud in real-time (Figure 62). Second, it

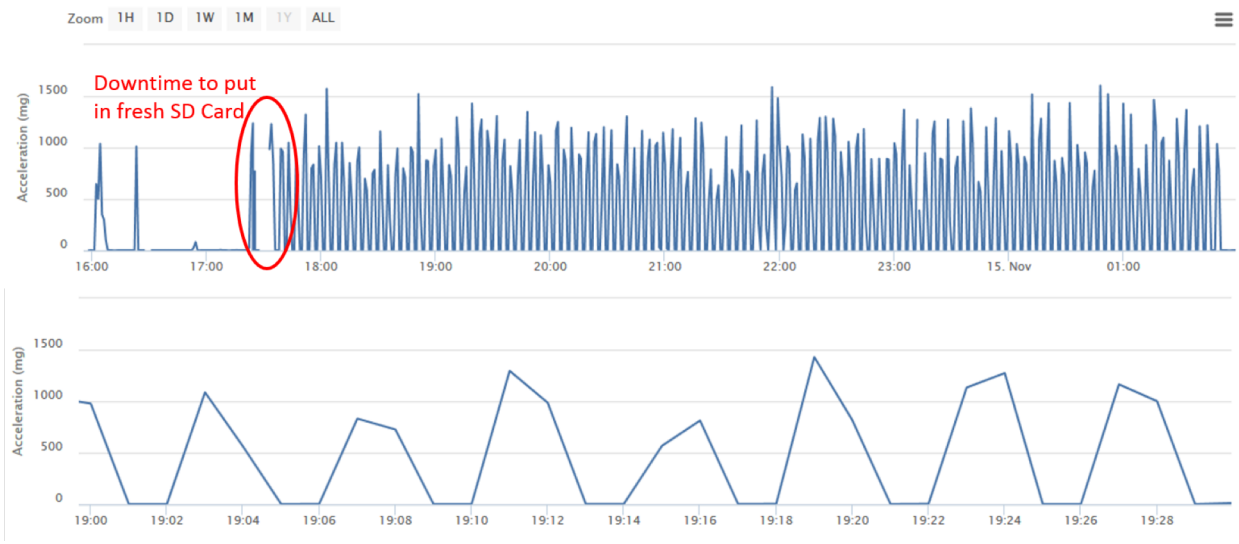

Figure 63. Night 1 processed maximum acceleration data on Civionics' web-based UI

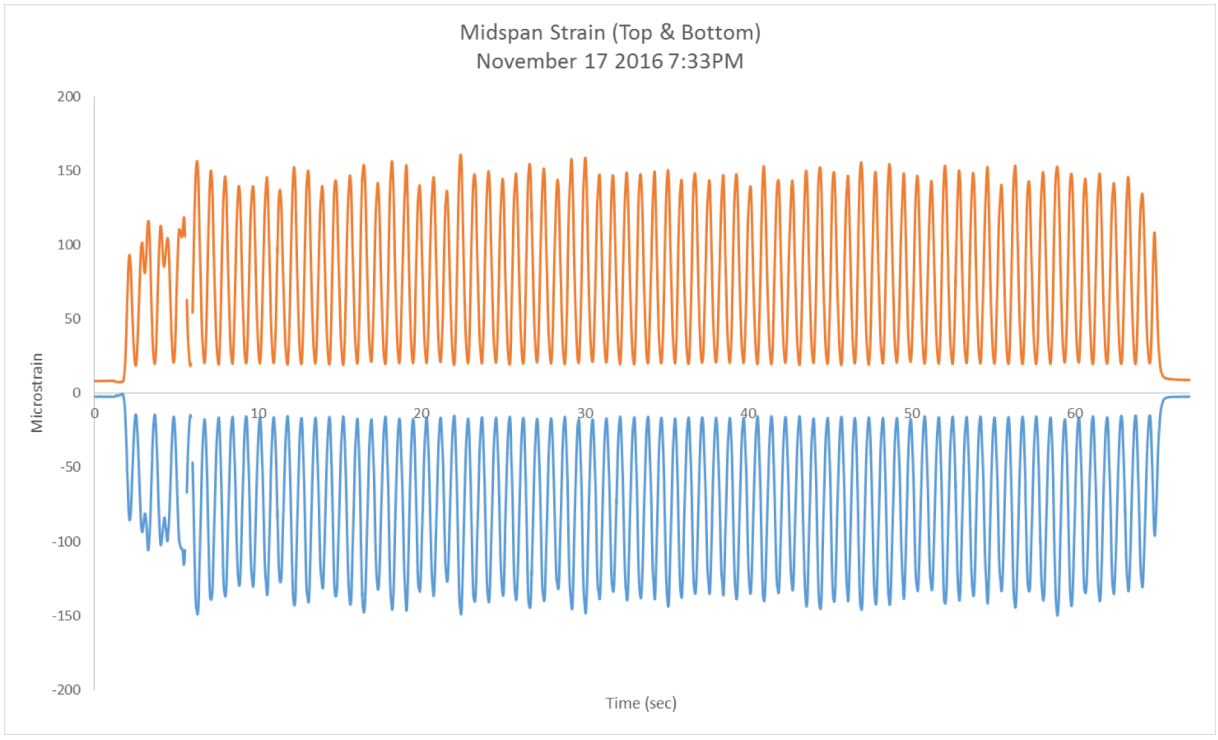

Figure 64. Night 4 raw mid-span strain data (top and bottom) as captured on SD card

captured the maximum acceleration to occur on the bridge during every one minute interval and sent this data to the cloud in real-time (Figure 63). Lastly, it triggered an analysis on the collected strain data whenever that data exceeded 50 µstrain. Because of the academic nature of these tests all triggered strain data was logged on an embedded SD card so it would be available for later comparison to data collected by TTCI's existing data acquisition system (Figure 64).

In the end, these tests showed the ability of Civionics' wireless data acquisition and data processing hardware to be quickly deployed with minimal resource need, and validated the ability of low-cost wireless sensing technology in the railroad setting to: 1) collect high quality strain, acceleration, and temperature data, 2) push both raw and processed data to the cloud for data storage and visualization, 3) locally store large quantities of raw data via SD card, and 4) process collected data onboard for enhanced battery life and ease of use.

As a follow-up to these initial tests, the project team returned to TTCI in early Spring 2017 in order to further validate the project technology with a focus on embedding some of the project's algorithms in the computational core of Civionics' wireless sensing nodes. In this return trip, a single Civionics Percēv Node was deployed to monitor two of the pre-installed strain gauges, and was programmed to assess both static and dynamic strain in real-time. This focus was a first step towards providing an out-of-the-box system for evaluating DLFs in real-time as trains cross a monitored bridge. The deployed node, which also contained a cell modem and battery pack for remote connection to Civionics' cloud-based data services, was set up and configured on the TTCI infrastructure in under 20 minutes.

In this set of tests, an assessment of static and dynamic strain was triggered every time the TTCI train crossed the monitored bridge, and results of each bogey crossing was pushed to the internet in real time over the Percēv node's cellular connection. Figure 65 shows the first six captured transits, as the train gained speed for its nightly run around the TTCI track (with one transit of the bridge roughly every four minutes.

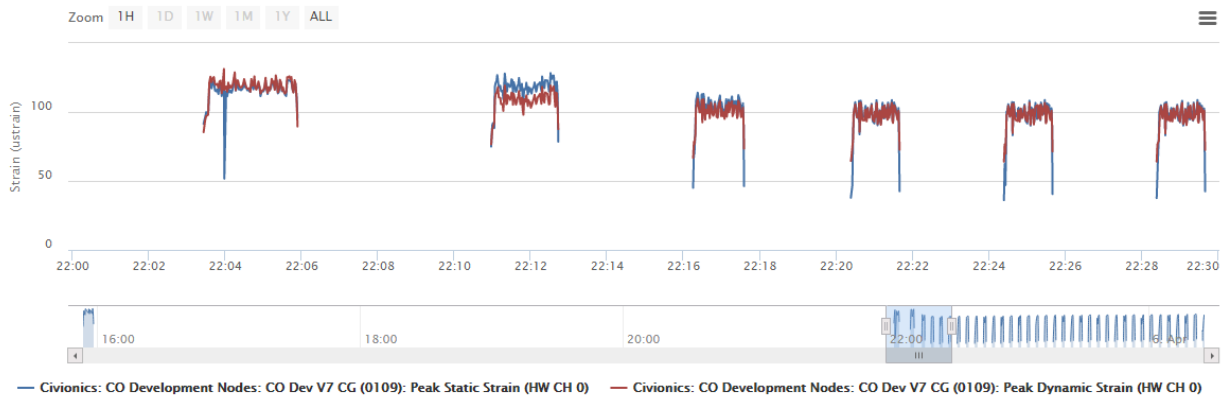

Figure 65. Spring 2017 Real-Time Embedded DLF Analysis at TTCI

REFERENCES

AASHTO (2012). *LRFD Bridge Design Specifications*. American Association of State Highway and Transportation Officials, Washington DC.

AREMA (2006). *Manual for Railway Engineering*, American Railway Engineering and Maintenance of-Way Association, Lanham, MD.

ASCE (2103). *2013 Report Card for America's Infrastructure*, American Society of Civil Engineers, Reston, VA.

Blevins, R. D. (2016). "Natural Frequency of Beams." *Formulas for Dynamics, Acoustics and Vibration*, John Wiley & Sons, Somerset, pp. 134–202.

Bruneau, M., Chang, S., Eguchi, R., O'Rourke, T., Reinhorn, A., Shinozuka, M., Tierney, K., Wallace, W., Winterfelt, D. (2003). "A Framework to Qualitatively Assess and Enhance the Seismic Resilience of Communities," *Earthquake Spectra*, Vol. 19, No. 4, pp. 733-752.

CSI (2016). *CSiBridge 2016: Introduction to CSiBridge*, Computers and Structures Inc. Berkeley, CA.

DHS (2011a), *Integrated Rapid Visual of Screening of Buildings,* Building and Infrastructure Protection Series, Department of Homeland Security, Washington, DC.

DHS (2011b), *Integrated Rapid Visual Screening of Mass Transit Stations*, Building and Infrastructure Protection Series, Department of Homeland Security, Washington, DC.

DHS (2011c), *Integrated Rapid Visual Screening of Tunnels*, Building and Infrastructure Protection Series, Department of Homeland Security, Washington, DC.

EM-DAT (2017). *EM-DAT: The OFDA/CRED International Disaster Database*, Université Catholique de Louvain, Brussels, Belgium (www.emdat.be, accessed on May 2017).

Ettouney, M., Alampalli, S. (2012a). *Infrastructure Health in Civil Engineering: Theory and Components*, CRC Press, Boca Raton, FL.

Ettouney, M., Alampalli, S. (2012b), *Infrastructure Health in Civil Engineering: Applications and Management*, CRC Press, Boca Raton, FL.

Ettouney, M., Alampalli, S. (2017a), *Risk Management in Civil Infrastructure*, CRC Press, Boca Raton, FL.

Ettouney, M., Alampalli, S. (2017b), *Multihazards Considerations in Civil Infrastructure*, CRC Press, Boca Raton, FL.

Ettouney, M. (2014), "Bouncing Back from Disaster: Then New and Growing Field of Resilience Management and How it is Becoming Essential to Civil Infrastructure Recovery," *McGraw Hill Financial Global Institute*, New York, NY.

FEMA (1996), "Costs and Benefits of Natural Hazard Mitigation," Federal Emergency Management Agency, Washington, DC.

Flanigan, K. A., O'Connor, S., Lynch, J.P., Ettouney, M. (2017). "Reliability-Based Framework for Health Assessment of Link Plate Assemblies using Long-Term Bridge Monitoring Data," *Proceedings of the 12th International Conference on Structural Safety & Reliability,* Vienna, Austria.

FRA (2014). *Freight Rail Today*. Federal Railroad Administration, Washington D.C. (http://www.fra.dot.gov/Page/P0362, accessed on July 2016).

GAO (2007). "Railroad Bridges and Tunnels: Federal Role in Providing Safety Oversight and Freight Infrastructure Investment Could Be Better Targeted," Document Number GAO-07-770, *U.S. Government Accountability Office*, Washington, D.C.

Gostautas, R. S., Tamutus, T. A. (2015). "SHM of the Eyebars of the Old San Francisco Oakland Bay Bridge" *Proceedings of the 10th International Workshop on Structural Health Monitoring*, Stanford, CA.

Hess, P. E., Bruchman, D., Assakkaf, I. A., Ayyub, B.M. (2002). "Uncertainties in Material and Geometric Strength and Load Variables," Naval Engineers Journal, Vol. 114, No. 2, pp. 139–166.

Hibbeler, R. C. (2011). "Buckling of Columns." *Mechanics of Materials*, Prentice Hall, Boston, pp. 657–783.

Hughes, J.F., Healy, K. (2014). *Measuring the Resilience of Transport Infrastructure*, Research Report 546, New Zealand Transport Agency, Wellington, New Zealand.

Kane, M. B., Peckens, C. and Lynch, J. P. (2014). "Introduction to Wireless Structural Monitoring Systems: Design and Selection," in *Sensor Technologies for Civil Infrastructures: Performance Assessment & Health Monitoring* (ed. Ming Wang, Jerome P. Lynch, and Hoon Sohn), Volume 1, Woodhead Publishing, London, pp. 446-479.

Kollár, L. (2003). *Structural Stability in Engineering Practice*. CRC Press, New York, NY.

Miner, M. A. (1945). "Cumulative Fatigue Damage." ASME Journal of Applied Mechanics, Vol. 12, No. 3, pp. A159–A164.

MMC (2005). *Natural Hazards Mitigation Saves: An Independent Study to Assess the Future Savings from Mitigation Activities: Volume 1 – Findings, Conclusions, and Recommendations*, Multihazards Mitigation Council, National Institute of Building Sciences, Washington, DC.

Moore, M., Phares, B., Graybeal, B., Rolander, D., Washer, G. (2001). *Reliability of Visual Inspection for Highway Bridges*, Report FHWA-RD-01-020, Federal Highway Administration, Washington DC.

Moreu, F., LaFave, J., Spencer, B. F. (2012). "Structural Health Monitoring of Railroad Bridges - Research Needs and Preliminary Results," *Structures Congress 2012*, Chicago, IL, 2012.

Munich RE (2013), *Munich Reinsurance America, Inc.*, New York, NY.

Munich RE (2014), *Munich Reinsurance America, Inc.*, New York, NY.

NIAC (2009). *Critical Infrastructure Resilience Final Report and Recommendations*, National Infrastructure Advisory Council, Washington, DC.

Nowak, A.S. (1999). "Calibration of LRFD Bridge Design Code." NCHRP Report 368, Transportation Research Board, Washington, DC.

O'Connor, S., Zhang, Y., Lynch, J. P., Ettouney, M., and Jansson, P. O. (2017). "Long-Term Performance Assessment of the Telegraph Road Bridge using a Permanent Wireless Monitoring System and Automated Statistical Process Control Analytics," *Structure and Infrastructure Engineering,* Taylor & Francis, 13(5): 604-624.

Otter, D., Joy, R., Jones, M. C., Maal, L. (2012). "Need for bridge monitoring systems to counter railroad bridge service interruptions," *Transportation Research Record: Journal of the Transportation Research Board*, Vol. 2313, pp. 134-143.

Palley, J. (2013). *Freight Railroads Background,* Federal Railroad Administration, Washington, D.C.

Peckens, C., Kane, M. B., Zhang, Y. and Lynch, J. P. (2014). "Introduction to Wireless Structural Monitoring Systems: Permanent Installation in Infrastructure Systems," in *Sensor Technologies for Civil Infrastructures: Performance Assessment & Health Monitoring* (ed. Ming Wang, Jerome P. Lynch, and Hoon Sohn), Volume 1, Woodhead Publishing, London, pp. 480-509.

Reid, R. L. (2010). "Damaged Eyebar Section Replaced On San Francisco--Oakland Bay Bridge." *Civil Engineering Magazine*, American Society of Civil Engineers, Vol. 80, No. 4.

Swartz, R. A., Jung, D., Lynch, J. P., Wang, Y., Shi, D., Flynn, M. P. (2005). "Design of a Wireless Sensor for Scalable Distributed In-network Computation in a Structural Health Monitoring System." *Proceedings of the 5th International Workshop on Structural Health Monitoring*, Stanford, CA.

Thoft-Christensen, P., Baker, M.J. (1982). *Structural Reliability Theory and its Applications*. Springer, New York, NY.

Vose, D. (2009), *Risk Analysis: A Quantitative Guide*, John Wiley and Sons, Hoboken, NJ.

Zhang, Y., Kurata, M., and Lynch, J. P. (2017). "Long-Term Modal Analysis of Wireless Structural Monitoring Data from a Suspension Bridge under Varying Environmental and Operational Conditions: System Design and Automated Modal Analysis," *Journal of Engineering Mechanics*, ASCE, 143(4): 04016124.

APPENDIX A: PROJECT DELIVERABLES

- Conduct meeting with Union Pacific engineers and identify three deck-plate girder union pacific bridges to be instrumented on the Chester and Jonesboro subdivisions. Report on identified bridges to USDOT within nine (9) months of the effective date of the agreement. (Del – 1a)
    - *Delivered via Q3 report (July 15, 2015)*

- Sensor plans, including remote sensing, etc. Report on results (requirements document) due to USDOT within nine (9) months of the effective date of the agreement. (Del – 2a)
    - *Delivered via Q5 report (January 15, 2016)*

- Reliability, risk, and resilience methodologies report. Report on results due to USDOT within twenty one (21) months of the effective date of the agreement. (Del – 3a)
    - *Delivered herein (May 30, 2017)*

- Instrument Harahan Bridge with remote wireless sensors. Report due to USDOT within fifteen (15) months of effective data of the agreement. (Del – 4a)
    - *Delivered via Q6 report (April 15, 2016)*

- Identify list of industry stakeholders for commercialization promotion. Report due to USDOT within fifteen (15) months of effective data of the agreement. (Del – 5a)
    - *Delivered via Q7 report (July 15, 2016)*

- Instrument one deck-plate girder bridge with remote wireless sensors. Report due to USDOT within twenty one (21) months of effective date of the agreement. (Del – 6a).
    - *Delivered via Q6 report (April 15, 2016)*

- Create commercialization report (*i.e.,* go-to-market commercialization roadmap) detailing promotion efforts planned for the developed products. Report due to USDOT within twenty seven (27) months of effective date of the agreement. (Del – 7a).
    - *Delivered via Q9 report (January 15, 2017)*

- Database structure reported in design document. Validate decision making toolchest (DMT) system using data. Evaluate analysis models and document the predicted outcomes. Report on results due to USDOT within twenty seven (27) months of the effective date of agreement. (Del – 8a)
    - *Delivered via Q10 report (April 15, 2017)*

- Decision making tool description and user guide. Report due to USDOT within thirty two (32) months of the effective date of the agreement. (Del – 9a)
    - *Delivered via Q10 report (April 15, 2017)*

- Paper submission to conference presentations and publication to peer review journals. Due to USDOT within thirty two (32) months of the effective date of the agreement. (Del – 10a)
    - *16 invited presentations and 6 conference/journal papers (Appendix B)*

- Create train load estimation algorithm. Report on results due to USDOT within twenty seven (27) months of effective data of the agreement. (Del – 11a)
    - *Delivered herein (May 30, 2017)*

- Create a public website highlighting the project developments within three (3) months of effective data of the agreement. (Del – 12a)
    - *http://www-personal.umich.edu/~jerlynch/rita/index.html*

- Create a webinar demonstrating CRS&SI and DMT technologies and presenting cost-benefit analysis for potential customers. (Del – 13a)
    - *Delivered herein (May 30, 2017)*

- Conduct semi-annual TAC conference call. (Del -14a)
    - *TAC call #1 completed (January 24, 2016)*
    - *TAC call #2 completed (July 27, 2016)*
    - *TAC call #3 completed (October 11, 2016)*

- Quarterly status and progress reports and final project report will be prepared and submitted in accordance with deliverables matrix of the basic agreement. (QPR – 1 through 8, FR – 1)
    - *Q1 through Q10 all submitted on time*

APPENDIX B: PRESENTATIONS AND PUBLICATIONS

Presentations:

- [October 24, 2014] Ettouney, M., and Lynch, J. P., "Union Pacific-University of Michigan: Intelligent Railroad Systems Initiative," presented to UP executive team, Union Pacific Railroad, Omaha, NE.
- [December 10, 2014] Lynch, J. P., "Wireless Cyber-Physical System Technologies for Enhancement of Infrastructure Resiliency," presented to the Department of Civil and Environmental Engineering, Massachusetts Institute of Technology (MIT), Boston, MA.
- [May 27, 2015] Ettouney, M., and Lynch, J. P., "Health Assessment and Risk Mitigation of Railroad Networks Exposed to Natural Hazards using Commercial Remote Sensing and Spatial Information Technologies," presented to UP Bridge Engineering Team, Union Pacific Railroad, Omaha, NE.
- [June 17, 2015] Ettouney, M., and Lynch, J. P., "Demand-Capacity Monitoring Paradigm for Risk-based Asset Management of Highway Bridges," presented to the 2015 American Society of Civil Engineers Engineering Mechanics Institute Meeting, Stanford, CA.
- [October 26, 2015] Lynch, J. P., and Zhang, Y., "Load Estimation of Highway Bridges using Structural Monitoring Data," Connecticut Bridge Weigh-in-Motion Workshop, Mystic CT
- [December 2, 2015] Zimmerman, A., and Lynch J. P. "A University Startup's Perspective on CRS&SI Business Planning and Market Analysis," presented at the USDOT CRS&SI Technologies Program Workshop #2, Oklahoma City, Oklahoma.
- [February 22, 2016] Ettouney, M., and Lynch, J. P., "Review of Project Activity: Instrumentation Status and Load Rating Methodology" presented to UP Bridge Engineering Team, Union Pacific Railroad, Omaha, NE.
- [March 22, 2016] Alampalli, S., Ettouney, M., and Alampalli, S., "Essentiality and Applications of Tripod Analogy for SHM Use in Bridge Management," *SPIE Smart Structures NDE Conference*, Las Vegas, NV.
- [March 22, 2016] Alampalli, S., Alampalli, S., and Ettouney, M., "Use of Big Data and High-Performance Analytics for SHM Use in Bridge Management" *SPIE Smart Structures NDE Conference*, Las Vegas, NV.
- [October 26, 2016] Alampalli, S., Alampalli, S., Ettouney, M., and Lynch, J. "Decision-Making Framework for Railroad Bridges Using Structural Health Monitoring and Big Data Analytics," *ASNT Annual Conference*, Long Beach, CA.
- [October 26, 2016] Ettouney, M., Alampalli, S., and Alampalli, S. "Resilience Monitoring of Single Bridges," ASNT Annual Conference, Long Beach, CA.
- [January 10, 2017] Lynch, J. P., "Health Assessment and Risk Mitigation of Railroad Networks Exposed to Natural Hazards using Commercial Remote Sensing and Spatial Information Technologies," USDOT RITA Booth, Transportation Research Board Annual Meeting, Washington DC.

- [January 11, 2017] Lynch, J. P., "Development of a Health Assessment and Risk Mitigation Strategy for Railroad Networks using Wireless Monitoring Technologies," Transportation Research Board Annual Meeting, Washington DC.
- [March 29, 2017] Flanigan, K., Johnson, N., and Lynch, J. P., "Utilization of Wireless Structural Health Monitoring as Decision Making Tools for a Condition and Reliability-Based Assessment of Railroad Bridges," *SPIE Smart Structures NDE Conf*erence, Portland, OR.
- [June 5, 2017] Lynch, J. P., Flanigan, K., Moreau, F., "Objective Resiliency Framework for Ensuring Railroad Network Safety and Efficiency," *Engineering Mechanics Conference (EMI) 2017*, San Diego, CA.
- [August 2017] Alampalli, S., Alampalli, S., Ettouney, M., and Lynch, J. "Data-to-Decision Framework for Monitoring Railroad Bridges," *9th NYC Bridge Conference*, New York City, NY.

Papers:

- O'Connor, S., Zhang, Y., Lynch, J. P., Ettouney, M., and Jansson, P. O. (2017). "Long-Term Performance Assessment of the Telegraph Road Bridge using a Permanent Wireless Monitoring System and Automated Statistical Process Control Analytics," *Structure and Infrastructure Engineering*, Taylor & Francis, 13(5): 604-624.
- Zhang, Y., O'Connor, S. M., van der Linden, G., Prakash, A., and Lynch, J. P. (2015). "SenStore: A Scalable Cyberinfrastructure Platform for Implementation of Data-to-Decision Frameworks for Infrastructure Health Management," *Journal of Computing in Civil Engineering*, ASCE, 30(5): 04016012.
- Jeong, S., Zhang, Y., Lynch, J. P., Sohn, H. and Law, K. H. (2015). "A NoSQL-Based Data Management Infrastructure for Bridge Monitoring Database," *Proceedings of the 10th International Workshop on Structural Health Monitoring*, Stanford, CA.
- Zhang, Y., O'Connor, S. M., and Lynch, J. P. (2015). "Automated Data-driven Load Estimation of Highway Bridges using Structural Monitoring Data," *Proceedings of the 7th International Conference on Structural Health Monitoring of Intelligent Infrastructure*, Turin, Italy.
- Lynch, J. P. (2015). "Wireless Sensor Network Technology for the Monitoring of Civil Engineering Structures," *Proceedings of the ASCE Metropolitan Section Infrastructure Group Emerging Technology in Infrastructure Management and Monitoring Seminar*, Brooklyn, NY.
- Alampalli, S., Alampalli, S., and Ettouney, M. (2016). "Use of Big Data and High-Performance Analytics for SHM Use in Bridge Management" *Proceedings of SPIE Smart Structures NDE Conference*, Las Vegas, NV.

APPENDIX C: WILD DATA ANALYSIS TO MODEL TRAIN LOADS ON MEMPHIS SUBJUNCTION

The purpose of this section is to provide histograms that give information about specific train types, and provide information explaining why certain structural responses at the Parkin and Harahan Bridges are observed in the study. Union Pacific provided WILD (entire network) and HBD (at the Presley Station) data from May 27, 2015 to January 28, 2016 (8 months). The HBD data was used to identify trains on the Memphis subjunction; using train identifiers, the same train was then identified in the WILD data base with train attributes (such as axle loads) extracted.

Train Car Weights and Axle Counts

The initial histograms for the length of each car, weight of each car, and number of axles in each car indicate that, while there is little variation in the locomotive characteristics, there was a wide variety of freight cars that pass by the WILD detectors. In order to understand the behavior of each type of car, car characteristics will be categorized in the following two ways:

- First, histograms are created for the length (distance from front axle to back axle) and weight of each freight car categorized by cars with four axles, six axles, eight axles, and twelve axles.
- Second, histograms are created for the length (distance from front axle to back axle) and weight of each freight car based on car code type. Car code types are based on AAR Equipment Type and Trailer/Container Type Codes. Table C1 provides descriptions of the code, the number of cars that fall into each code category (for the eight months of WILD data), and the number of axles that each car has.

Based on Table C1, looking at the frequency of each car type per code based on number of axles (highlighted by the red box), it can be seen that even when cars are categorized by code type, the number of axles in each car can vary within each specific type. For example, 681 type “F” flat cars have four axles (98.6% of all type “F” cars), 9 have eight axles (just 1.3% of all type “F” cars), and 1 has twelve axles (just 0.14% of all type “F” cars). Additional axles in a car (such as in the case of type “F” cars) would directly impact the histograms for the length and weight of each car per code type. Further investigation was undertaken to confirm that this was not an error in the WILD data or an error in the data processing approach to filter the eight months of WILD data.

Two significant findings were made that relate to the parsing of WILD data:

- *Finding 1:* Public railroad information archives online collect data (including pictures) on individual train cars from across the United States. These archives include a significant portion of the cars that our team considered in the eight-month time period. The team isolated one of the nine type “F” cars that has eight axles, located the car in the archive, and have included a photo of the car in Figure C1: the car does in fact have eight axles. This process was repeated for the other outlying data (such as the locomotive in Figure C2) with the findings supportting the information in Table C1. In addition, the team

Table C1: Categorization of cars by train type (May 27, 2015 – January 28, 2016)

Categorization by train type (based on AAR Equipment Type and Trailer/Container Type Codes)		Frequency of each car type (per code) based on number of axles			
Code	Description	Four Axles	Six Axles	Eight Axles	Twelve Axles
A	Equipped box cars	656	0	0	0
B	Unequipped box cars	120	0	0	0
C	Covered hopper cars	6085	0	0	0
D	Locomotive	3	1221	0	0
E	Equipped gondola	552	0	0	0
F	Flat cars	681	0	9	1
G	Unequipped gondola	97	0	0	0
H	Unequipped Hopper	389	0	0	0
J	Gondola car	13	0	0	0
K	Equipped hopper cars	7550	0	0	0
L	Special type cars	1	0	0	0
M	M-O-W, Scale, Passenger, Caboose, and End-of-train information systems	78	0	0	0
P	Conventional intermodal cars				
Q	Lighter weight, Low-profile intermodal cars	0	0	158	133
R	Refrigerator cars	37	0	0	0
S	Stack car	1861	0	2182	306
T	Tank cars	4523	0	0	0
U	Containers				
V	Vehicular flat cars	7879	280	0	0
Z	Trailers				

researched the different types of cars that are considered in the AAR Equipment Type code and confirmed that all of our results fit reasonably within the range of lengths and number of axles that can be seen in each type of freight car. Figure C3, C4 and C5 show a six-axle locomotive, twelve-axle flat car, and four-axle intermodal car.

- *Finding 2:* Based on the types of trains that are encountered in the WILD data, it is very unlikely that a single freight car would have twelve axles. However, Table 1 shows that types “F”, “Q”, and “S” contain cars with twelve axles. These codes correspond to flat cars, intermodal cars, and stack cars respectively. It will be explained how in one case this is true (a single car has twelve axles), but in the other cases the identification of a car as having “twelve axles” (or even eight axles), is misleading. After researching more about these three types of cars, it can be stated:

Figure C1. The QTTX 130707 flat car (eight axles)

Figure C2. The GMTX 2128 locomotive (four axles)

Figure C3. Union Pacific locomotive (six axles)

- Even though the majority of type "F" flat cars have four axles, or even eight axles, as seen in Table 1, the team is able to identify the single twelve axles flat car from the WILD data within the online archive. The team created a diagram of the axle locations for the twelve axle flat car as seen in Figure C6.
- Intermodal cars and stack cars each have unique features. Intermodal transportation allows freight to be shipped via rail, ship, and truck, without the freight ever having to be handled. A standard eight-axle intermodal car is shown in Figure C7. Stack cars are built to be able to carry multiple layers of intermodal containers. Since stack cars carry up to two layers of containers, the carrying beds are lowered closer to the ground between the two sets of axles (known as a "well") in order to increase stability (Figure C8). While basic intermodal and stack cars consist of four axles, it is common for multiple cars to be permanently connected together to form a long car that consists

Figure C4. KRL #300300 heavy duty depressed center 12-axle flatcar

Figure C5. Four-axle intermodal car

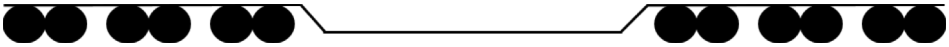

Figure C6. Format of the twelve-axle flat car

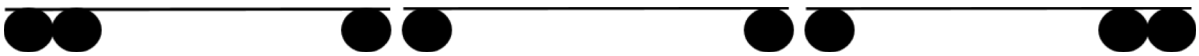

Figure C7. Format of eight axle intermodal car

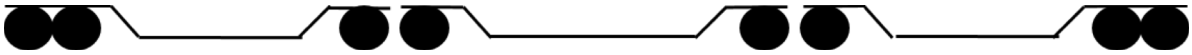

Figure C8. Format of eight axle stack car

of multiple units. Each unit within a multi-unit intermodal or stack car has very similar characteristics to a single car, but these units cannot be removed from each other. This is significant with respect to our analyses because the WILD detector records *all* of the units that are connected into a multi-unit intermodal or stack car as

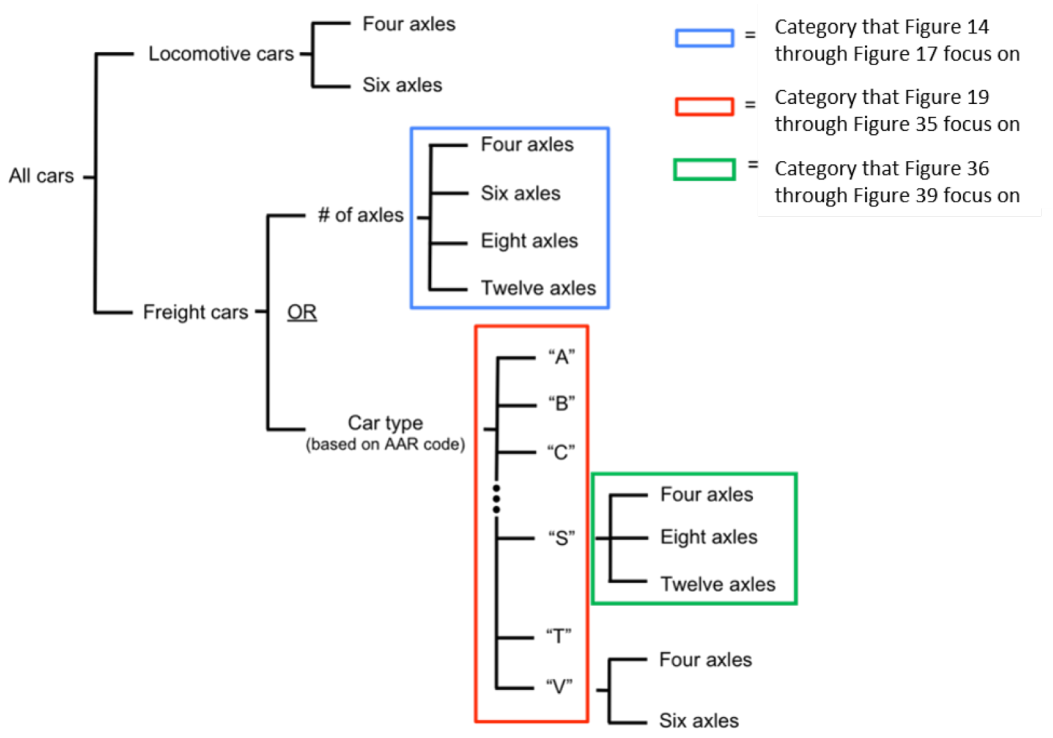

Figure C9. Levels of train type categorization

one single car (all categorized under a single car ID# and a single combined car weight). Thus, the WILD detector might read a stack car as being a single car with twelve axles that weighs 350 tons, when it is actually three cars (four axles each) that have a *combined* weight of 350 tons. This explains the outlying length and weight data in some of the histograms. The identification of this simplification that the WILD detector makes will allow us to take these special car structures into consideration during the development of future load histograms.

Levels of Train Type Categorization

Figure C9 provides a decision tree diagram that explains various ways to categorize different types of cars in the WILD data. Several histograms are included in this document that categorize the car data in three different ways. First, Figure C14 through Figure C17 provide histograms for the length of each car based on the number of axles per car. Second, Figure C19 through Figure C35 provide histograms for the length and weight of each car based on car type code. Third, Figure C36 through Figure C39 provide histograms for the length of each car based on car type code and further categorized by number of axles in each car. For the sake of space, only car type "S" has been categorized in this third way (Figure C36 through C39). It is pointed out the key features of each histogram within each diagram (when necessary). All histograms in this report are color coded according to the legend in Figure C6 so that it is easy to tell how they are categorized. In addition to the histograms that are attached to this report, our team can automatically create histograms for length of each car, weight of each car, avg./max load per

axle, distance between axles, and distance between cars, for any level of categorization within the decision tree presented in Figure C9.

Conclusions

The analysis performed provides a basis for assessing the loads imposed on the Memphis subjunction bridges (Parkin Bridge and Harahan Bridge). Specifically, the number of trains including locomotives and the different AAR train car types are quantified over the eight-month study period. Figure C10 and C11 provides histograms on the length of the locomotives and their associated number of axles (four versus six axles). Figure C18 provides a histogram for the different car types and their frequency over the eight-month period (similar to Table C1). Figure C19 through C35 provide histograms of length and weights associated with the different AAR car types observed in the WILD dataset. Finally, Figure C36 through C39 are histograms of lengths and weights of S-type AAR cars with different number of axles.

Figure 10: Length of loco (from front axle to back axle)

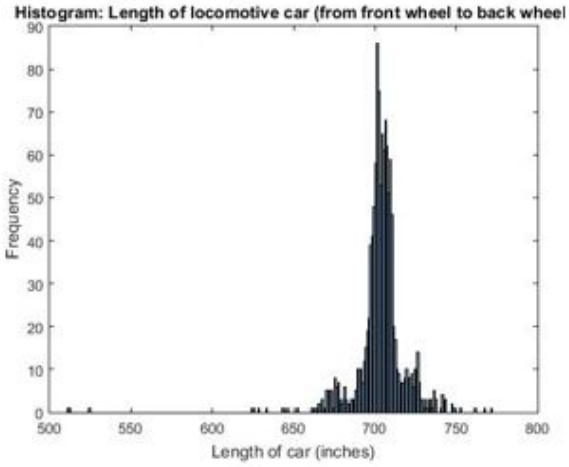

Figure 11: Number of axles per locomotive car

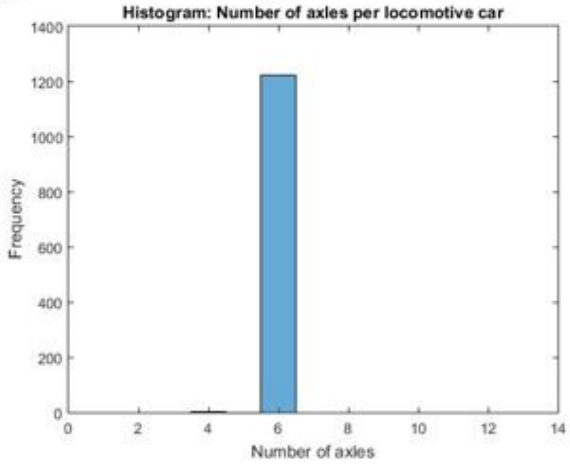

Figure 12: Length of freight (from front axle to back axle)

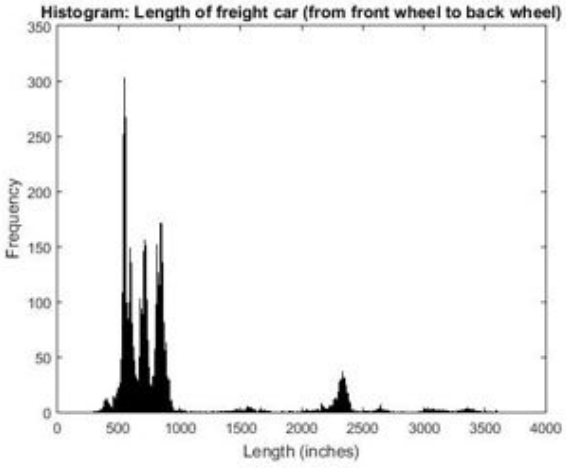

Figure 13: Number of axles per freight car

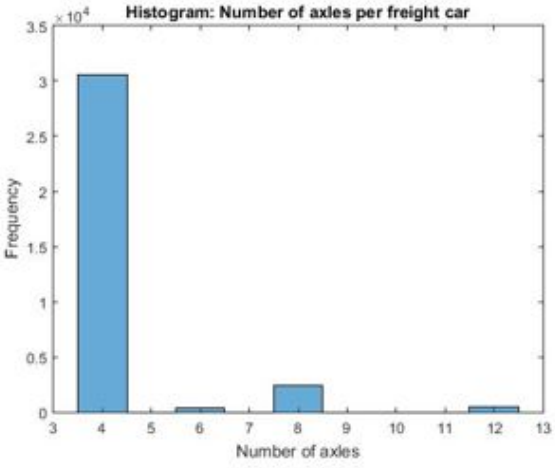

Figure 14: Length of car for all cars with four axles

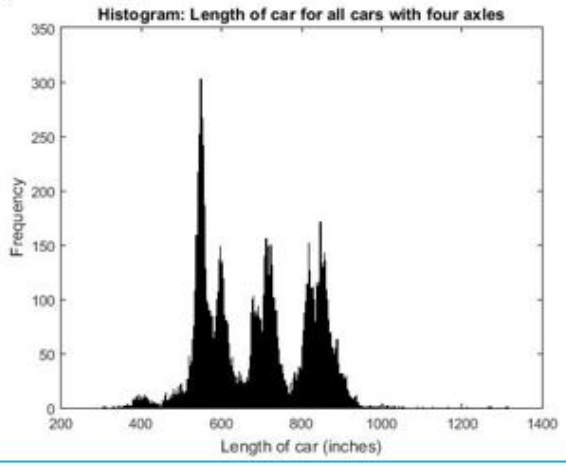

Figure 15: Length of car for all cars with six axles

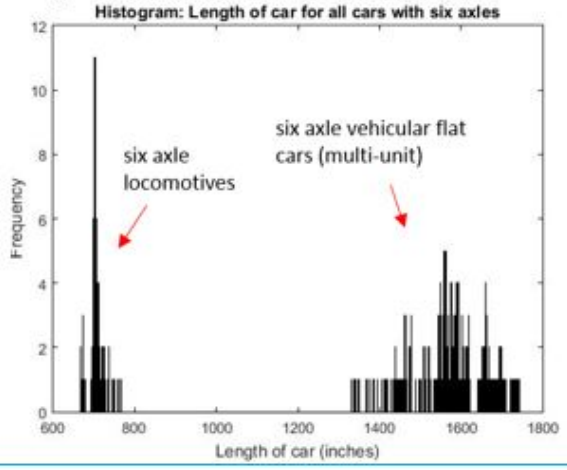

Figure 16: Length of car for all cars with eight axles

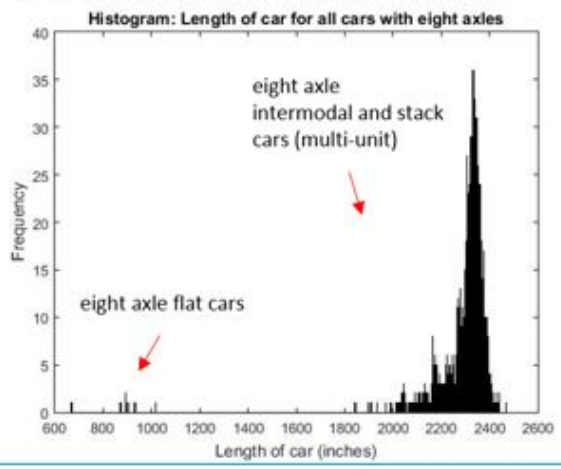

Figure 17: Length of car for all cars with twelve axles

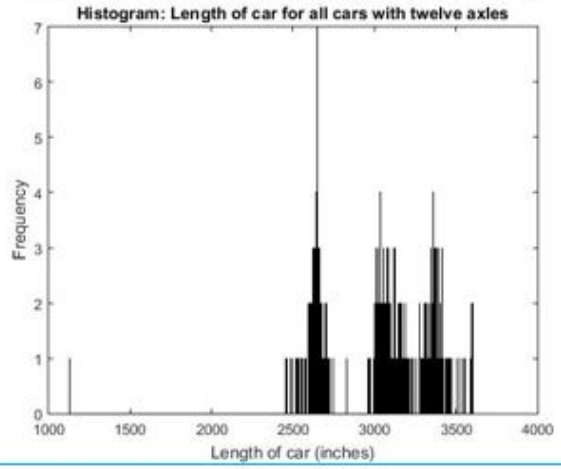

Figure 18: Equipment type of each car:

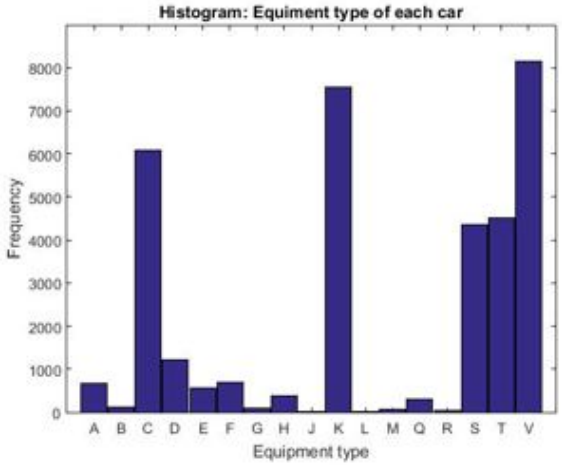

Figure 19a: Car type "A" length of car

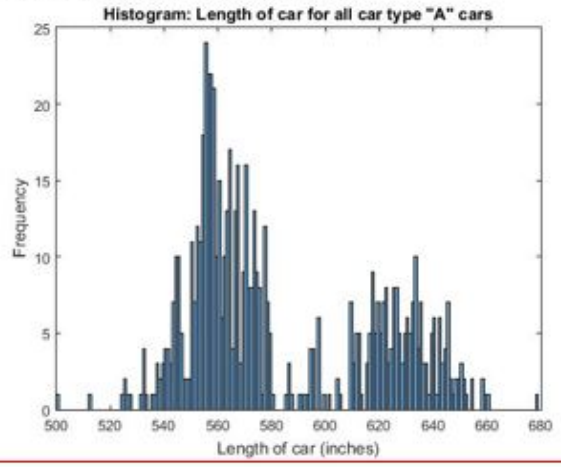

Figure 19b: Car type "A" weight of each car

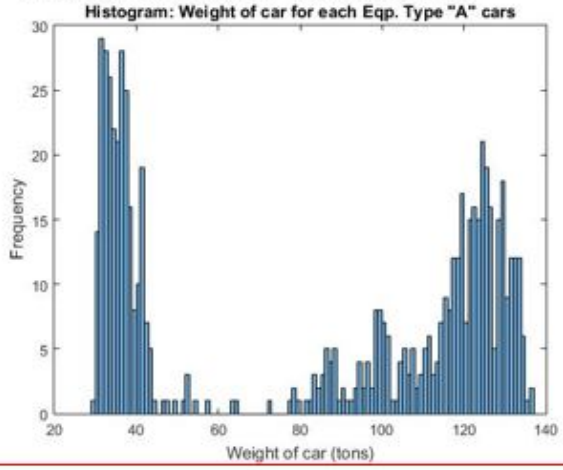

Figure 20a: Car type "B" length of car

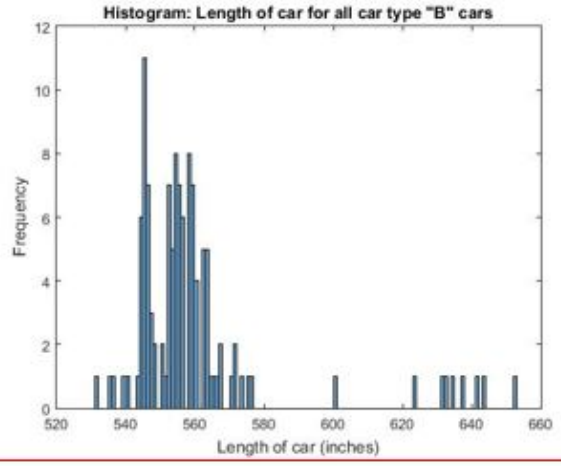

Figure 20b: Car type "B" weight of each car

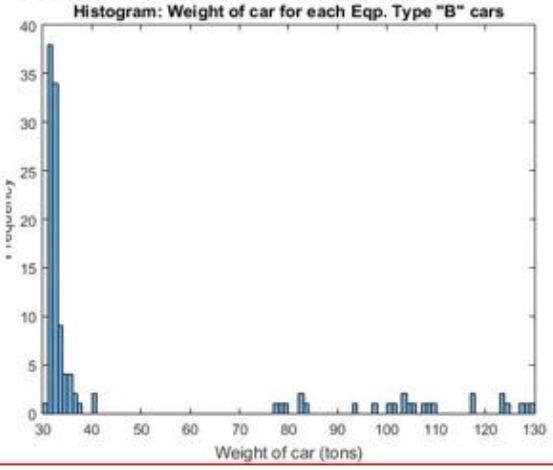

Figure 21a: Car type "C" length of car

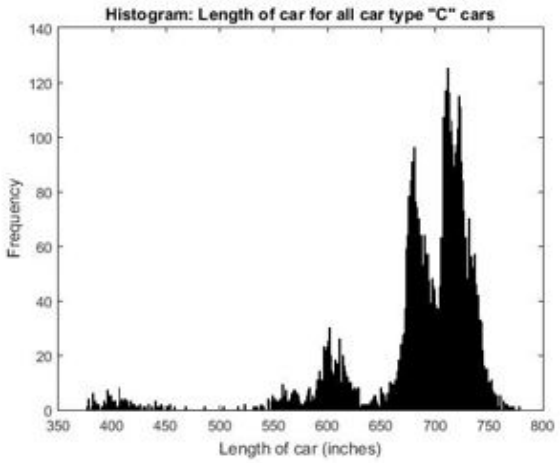

Figure 21b: Car type "C" weight of each car

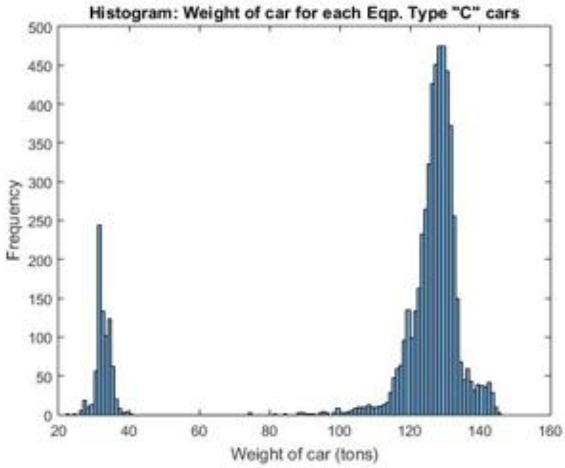

Figure 22a: Car type "D" length of car

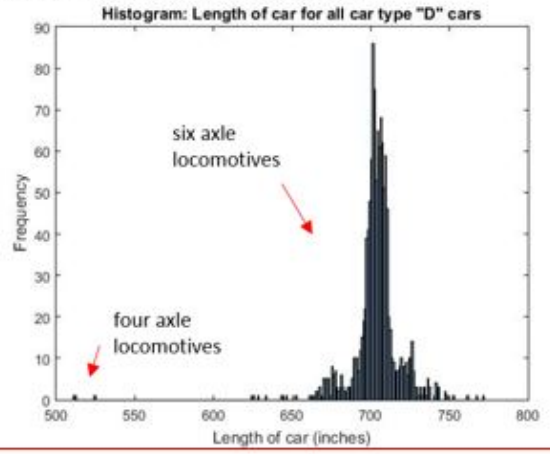

Figure 22b: Car type "D" weight of each car

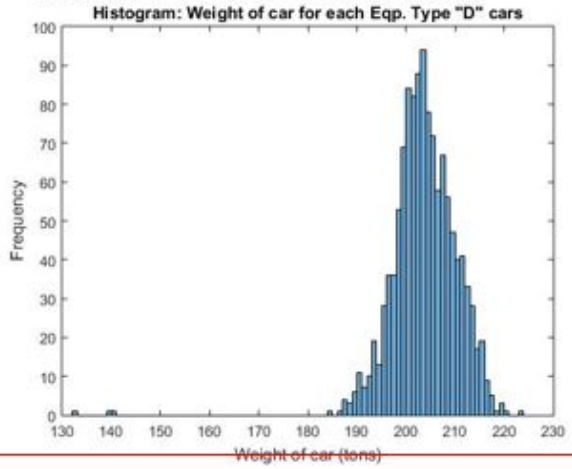

Figure 23a: Car type "E" length of car

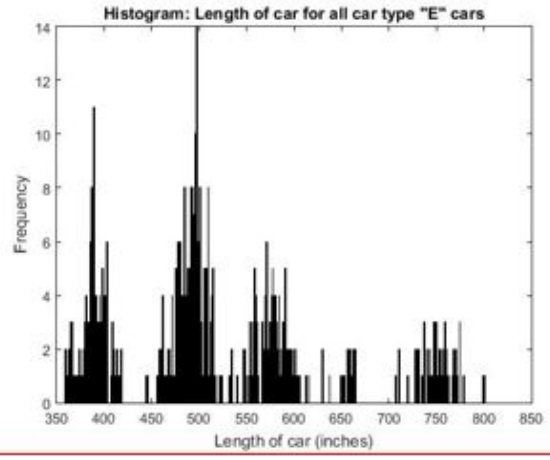

Figure 23b: Car type "E" weight of each car

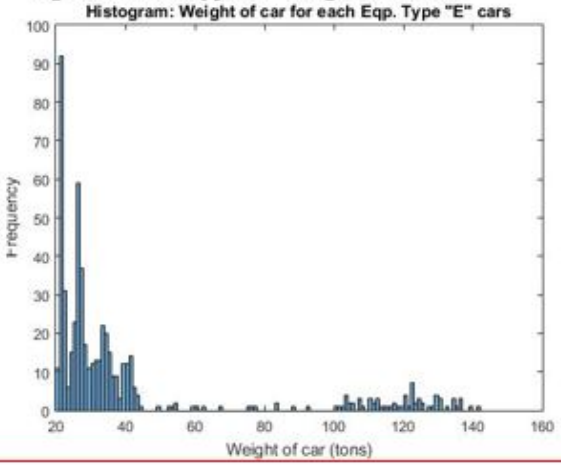

Figure 24a: Car type "F" length of car

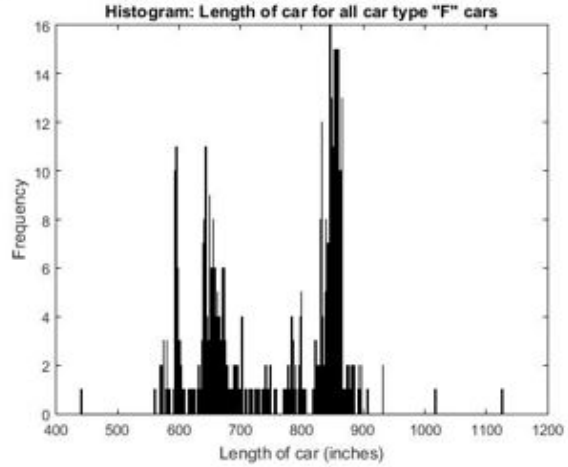

Figure 24b: Car type "F" weight of each car

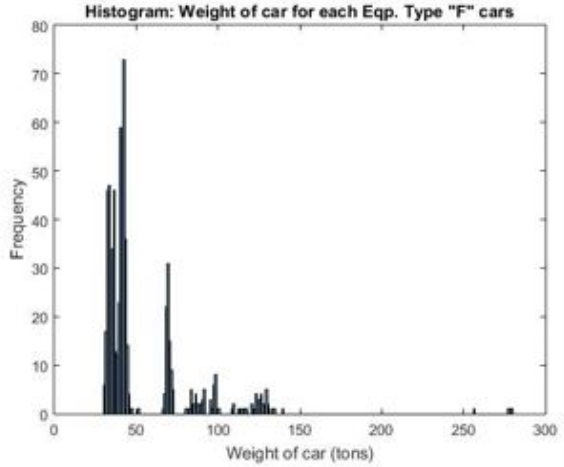

Figure 25a: Car type "G" length of car

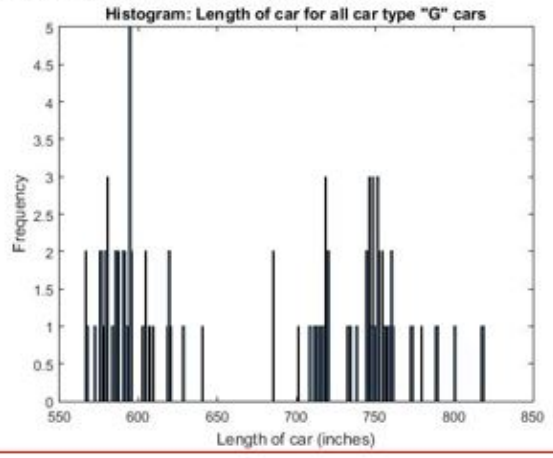

Figure 25b: Car type "G" weight of each car

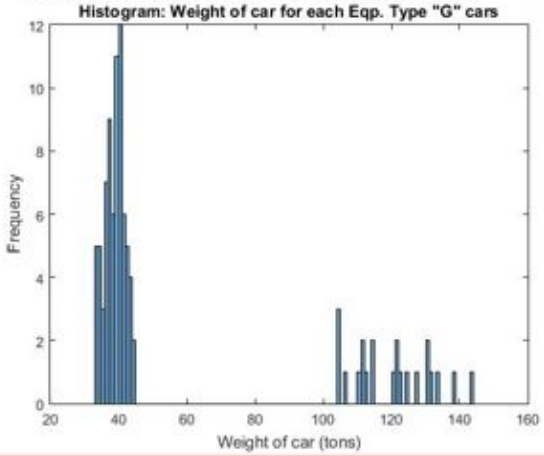

Figure 26a: Car type "H" length of car

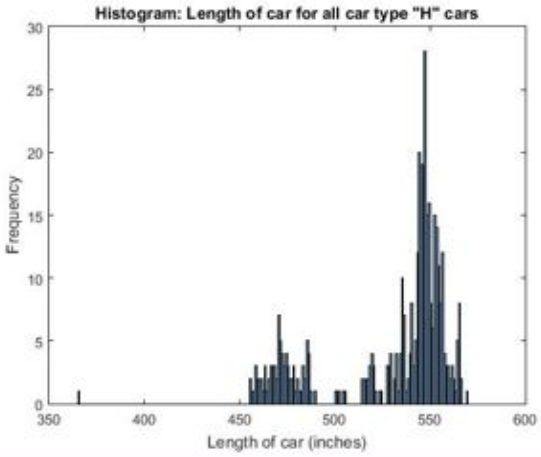

Figure 26b: Car type "H" weight of each car

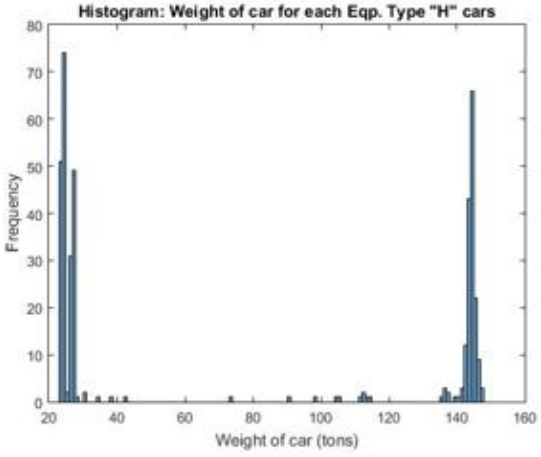

Figure 27a: Car type "J" length of car

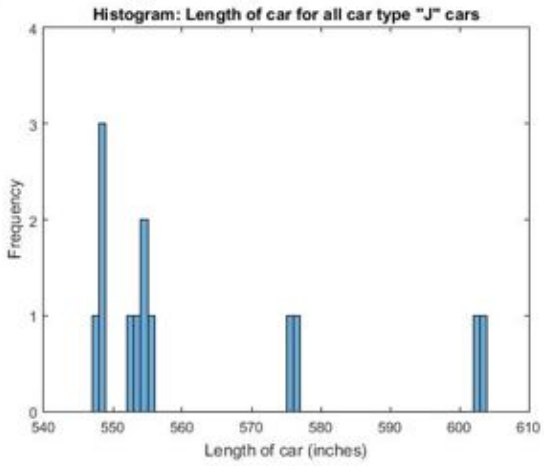

Figure 27b: Car type "J" weight of each car

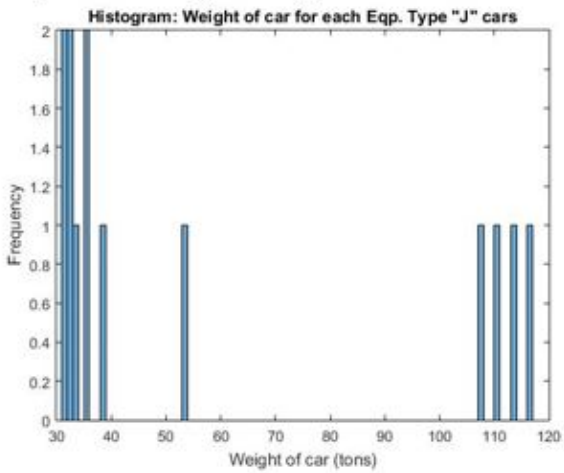

Figure 28a: Car type "K" length of car

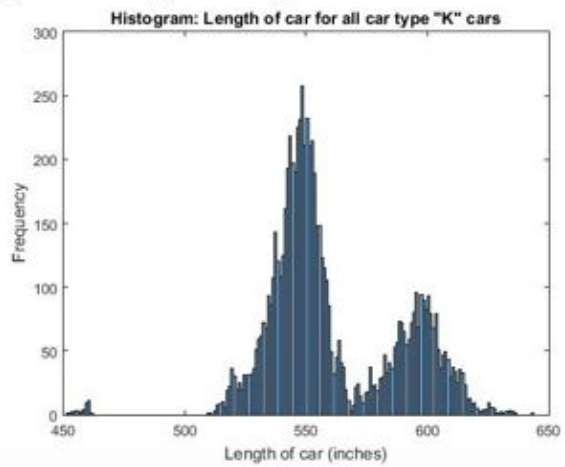

Figure 28b: Car type "K" weight of each car

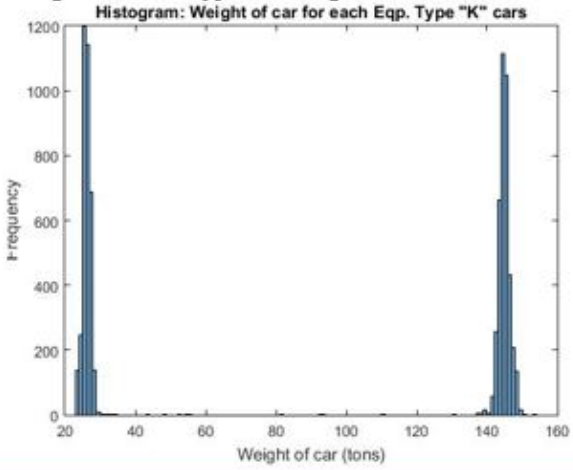

Figure 29a: Car type "L" length of car

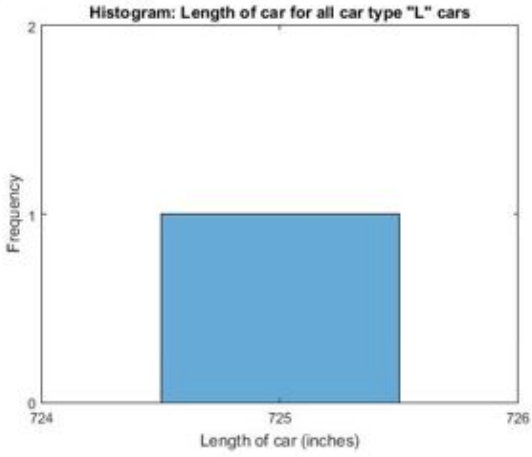

Figure 29b: Car type "L" weight of each car

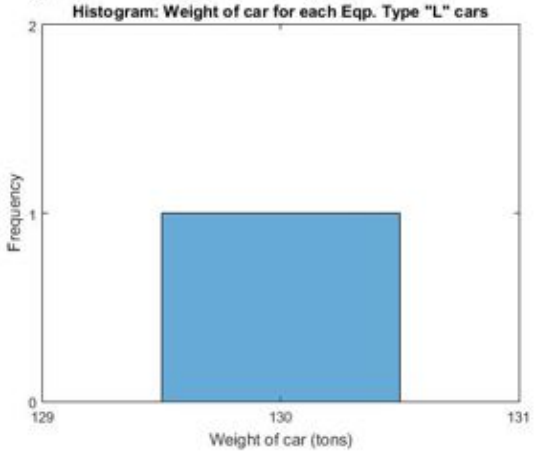

Figure 30a: Car type "M" length of car

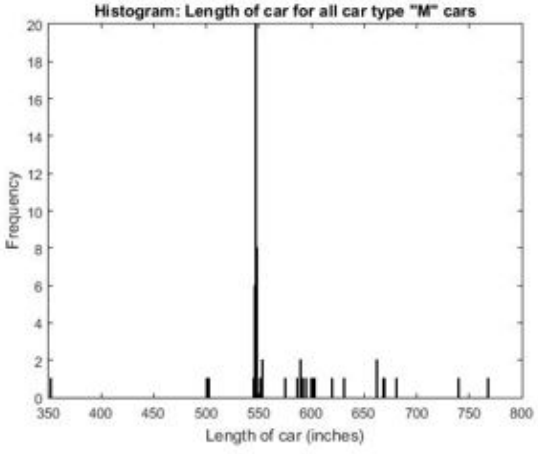

Figure 30b: Car type "M" weight of each car

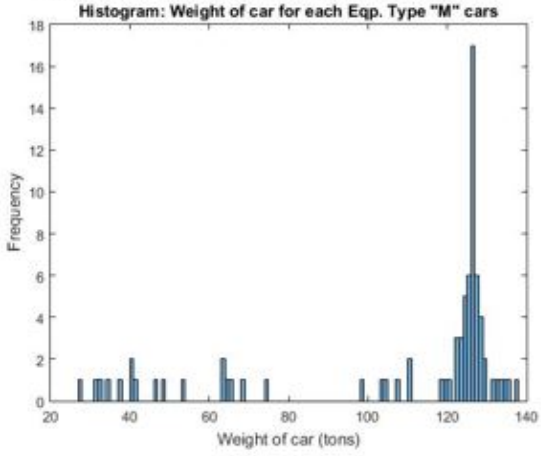

Figure 31a: Car type "Q" length of car

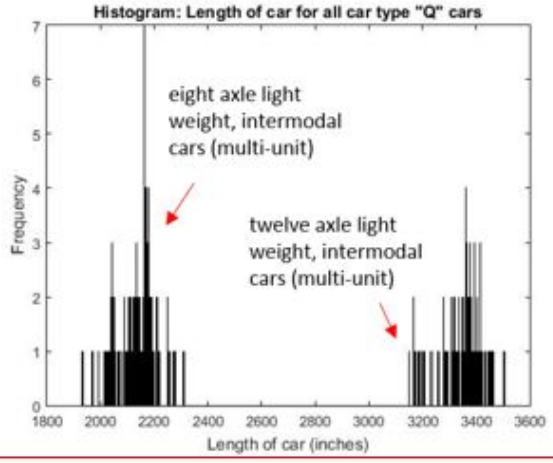

Figure 31b: Car type "Q" weight of each car

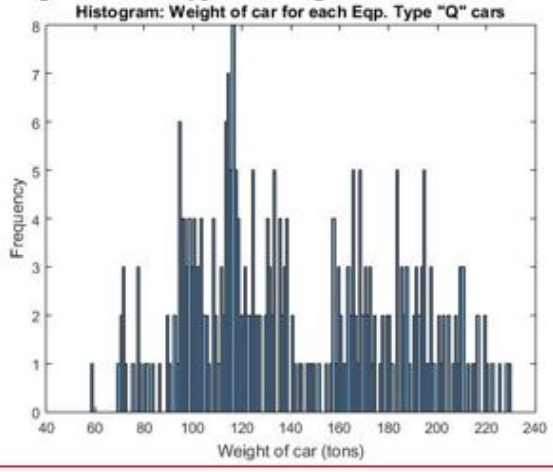

Figure 32a: Car type "R" length of car

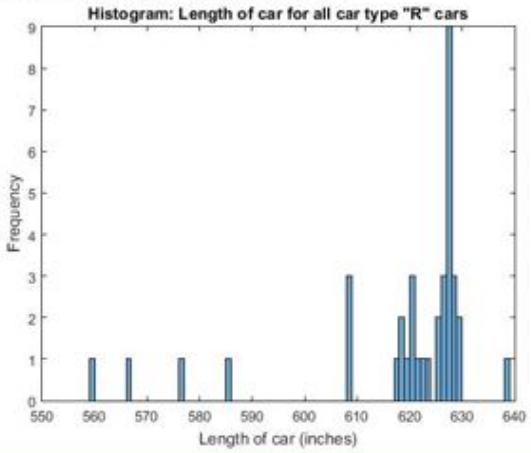

Figure 32b: Car type "R" weight of each car

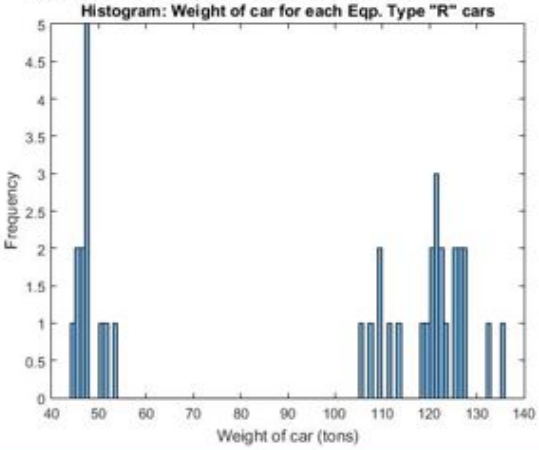

Figure 33a: Car type "S" length of car

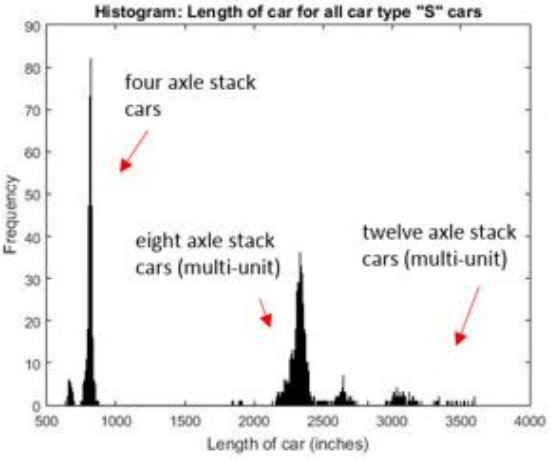

Figure 33b: Car type "S" weight of each car

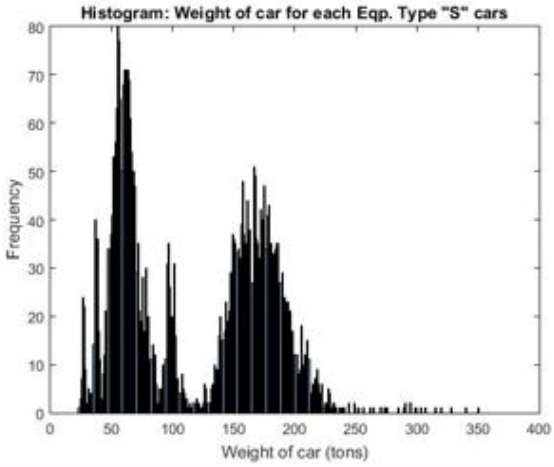

Figure 34a: Car type "T" length of car

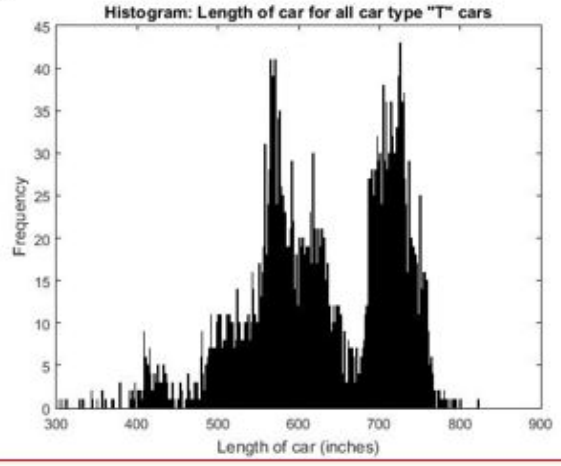

Figure 34b: Car type "T" weight of each car

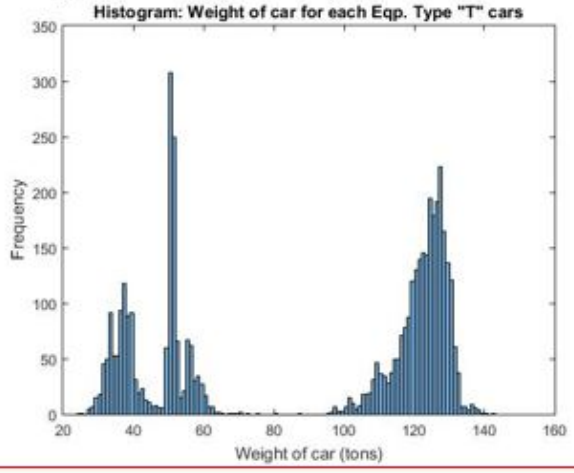

Figure 35a: Car type "V" length of car

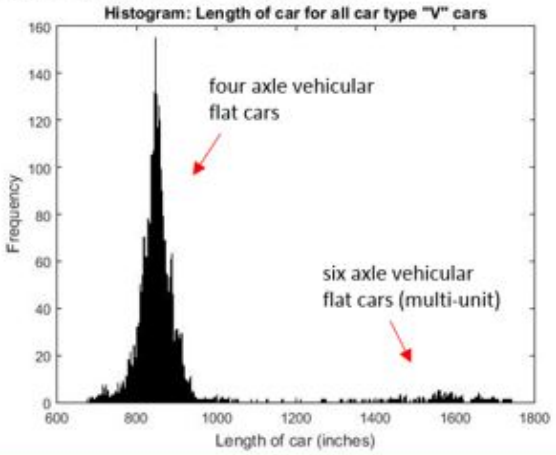

Figure 35b: Car type "V" weight of each car

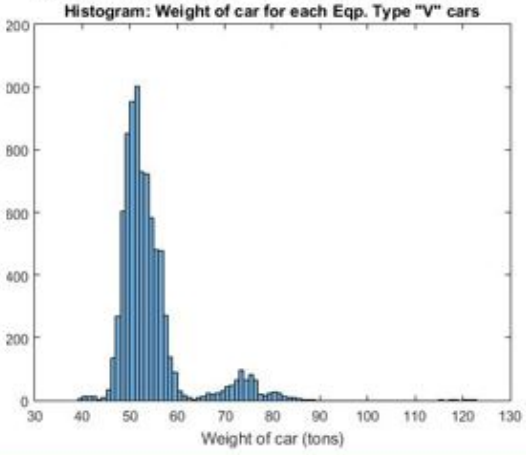

Figure 36: Car type "S" all axles included

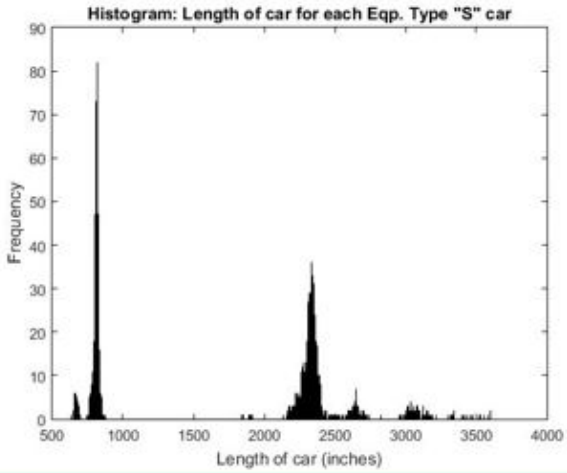

Figure 37: Car type "S" only cars with four axles

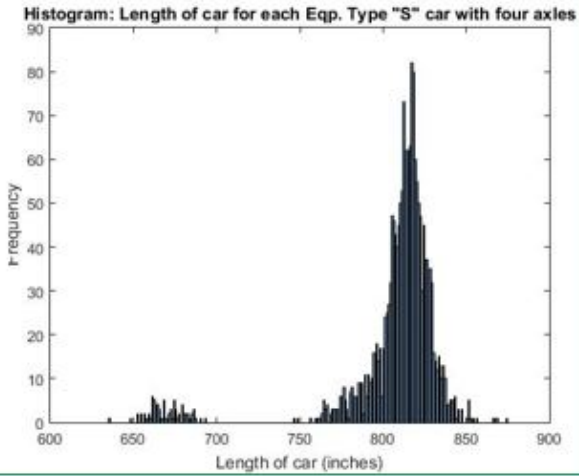

Figure 38: Car type “S” only cars with eight axles

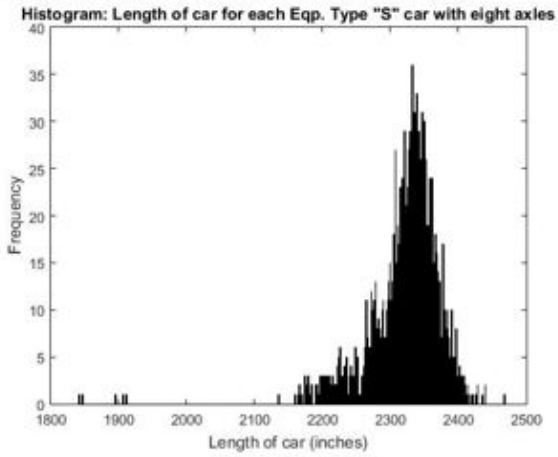

Figure 39: Car type “S” only cars with twelve axles